Transverse Sub-Assemblage Testing of the Inverted-T Bridge System

Matthew S. Mercer

Thesis submitted to the faculty of the
Virginia Polytechnic Institute and State University
in partial fulfillment of the requirements
for the degree of

MASTER OF SCIENCE
in
CIVIL ENGINEERING

Thomas E. Cousins, Co-Chair

Carin L. Roberts-Wollmann, Co-Chair

Cristopher D. Moen

June 12, 2012

Blacksburg, VA

Keywords: Inverted-T, Sub-assemblage, Embedded Plate, Extended Bar, Accelerated Bridge Construction, Prefabricated Bridge Construction, Poutre Dalle

Transverse Sub-Assemblage Testing of the Inverted-T Bridge System

Matthew S. Mercer

ABSTRACT

The inverted-T bridge system is a rapid bridge construction technique that consists of precast inverted-T girders placed adjacent to one another and covered with a cast-in-place deck. This system was first implemented in the U.S. by the Minnesota Department of Transportation (Mn/DOT). This research focuses on improving the constructability of the Mn/DOT system while maintaining the system's structural performance characteristics. To accomplish this goal, five sub-assemblage specimens were cast and tested in the structures laboratory at Virginia Tech. These tests focused on identifying an improved precast girder geometry and transverse sub-assemblage connection for this system.

From this study it was found that all of the proposed specimens behaved adequately at service load and strength. From these results, it is recommended to further evaluate a specimen with a tapered profile and no physical connection between precast girders for use in a Virginia Department of Transportation bridge near Richmond, VA.

ACKNOWLEDGMENTS

I would like to thank professors Dr. Tommy Cousins and Dr. Carin Roberts-Wollmann for the opportunity to work on this project. Their extensive knowledge, guidance, and interaction have been instrumental to my progress with this thesis and as a graduate student. I would also like to express my gratitude to Dr. Cris Moen for serving as a member of my thesis committee and for his contributions to my work.

I would like to extend my thanks to the members of VCTIR for their interest and input on this project. Furthermore, I would like to show my appreciation for the support of Fatmir Menkulasi, Douglas Nelson, Achmaa Vaanjilnorov, and all of the graduate students who helped with the concrete placements throughout the duration of this project. This project has been a team effort and would not have been possible without them.

I am very grateful for the efforts and support of David Mokarem, Brett Farmer, and Dennis Huffman. Their contributions and friendship have been valuable to me both in the structures laboratory and on a personal level. I would also like to thank all of my fellow SEM graduate students for the experience here at Virginia Tech. The last two years have been a great time and something I will never forget.

Lastly, I would like to thank my parents Randall and Kimberly Mercer. They, along with my sister Amanda Dowdy, have supported me in all that I have done throughout my life and continue to do so every day. Their guidance and encouragement extends far more than I could ever ask. I am so blessed and truly thankful for all that they have done for me.

TABLE OF CONTENTS

LIST OF FIGURES

LIST OF TABLES

INTRODUCTION

Background

Prefabricated bridge construction is a rapid construction process that includes both precast and cast-in-place (CIP) elements. This process consists of manufacturing girder elements in a precast concrete facility and then transporting the sections to the work site. The system can be made composite via the addition of a CIP deck. With this process time spent at the worksite is reduced and better quality control of the precast girder components is achieved. Some undesirable issues, however, are created. For adjacent girder systems such as adjacent boxes or voided slabs, these issues include differential shrinking of the precast and cast-in-place elements and durability of the system. Cracks can compromise the strength of the bridge and allow chlorides and other corrosive agents access to the reinforcing steel. Adjacent girder systems can also lose shear key connection which leads to decreased load sharing between girders. Many of these issues can be resolved by using the inverted-T bridge system.

The inverted-T system, a type of rapid bridge construction system, consists of inverted-T shaped girder sections with a CIP topping. The geometry of the inverted-T girders maximizes the amount of CIP concrete over the girder to girder joint. Figure 1 shows a comparison between the inverted-T and adjacent box girder systems. The depth of concrete over the girder to girder joint is much greater in the inverted-T system and therefore has better reflective crack control capabilities. The concrete over the joint in prefabricated adjacent girder systems is susceptible to reflective cracking due to the high tensile stress across the bottom of the bridge and lack of bond between girders. The tension stress is caused by transverse bending and differential deflection of the girders. The current practice for resisting the tensile stress and increasing load sharing between girders in the inverted-T concept is to extend rebar from the side of each girder over the joint and then cast the girders together with the deck concrete. This steel serves to carry the tensile forces that develop across the joint and reduce the reflective crack. Reducing the reflective cracking limits corrosion and helps maintain the strength of the bridge. The connection also ensures load sharing between adjacent members.

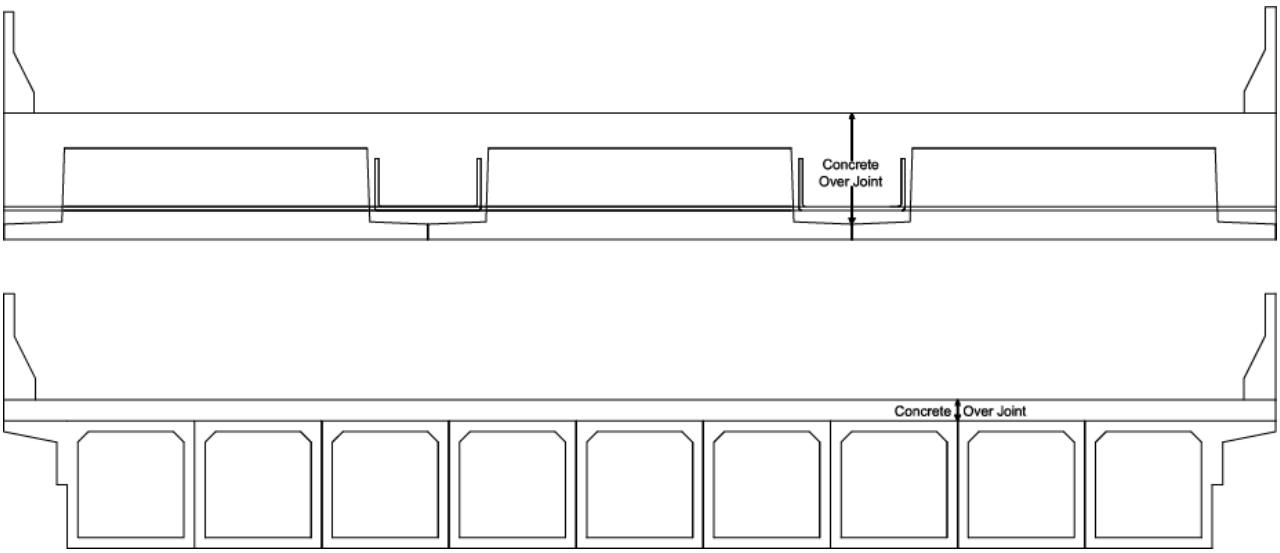

Figure 1: Depth of CIP Concrete over Longitudinal Joint of Inverted-T System (top) and Adjacent Box Girder System (bottom)

For the inverted-T system the CIP deck concrete serves a few purposes. The first of which is to provide a smooth wearing surface for drivers, by covering the joints of adjacent girders. Secondly, if the girders are properly roughened the deck acts compositely with the girder elements and contributes to the flexural strength of the system. Lastly, the CIP deck provides continuity along the longitudinal joint. The deck concrete distributes the loads among adjacent girders.

Objective

The objective of this research is to further develop the inverted-T to inverted-T connection for adjacent precast girders in the prefabricated inverted-T bridge system. The current design detail of extended bars protruding transversely from each precast girder (as developed by Mn/DOT) (French et al., 2011) creates constructability issues. These included obstacles with formwork to accommodate the bars extending from the formwork sides and difficulties with transportation and placement of the girders without causing damage the extended bars.

The developed inverted-T bridge system design should provide equivalent or better reflective crack control under service level conditions. Ultimately, the findings of this research will be used as the basis for full-scale testing and eventual implementation in a bridge in Virginia.

Organization

The next chapter of this thesis is a literature review that covers Accelerated Bridge Construction and the research and studies that have brought the inverted-T system to its current state. The next chapter presents the specimens tested as part of this research. It covers the purpose of each test and details the specifications of each specimen's design. The justification for parameters such as geometry and connection types is also laid out in this chapter. Following the introduction of the specimens is a chapter that documents the methods and processes by which the specimens were constructed and instrumented. This also includes details on the material testing and data acquisition procedures.

Following the physical descriptions of the specimens and test setup is a chapter that discusses the analytical methods used to calculate service level stresses and the loads required to simulate those stresses in a laboratory setup. Following the finite element models and calculations in the analytical methods section is the results chapter. This chapter presents all of the recorded data that is included in the discussion chapter.

The discussion chapter expands on all of the important results and behaviors that were recorded throughout the process of this research. The inferences of the discussion chapter are summarized into a few key points in the conclusions chapter. The recommendations chapter then presents what changes or further studies should be done based on the conclusions of this research. The recommendations are followed by the references used in this paper and a series of appendices that cover information that was not included in the body of the thesis.

LITERATURE REVIEW

Accelerated Bridge Construction and Prefabricated Bridge Superstructure Systems

The increasing traffic demands on bridge infrastructure present significant challenges for the state departments of transportation. One of these challenges is reducing construction time to minimize obstruction to the motoring public. A solution to this problem is to prefabricate bridge parts offsite and then transport and assemble the components at the jobsite.

In conventional bridge construction the majority of the concrete placement work is done onsite. Included in this work is the installation of substructure and superstructure forms. After the forms are installed they are filled with reinforcing steel and concrete. Once the concrete is placed time is apportioned to allow for curing. This entire process takes a significant amount of time and is also susceptible to delays due to adverse weather. The lengthy successive cycle and the delays add to the distress that construction projects cause to motorists. (Culmo, 2009)

The increased use of Accelerated Bridge Construction (ABC) has been driven by the need to limit the obstruction to the motoring public during bridge construction and rehabilitation projects. The ABC concept not only limits issues with traffic impedance, but also offers positive benefits within the context of bridge construction processes and quality. Culmo (2011) provides the following lists of advantages of the ABC concept.

ABC improves:

- Site constructability
- Total project delivery time
- Material quality and product durability
- Work-zone safety for the traveling public and contractor personnel

ABC reduces:

- Traffic impacts
- Onsite construction time
- Weather-related time delays

ABC can minimize:

- Environmental impacts
- Impacts to existing roadway alignment

- Utility relocations and right-of-way take

Casting bridge girders in a plant as opposed to in the field allows for better monitoring and quality control of the specimens. Fabricating the components in a controlled environment eliminates any issues that might arise in the field. More importantly, by casting and aging the girders offsite the time required onsite for forming and placing is reduced. The girders can simply be craned into place and prepared for deck placement immediately. (Ralls et al., 2002)

Prefabricated bridge design not only reduces construction time, but also promotes worker safety. Creating the formwork for cast-in-place bridge (CIP) systems can be hazardous work. CIP construction requires workers to work close to traffic, near power lines or over water. Performing that work in a controlled and safe environment eliminates any danger associated with placing workers in compromised positions during construction in the field. This is particularly valuable in situations that require workers to reach the underside of a bridge for the installation or removal of formwork. (Ralls, 2006)

There are several options to pursue within the scope of prefabricated bridge superstructure systems. Some examples of these options include full-depth precast deck panels with or without post-tensioning, Fiber Reinforced Polymer (FRP) deck panels, steel grids, orthotropic decks, adjacent deck bulb-T beams, adjacent double-T beams, adjacent inverted-T beams, adjacent box beams, ,voided slabs, modular beams with decks, full-width beam span with deck, and a total bridge fabrication. All of these options serve as solutions to accelerate bridge construction and provide minimal disturbance to the motoring public. It is up to the engineer's judgment to discern if the ABC approach is appropriate for a project and, if it is, which option is most suitable. (Culmo, 2011)

In adjacent member bridges, once placed in position, the girders are connected to one another to form continuity. This continuity promotes load sharing and distributes the stresses more evenly across the width of the bridge. Closure joints must be designed to distribute loads laterally without distortion. These joints must be sealed to prevent moisture from passing through the interface. Continuity is established by a few different methods including post-tensioned joints, passively reinforced joints, welded or bolted joints, or some combination of these components. (Ralls et al., 2004)

Post-tensioned joints typically use the compression created from the post-tensioning in combination with a shear key for load transfer. While typically effective, this process does

require the labor associated with post-tensioning. Passively reinforced joints use an arrangement of projecting lapped reinforcing steel to form continuity. These joints must be wide to allow the projecting bars to develop. This large area of concrete over the joint is susceptible to shrinkage cracking. Welded or bolted joints consist of vertical or inclined plates which are cast into the prefabricated elements and then welded together in the field. The process, though an effective means to form continuity, requires additional labor for both welding the connection and grouting the finished joint. (Ralls et al., 2004)

One significant disadvantage to prefabricated bridge construction is durability. All of the connections discussed above are susceptible to reflective cracking. This issue is a concern along the longitudinal joint between adjacent bridge girders. At this joint there is no stiffness provided by the girders and stresses develop in the deck due to differential deflection. Figure 2 shows the relationship between differential displacement and reflective cracking in prefabricated construction. (Bell et al., 2006)

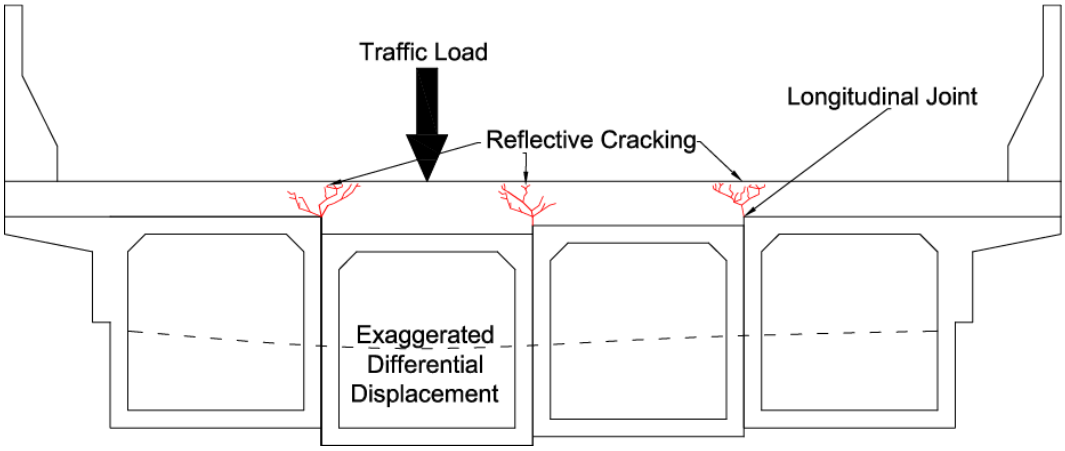

Figure 2: Reflective Cracking from Differential Displacement

Poutre Dalle System

In April of 2004 a group of engineers sponsored by the Federal Highway Administration (FHWA) and the American Association of State Highway and Transportation Officials (AASHTO) set out to obtain information on prefabricated bridge systems overseas. The group was interested in identifying the methods and processes that were being used in other industrialized countries in Europe and Asia. The study focused on Belgium, France, Germany, Japan, and the Netherlands. This study led to the discovery of 33 new technologies that to date

had not been implemented in the United States. Of these 33 the research team selected 10 that were of interest for further study. (Russell et al., 2005)

During the study conducted by the FHWA and AASHTO the group members were introduced to the Poutre Dalle system in France. This short-span (20 to 82 feet) system consists of beams that are placed next to one other and connected by a CIP deck. Each of the beams is a shallow, precast, prestressed concrete inverted tee-beam. Figure 3 shows a photo of a Poutre Dalle system inverted-T girder. Figure 4 shows a cutaway of the CIP deck and configuration of the inverted-T girders. The system was designed to provide transverse moment capacity for the longitudinally oriented girders. Transverse load distribution was achieved through the development of transversely oriented reinforcement protruding from the precast section and extending into the CIP concrete placed in the trough region created by adjacent panels. (French et al., 2011) Continuity between adjacent inverted-T beams was established using a series of 180 degree bent hooks protruding through the web of each precast girder. These hooks overlapped adjoining flanges and were cast into the deck concrete. Reports on the system provided the following advantages (Russell et al., 2005):

- Provides a precast solution with a range of sizes
- Does not require falsework.
- Can be placed across highways in service.
- Has short delivery time.
- Does not require skilled labor for erection.
- Has smooth bottom surface.
- Has thinner deck resulting in higher vertical clearance.
- Allows fast construction.
- Allows economical construction.
- Provides a safe working platform.

Figure 3: Poutre-Dalle Precast Girder from France (Courtesy of Federal Highway Administration)

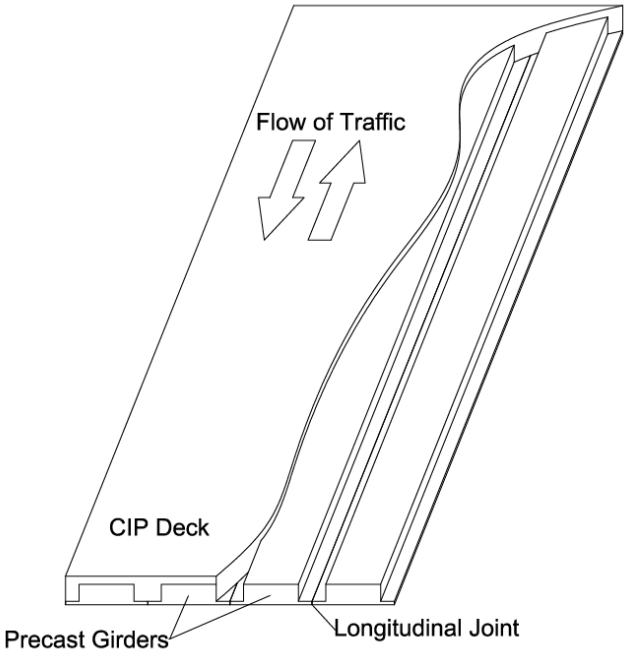

Figure 4: Model of Poutre Dalle System

Minnesota PCSSS

The Minnesota DOT (Mn/DOT) implemented the concepts of the Poutre Dalle system into a precast composite slab span system (PCSSS). This study led to the construction of two inverted-T bridges in the state of Minnesota in 2005. (Smith et al., 2008) In Project 10-71 for the National

Cooperative Highway Research Program (NCHRP) French and others further investigated the Poutre Dalle system in the paper *Cast-In-Place Concrete Connections for Precast Deck Systems* (French et al., 2011). At that time there were no published results regarding the performance of the Poutre Dalle system. In this study the researchers at the University of Minnesota modified a few of the practices of the French and tested a series of connections along the longitudinal joint. The main difference in the study performed in Minnesota was that the 180 degree hooked bars used in France were replaced with 90 degree hooks. This allowed a cage of reinforcement to be pre-tied and dropped into position over the inverted-T to inverted-T joint. This cage served to resist shear forces across the longitudinal joint. The modification of the hooks simplified the installation of the cage in the field. Figure 5 and Figure 6 show the 90 degree hooks and the alignment of the precast girders in the field.

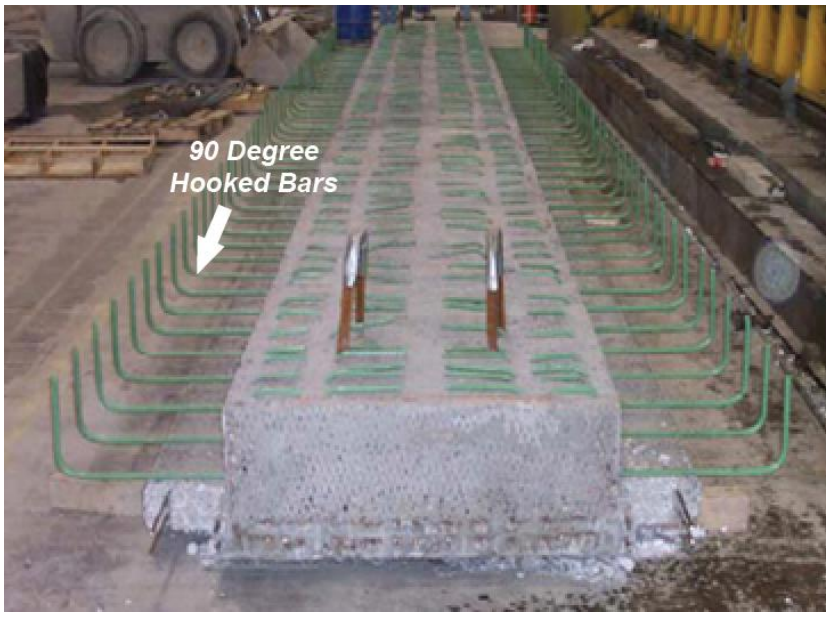

Figure 5: Precast Inverted-T Used by Minnesota Dept. of Trans (Mn/DOT) (Courtesy of Mn/DOT)

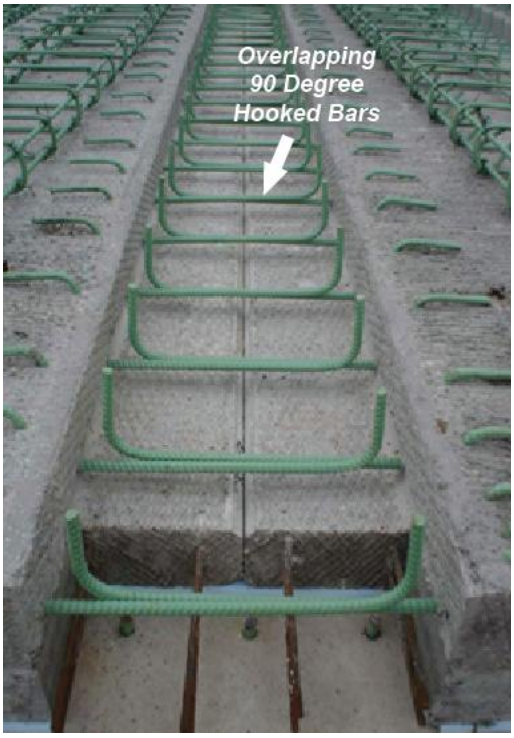

Figure 6: Field Installation of Precast Inverted-Ts before Installation of Drop-in Cage (Courtesy of Mn/DOT)

The work done by the University of Minnesota as part of the NCHRP project (French et al., 2011) included some optimization of the transverse connection along the longitudinal joint of the inverted-T bridge system. Seven sub-assemblage specimens were designed and tested to investigate the effects of spacing, size, and placement of the 90 degree hooked extended bars. Each specimen was designed to investigate a single attribute and identify the crack control performance of the system with the variable component. The results of this research indicated that using larger extended bars with tighter spacing and minimal cage reinforcement was preferable over other economically equivalent combinations of extended bar sizes, spacing, and cage reinforcement details.

The University of Minnesota test specimen consisted of two adjacent precast girder sections combined with a cast-in-place deck section. This setup is shown in Figure 7. A vertical clamping system was also used adjacent to the applied load to simulate the effects of rotational restraint. The clamping restraint can be seen in Figure 8. The specimens were exposed to a set loading regimen that included several thousand cycles at each load step. The specimens were instrumented with a series of concrete embedment, steel resistance, and vibrating wire gages. There was also a series of LVDTs and wirepots attached to the side and bottom of the specimen.

Cores were taken from each sample after testing to help identify the maximum height of the crack. The results of this work were developed into a design guide for inverted-T bridges. (French et al., 2011)

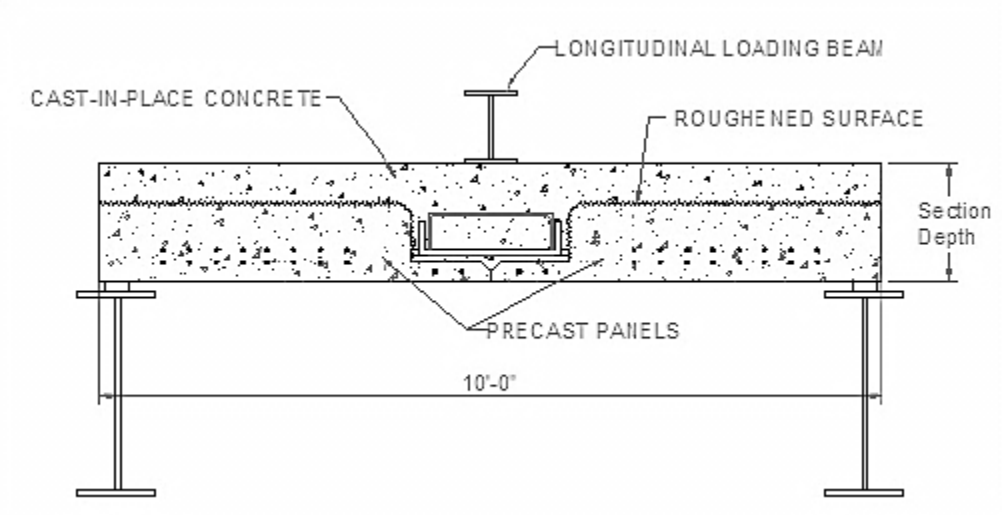

Figure 7: Elevation View of Sub-assemblage Specimens (Courtesy of Mn/DOT)

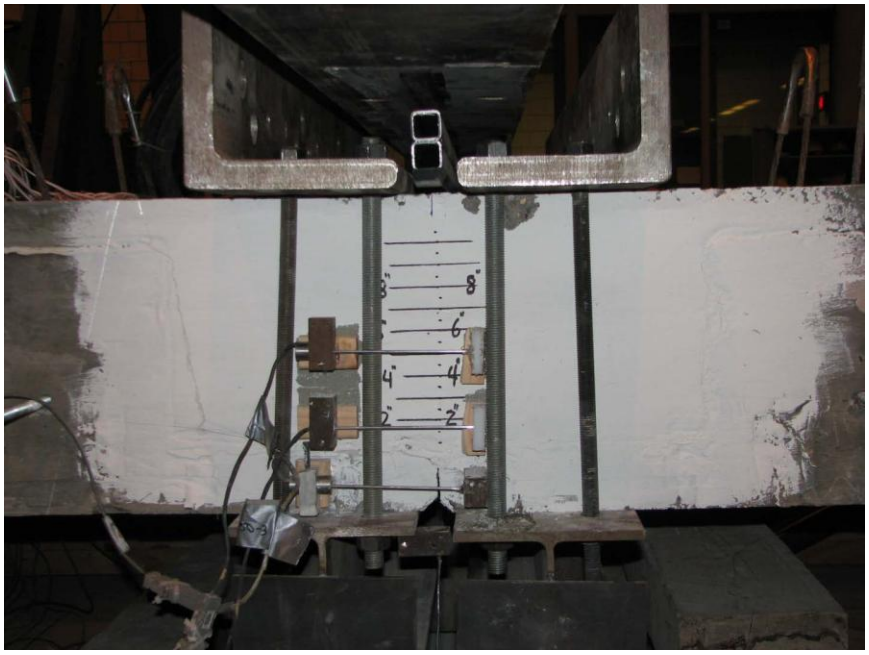

Figure 8: Clamping System Used to Provide Rotational Restraint (Courtesy of Mn/DOT)

The design guide set forth in NCHRP 10-71 based on the results of the sub-assemblage testing done at the University of Minnesota made several recommendations for the implementation of the inverted-T concept. The first conclusion was that reflective cracking

originating at the longitudinal joint between adjacent precast flanges can be controlled through the addition of a drop-in reinforcing cage. The research also indicated that the reinforcement spacing for crack control is defined as the maximum spacing between the reinforcement crossing the joint regardless of whether it is part of the drop-in cage or the transverse hooked bars. The publication also set forth guidelines for allowable dimensions and cover depths of the concrete components of the system. (French et al., 2011)

TEST SPECIMENS

This chapter presents the specimens tested and explains why each was selected. It discusses the manner in which the test setup was chosen and what limitations controlled the tests. Along with descriptions of each connection that was tested, some rejected options are included to show the thought process of why the chosen specimens were selected.

Transverse Orientation

The component of interest for this research is the longitudinal connection between adjacent bridge girders. The goal was to mimic the transverse stress at this connection which occurs under service load conditions. Full-scale testing is not within the scope of this portion of the project so a section of the bridge was selected to best represent the performance of the system as a whole. Preliminary discussions considered three girder sections with two connections per test, but specimen size and weight restrictions limited further consideration. Therefore, on transverse connection was included in each test specimen. This left a test setup that consisted of two full girder sections with one connection between them. This arrangement was replicated with different girder and connection details to optimize the design. The load applied caused similar transverse stress conditions to that of the actual bridge.

The specimens were sized to conform to the constraints of the test environment. All testing was done at the Thomas Murray Structures Laboratory at Virginia Tech. The lab contains two overhead cranes each with a capacity of five tons. This limited the overall weight of each specimen to 20,000 lbs. During the preliminary, full-bridge design conducted in the summer of 2011, 6 ft wide, 18 in. tall girders with a 7 in. cast-in-place deck were prescribed. These dimensions were based on the work done at the University of Minnesota (French et al., 2011) with adjustments made to meet the specific design needs of the test bridge in Virginia. Since these parameters had already been selected and designed, it was concluded that using a 4 ft wide test section would give the best behavior and connection alignment (which is discussed later in this chapter) while still meeting the constraints of the overhead cranes.

Each specimen was constructed of two separate precast girders with varying geometries and connection types. These girder pieces were placed adjacent to one another and joined with

the cast-in-place (CIP) deck. Once cured, the entire specimen was moved as one unit into the testing area using a spreader beam and both overhead cranes. In an actual bridge application, each girder has a flange on either side of the web. Since flanges were time consuming and difficult to cast, only one flange was cast per precast girder. The normally CIP region above the flange was treated as part of the girder and cast as such. Since this portion of the test was located far from the connection being tested this adjustment did not affect the results of the test.

Connections

The goal of this research was to provide the best resistance to reflective cracking over the joint of the adjacent bridge girders. Ideally, from a research perspective, the best way to identify the components that promote the best performance would be to test each deviation from the existing system as the only variable and compare the results of each change to the control. Lab space and time restrictions, however, limited the experimentation to a total of four tests. Since there were several variables of interest, it was decided to investigate combinations of different variables in each of three tests. Those results were compared to the control to identify which properties provided the best performance.

The control for these tests was the inverted-T design developed based on the research and implementation done at the University of Minnesota as shown in Figure 9. Further details of the full test specimen are illustrated in Figure 10 through Figure 12.

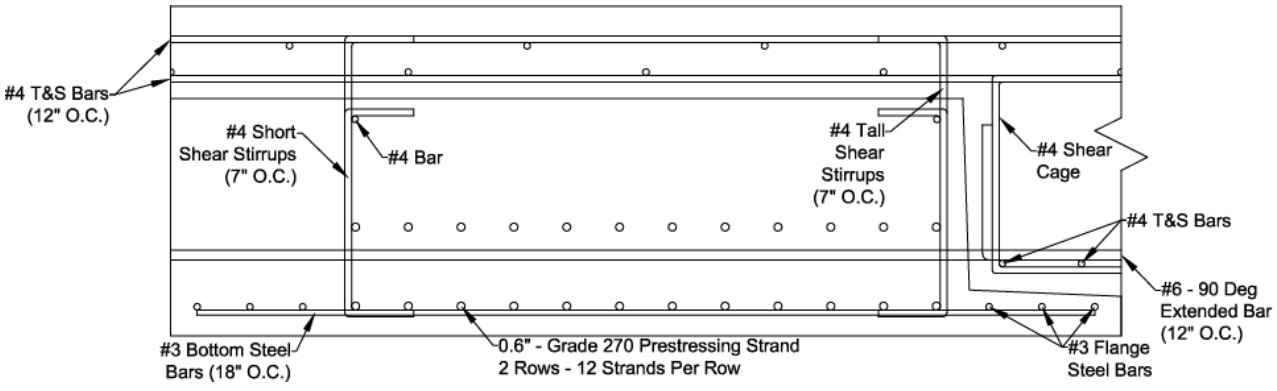

Figure 9: Extended Bar Control Test Section

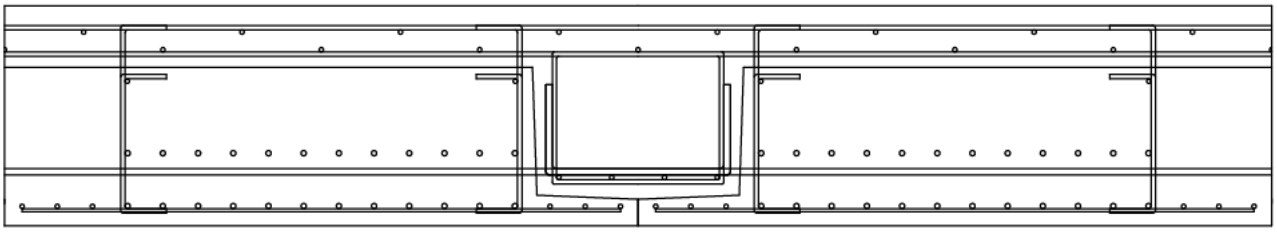

Figure 10: Profile View of Extended Bar Test Specimen

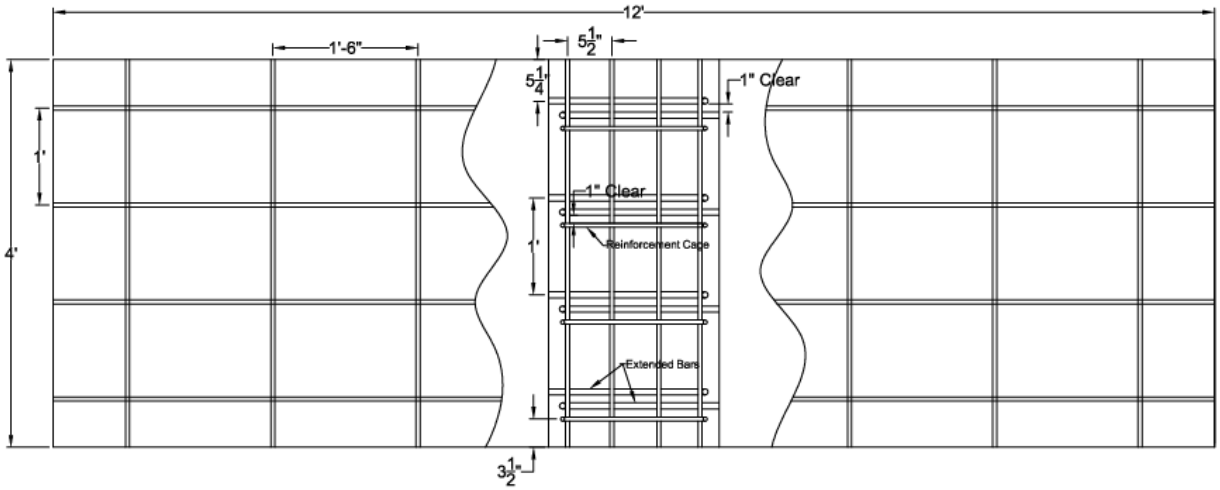

Figure 11: Plan View of Extended Bar Test Specimen

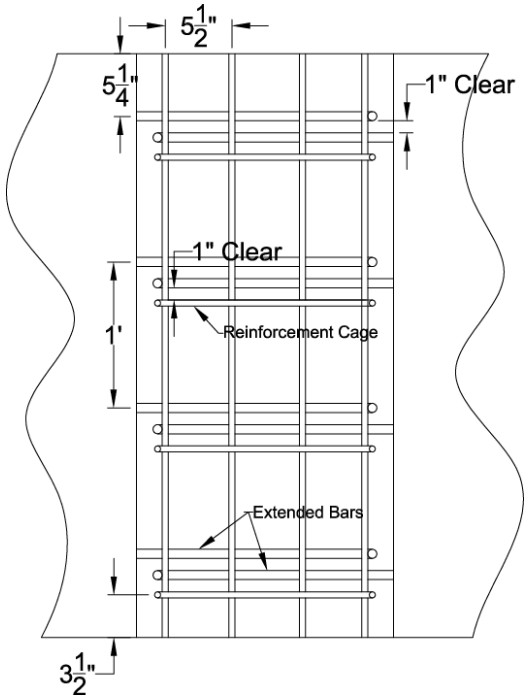

Figure 12: Zoomed in Detail of Extended Bars

Figure 10 and Figure 11 show the complete specimen that was tested in the laboratory from an elevation and plan perspective. In Figure 11 the top mats of reinforcement have been cut away to expose the steel layout in the region over the longitudinal joint. It is this layout that exemplifies the benefit of the four foot wide specimen. The 4 ft width allowed the inclusion of four reinforcement connections from each girder (eight total) which allowed the specimen to replicate the system behavior that would be seen in the field.

The extended bars of the existing control specimens are a fabrication, transportation, and placement issue. From the standpoint of the prestressed girder fabricator, the extended bars require special formwork that allows the bars to protrude from the geometry of the girder. This special requirement means that in order for a precaster to be selected for a project they must be willing to accommodate this need. In meetings held in the fall of 2011, several precasters expressed this as an issue they would prefer to not have to deal with. Eliminating the extended bars was seen as a desirable change to the system as it would eliminate this issue and curtail any potential cost increases as a result of special fabrication requirements.

The protrusion of the bars from the girder side also serves as an issue during transportation and placement in the field. The extended bars add about one foot of width to either side of the girder. For the design profile used in this test that is a 33% increase in width. The extended bars are also vulnerable to damage during transportation to the construction site. Figure 13 shows some of the difficulty in aligning the girders with the extended bars.

Figure 13: Workers Installing Inverted-T with Extended Bars Into Position (Gonzalez)

As an alternative to the extended bar connection, a welded connection between the precast girders was investigated, as can be seen in Figure 14. The original design consisted of small metal plates embedded in the top of each precast girder and welded at intervals along the length of the span. These plates were welded to rebar embedded into the precast girders to carry the tension force across the weld.

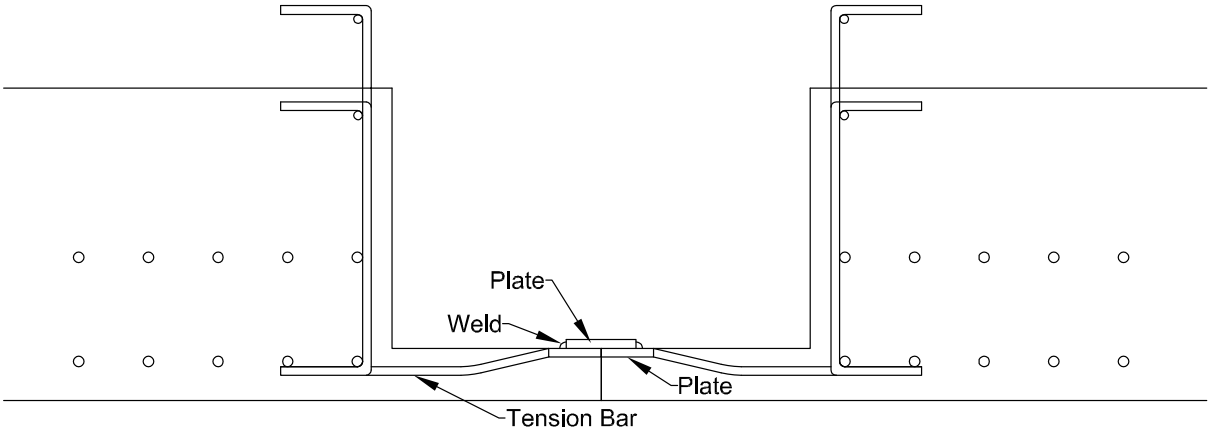

Figure 14: Original Welded Plate Design

The welded plate connection produced both desirable and undesirable changes to the extended bar system. On the positive side, the welded connection eliminated the need for

complicated formwork during fabrication and eliminated issues with damaged connection bars. Since the connection was located at the top of the precast flange, the distance between the tension steel and compression resultant increased, which provided more moment resistance. The geometry of the system moved the tension steel from 6 in. above the bottom of the precast element to about 3.5 in. above. The absence of the extended bars also creates a safer work environment for contractors and their crews. On the negative side, the connection required field welding of the connection plate. This added time to a process which was desired to be rapid construction. Also, the design left little tolerance for differential camber of the precast girders. The plates embedded into the top faces of the flanges should be aligned at approximately the same height in order to form a solid welded connection. Due to these drawbacks, refinements to the welded plate connection were investigated.

A solution was found by means of another precast concrete usage. JVI manufactures a weldable connection called the Vector Connector whose primary use is in double-T girder flanges in parking garages as shown in Figure 15. This concept was considered for use in the bottom flange connection of the inverted-T. The benefit of the Vector Connector connection is that the tapered face of each end of the connection allows for a tolerance in installation. The setup requires a piece of weldable rebar to be dropped between the two adjoining faces and welded in to place. The tension force is then carried into the legs of the Vector Connector which transfers the tension force into the precast double-T.

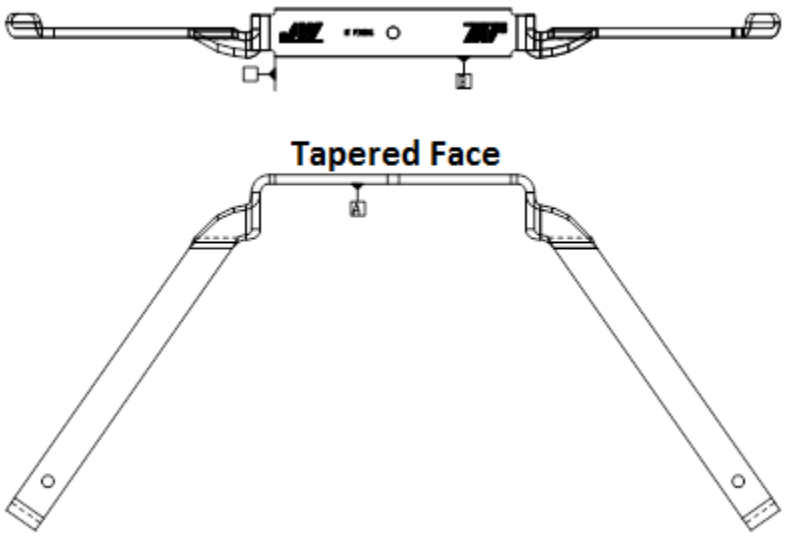

Figure 15: Mini V-Square Vector Connector (courtesy of JVI)

The concept of the Vector Connector provided a solution to the tolerance issue, but created a few others. For one, the standard Vector Connector is designed for use in a minimum of 4 in. thick precast flanges. The desired flange thickness of the inverted-T test specimens is 3 in. JVI also offered a Mini Vector Connector applicable to flange thicknesses as small as 2 in., but these were not able to carry the calculated tensile forces within a reasonable spacing. Given the limitations of the off-the-shelf product, it was decided to take the primary concept of the Vector Connector and modify it for the forces and dimensions of the inverted-T.

A specially fabricated plate that transfers the tension force into the concrete (as shown in Figure 16 and Figure 17) was used instead of the JVI connector. The tension force is transferred across the precast element with a No. 6 rebar welded to the connection plates on each flange tip. This provides a connection solution that can be simply produced at the precasting facility.

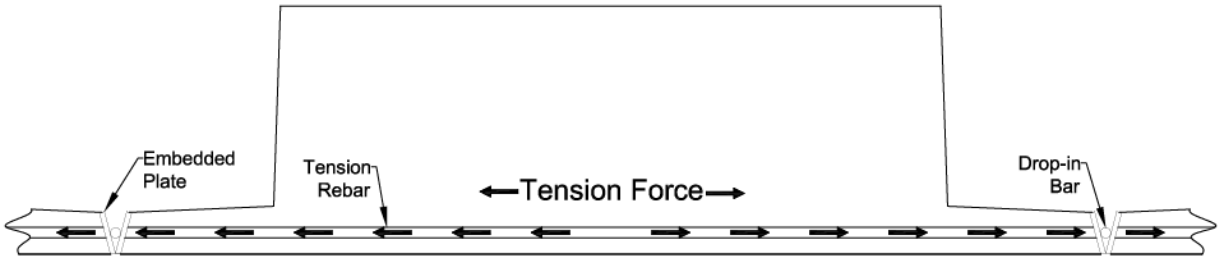

Figure 16: Tension Rebar between Embedded Plates

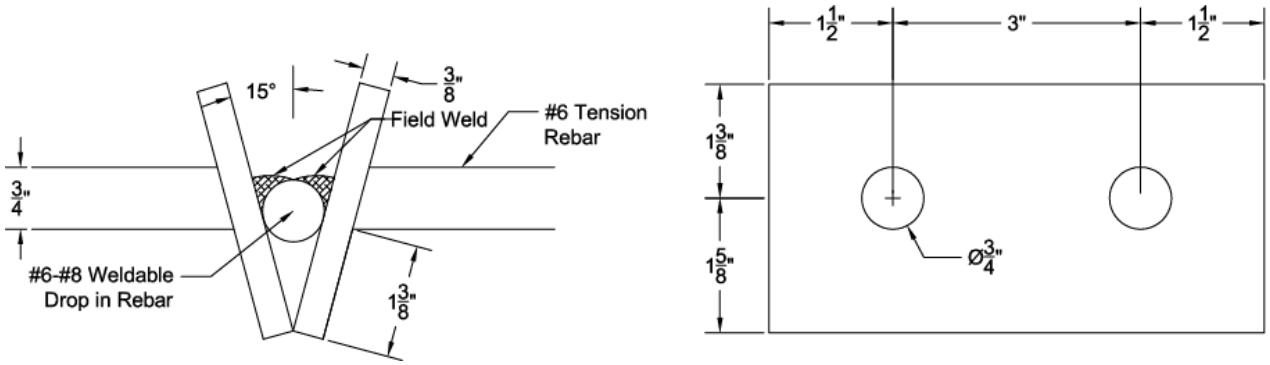

Figure 17: Homemade Embedded Plate Connection

As Figure 17 shows, the embedded plate connection is comprised of a plate located at the end of both adjoining girders that can be joined by a welded drop-in rebar. The plate is attached to the transverse tension bar with a full-penetration weld. One side of each connection is placed into the girder formwork and then cast into the precast section. After the girders were cast and

sufficiently aged they were butted up against one other. Once together, a No. 6 to No. 8 rebar (depending on the size of the gap) was dropped between the plates and the remaining gap was filled with weld. The connection was designed so that if the girders are properly aligned the tension steel will be in plane with the location of the weld. If the girders do not align as shown in Figure 18 the connection will still work. The difference is that modifications need to be made to the size of the drop-in bar and that the tension force will create some moment at the weld, which has been accounted for in the design.

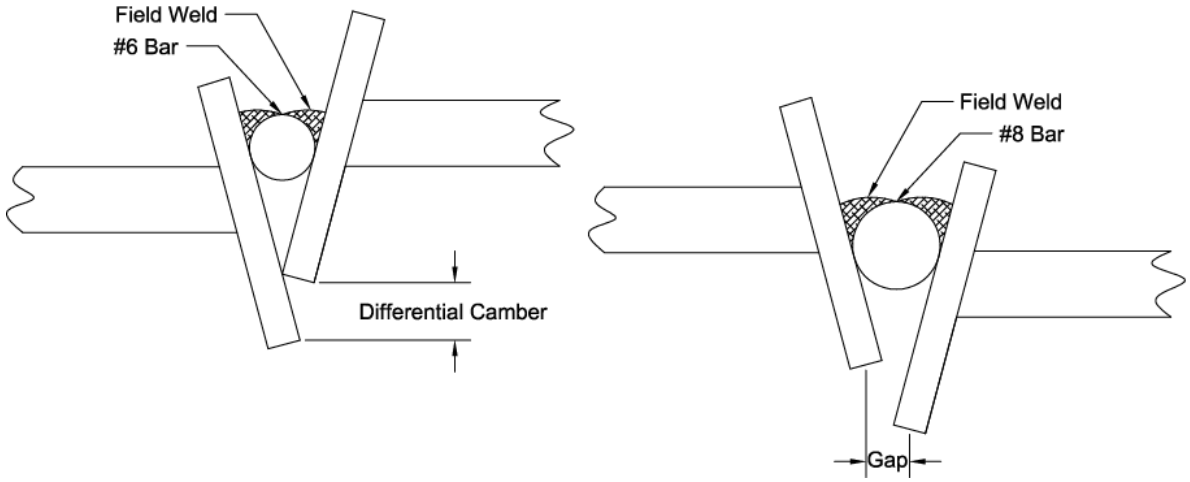

Figure 18: Corrective Alignment for Embedded Plate Connection

In order to capture the performance of the embedded plate connection the specimen shown in Figure 19 was chosen for testing. This specimen is analogous to the extended bar connection with a few exceptions. The obvious difference between the two test specimens is the embedded plate takes the place of the extended bars. Also, since the bars designed to carry the tensile force from the embedded plate connection ran across the bottom of the section the No. 3 bars at 18 in. spacing were replaced by the two No. 6 bars per embedded plate connection. The embedded plate connections were sized to be placed every 2 ft. In addition, the shear cage was eliminated from the existing extended bar connection detail. The inclusion of the cage would add to the tension steel of the specimen to some degree. By eliminating this cage, behavior of just the welded connection between the precast girders would be made more evident. Beyond those changes, all geometry, prestressing, and mild steel configurations remained the same to provide a direct comparison between the two connection profiles. Figure 20 and Figure 21 show the layout of the full test specimen.

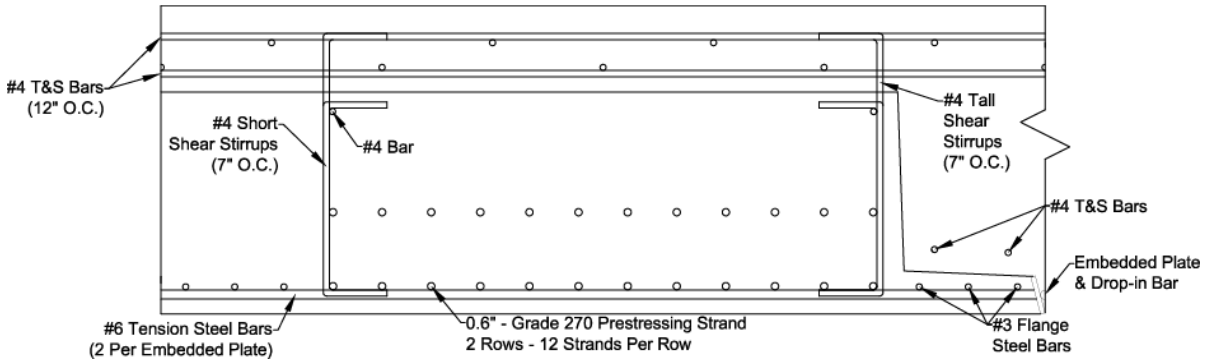

Figure 19: Embedded Plate Inverted-T Shaped Test Section

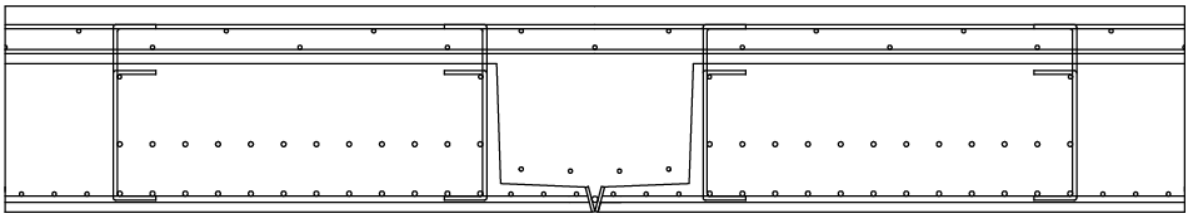

Figure 20: Profile View of Embedded Plate Test Specimen

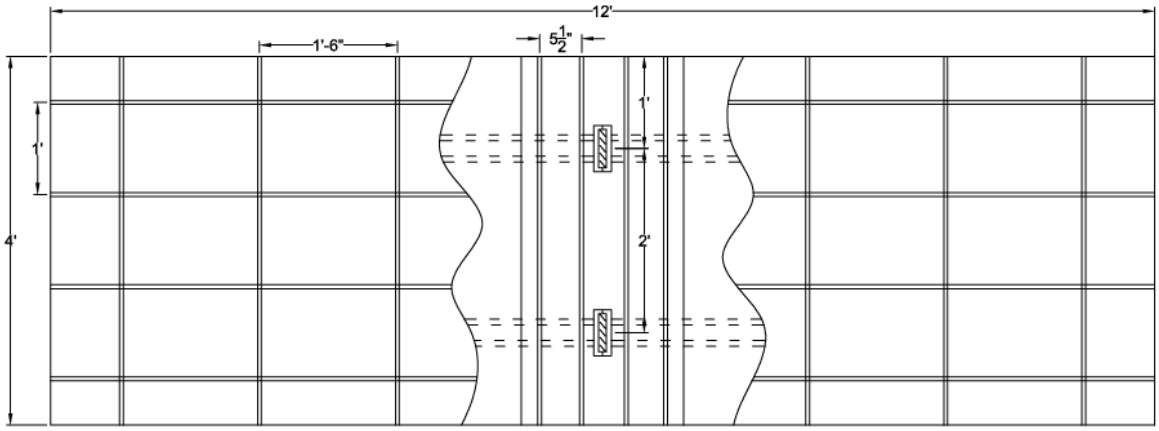

Figure 21: Plan View Embedded Plate Test Specimen

Geometry

The inverted-T system gets its name from the fact that the girders resemble an upside-down "T". This geometry has both desirable and undesirable qualities. One benefit of the inverted-T shape is that the thick middle portion provides a place for multiple rows of prestressing in the longitudinal direction. The thick web also contributes to the longitudinal

strength because it is designed with a higher strength concrete than the CIP deck. The flanges on either side of the web allow a transverse connection to be made without significant loss of section over the joint. Since the flange tips are not bonded together the only effective concrete at the joint is that which is included in the CIP deck. Reducing the thickness of the flange increases the depth of the deck over the joint and increases the effective section at that location. Some negative properties of the inverted-T shape arise from the 90 degree angles at the flanges and outer edges of the middle portions. From a precasters perspective these 90 degree angles create issues for removal of formwork after casting. This, however, can be resolved by adding a slight taper to both the top of the flange and the vertical face of the girders. Even with that adjustment to ease fabrication, the angles of interest are still close to 90 degrees, which makes the areas prone to stress concentrations.

In order to alleviate stress concentrations caused by the sharp angles of the inverted-T system, it was decided to investigate tapered sections as shown in Figure 22. By tapering the vertical face of the girder, the stress concentrations created at the corner where the girder flange and web meet and at the top corner of the girder are reduced. This also lowers the elevation of the bottom temperature and shrinkage mat of reinforcement. In the Mn/DOT profile both mats of temperature and shrinkage reinforcement were placed at a constant elevation near the top of the composite section. With the tapered section the bottom layer of temperature and shrinkage reinforcement can easily be lowered to just above the elevation of the flange. This allows the transverse temperature and shrinkage steel in the bottom layer to contribute to the transverse moment capacity of the section over the joint.

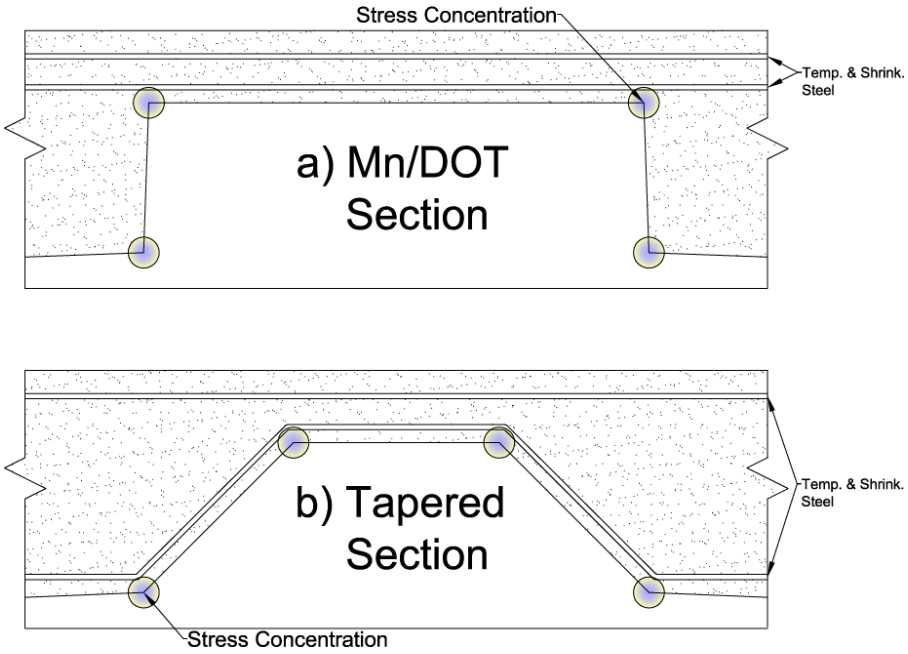

Figure 22: a) Inverted-T vs. b) Tapered Profiles

In addition to relieving stress concentrations, tapering the vertical face of the girders creates a better bond between the precast and CIP sections. For two vertical faces cast against one another there is very little interlock to carry the transverse tension across the interface. However, by shifting the angle to 45 degrees a significant amount of the transverse tension can be resisted across the interface. Since the force at this interface is tension this friction resists interface debonding. This produces better composite action and reduced cracking at that interface as shown in Figure 23.

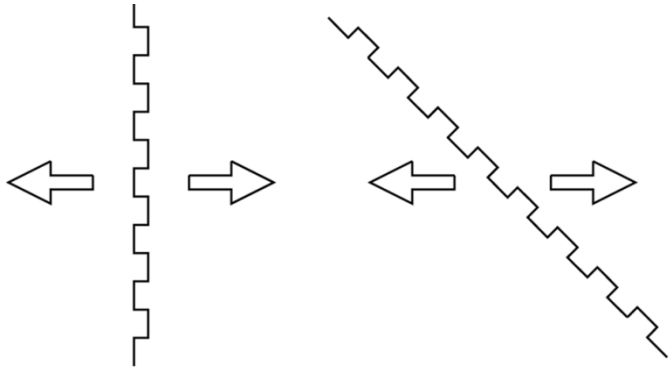

Figure 23: Interface Interlock

As Figure 22 shows the flange dimensions were kept the same for the two geometries. Cutting the flange width in half to limit the amount of precast girder removed by tapering the vertical face was considered. This idea was discarded, however, in favor of keeping the flange width the same in order to keep a sufficient amount of CIP concrete over the joint. This does, however, reduce the total area of the precast girder and thus some of the stronger concrete of the composite section. The 11 ½ in. dimension for the flange was chosen in lieu of the original 12 in. flange in order to allow a slight taper to the vertical interface on the inverted-T profile. This taper was introduced to ease the form removal process. Though no longer necessary for the 45 degree tapered profile, the flange dimension was kept at 11 ½ in. to provide consistency between tests.

In order to make a comparison between the two geometries it was advantageous to test two specimens with the only difference being their geometries. This decision brought about the inclusion of the specimen in Figure 24. This profile is a replica of the inverted-T shape with embedded plate connection only now with the tapered section profile and necessary consequent adjustments. These adjustments include relocating the shear stirrups closer to the center where the top face of the precast girder is level and adjusting the spacing of the prestressing strand in the second layer to keep all of the strands within the girder bounds. This specimen also takes advantage of the dropped bottom layer of temperature and shrinkage reinforcement.

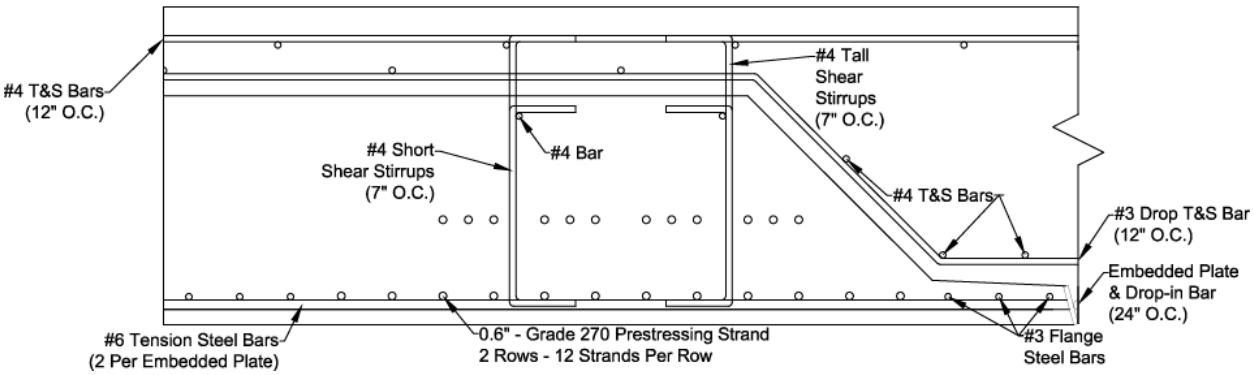

Figure 24: Embedded Plate Tapered Shape Test Section

As a fourth test profile, a tapered section with no physical transverse connection between the precast girders was tested. This section can be seen in Figure 25. For simplicity, this specimen will be referred to as the "no connection" test throughout this thesis. This specimen was tested to determine if the complexity of providing the connection reinforcement across the transverse joints was necessary when using a tapered profile. Eliminating the connection saves a

significant amount of time during both fabrication and in the field. The rationalization behind the "no connection" test setup was to increase the size of the drop bar from the temperature and shrinkage mat to carry the tensile force along the joint. As the drop bar begins to bend up along the tapered face of the girder, the force can then be transferred to the transverse flange steel and carried across the bottom of each precast girder. Issues did arise due to some of the assumptions made about this force transfer. These issues can be found in the Discussion chapter of this thesis.

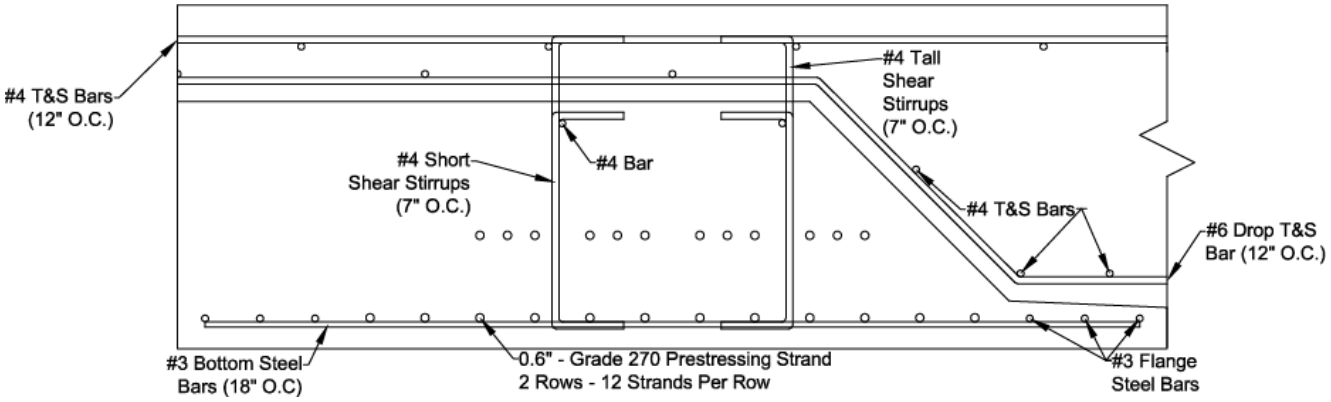

Figure 25: No Connection Tapered Test Section

The four profiles selected for this research were designed in order to improve the Mn/DOT system. Each of the three non-control specimens presented either a new variable or a system of changes that serve as a potential improvement to the Mn/DOT system. These variables are presented in Table 1. Given considerations like time and ease of construction, along with cost, it was not appropriate to compare the trials by a direct strength and cracking behavior basis only. Instead these tests and corresponding results were configured to find a system or group of unique variables that created the most favorable product for application in the inverted-T bridge system. Full details of the steel layout for each specimen can be found in Appendix A.

Table 1: Test Matrix

Test	Geometry	Connection	Shear Cage	Drop-Bar
1	Inverted-T	Extended Bar	Yes	No
2	Inverted-T	Embedded Plate	No	No
3	Tapered	Embedded Plate	No	Yes
4	Tapered	No Connection	No	Yes

EXPERIMENTAL METHODS

This chapter discusses the test setup and how the tests were conducted. An introduction to the load regimen is included along with an explanation of the process. The instrumentation and layout used for the tests is detailed and justified as such.

Testing Setup

The purpose of the physical testing was to replicate the behavior of the inverted-T to inverted-T joing in a scaled, laboratory setting. Studies were performed to determine the appropriate specimen layout and loading configuration to most suitably replicate actual bridge conditions. The sub-assemblage testing was intended as a precursor to full-scale testing of the inverted-T system. The ultimate goal of the sub-assemblage and full-scale testing is to provide the Virginia Department of Transportation recommended fabrication and design details for construction of the U.S. 360 Bridge of over the Chickahominy River.

The first step in designing the test setup was to model the behavior of the bridge. A finite element model was created by Fatmir Menkulasi (Ph. D candidate, Virginia Tech). With this model, Menkulasi was able to apply a series of load combinations and identify the worst-case service loading configuration on the bridge. From that configuration, he calculated the worst-case service stresses in the bridge. The sub-assemblage test was designed to re-produce this state of stress at the inverted-T to inverted-T connection. Further discussion of this modeling is included in the Analytical Methods chapter of this thesis.

The finite element model showed that in all loading cases the transverse shear stress was very small. The region of interest for these transverse sub-assemblage connection tests was the area over the precast girder joints and at the vertical or tapered interfaces between the girder and CIP concrete. To create a region of constant moment and negligible shear in the region of interest the specimens were loaded at quarter points. Figure 26 shows the shear and moment created in the test specimen from the four point loading. Loading at points six feet apart and over a 9 in. x 18 in. contact area simulated the AASHTO truck wheel patch load. According to AASHTO (AASHTO, 2010) the design tandem wheel loads are 6 ft on center with a patch size

of 10 in. x 20 in. The target bending stress across the longitudinal joint was calculated in the finite element model as 0.18 ksi. The test setup minimized the effect of shear on the joint area.

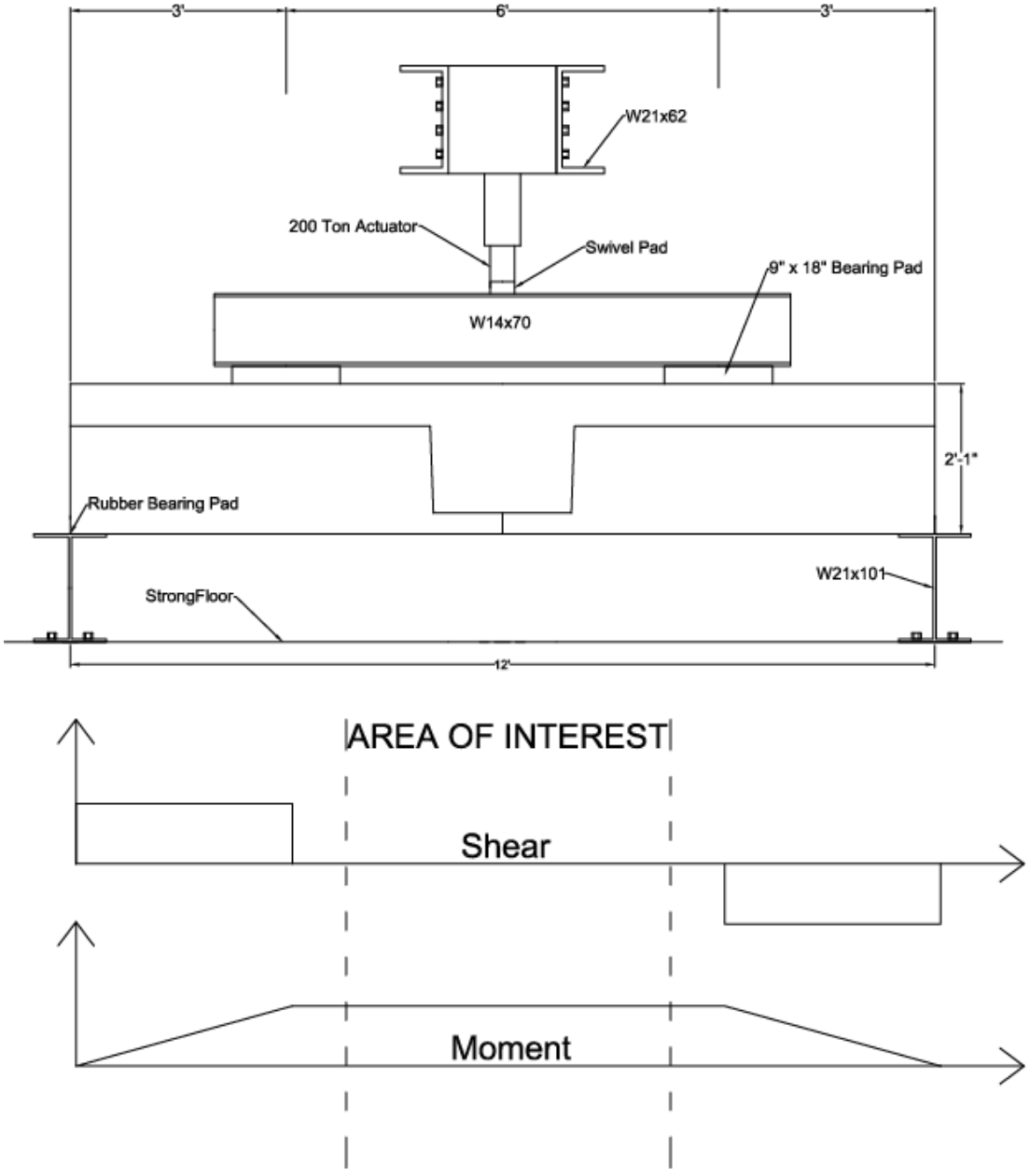

Figure 26: Test Setup with Shear and Moment Diagrams

A load frame setup was developed to apply the quarter point loads. The completed setup can be seen in Figure 26. The frame was constructed of two W21x62 columns mounted to the strongfloor with four 1 in. diameter A325 bolts per column. Spanning the columns were two W21x62 crossbeams held in place with six 3/4 in. diameter A325 bolts per connection. A RR-

20013 Enerpac 200 ton actuator was used to apply the vertical load to the test specimens. This was attached to the crossbeams by way of a custom steel mount that was supported by eight 3/4 in. diameter A325 bolts per side. The actuator was attached to the mount with four 3/4 in. diameter A325 bolts. From the actuator, the load was transferred to a stiffened W14x70 spreader beam. The spreader beam transferred the load to two 9 in. x 18 in., 2 in. thick rubber pads. The specimen sat upon two rubber bearing pads each placed atop stiffened W21x101 support beams. These beams were connected to the strong floor with eight 1 in. diameter A325 bolts. This setup provided a simply supported condition for the specimen.

The calculated frame capacity placed an upper bound on the load that could safely be applied to the specimens. Though the actuator was capable of applying a load of 400 kips, the capacity of the frame limited the applied load to 300 kips. The controlling component of the setup was shear in the bolts connecting the actuator to the crossbeams. The limit of 300 kips was significantly more than the calculated 25 kip applied load required to induce service load stresses at the connection. This was deemed as an adequate upper limit for testing the system for realistic loads. A photo of the setup with specimen in-place can be seen in Figure 27.

Figure 27: Test Frame Setup (Photo)

Testing Regimen

Beyond just testing the specimens at the calculated service stress, there was also interest to know the behavior of the specimens above service strength up to flexural strength. A testing regimen was created that captured that behavior and also tracked crack growth induced from cyclic loading. Another finite element model was created by Menkulasi to model the test setup. From that model, and considering self-weight effects, it was determined that the applied load necessary to cause a service level stress of 0.18 ksi at the longitudinal joint was 25 kips (12.5 kips at each loading point). In order to track the behavior of the specimens the load increment was set at 5 kips. Beyond 30 kips, the load was increased to 10 kips per load step. This process was continued until the first crack was identified. At that point the cracks were traced and crack height and width were documented. After recording the crack data, the load was released and cycled to the cracking load five times. Crack propagation and opening was then checked again.. The cycling process was repeated for three more cycles and the cracks were checked again. After completing those eight cycles the specimen was loaded and unloaded one cycle at a time until three subsequent loads showed no crack propagation or opening. From there, the load was again increased by 10 kip increments as crack initiation, propagation, and width were documented at each load step. This process was continued until either the capacity of the load frame was reached or the specimens could not carry increased load.

There was interest in fatigue testing, particularly for the welded connections. A limited availability of actuators in the laboratory capable of performing such cyclic loading, however, eliminated such testing as an option. Crack propagation was investigated under cyclic loads via the manual cycling process stated above. The behavior of the systems under a lifecycle of traffic loads, however, still remained a question.

Instrumentation

The ultimate goal of the tests was to identify which connections, geometries, systems, etc. best limited reflective cracking at the inverted-T to inverted-T joint. This was achieved by the visual documentation of crack formation and propagation at given loads and the use of instrumentation to measure crack openings, reinforcement strain, vertical deflection, and applied load.

Cracks can be visually observed on the order of around 0.002 in. wide. For the most part, a crack of this size is the first of which worth noting in terms of reflective cracking. However, with the use of instrumentation, smaller cracks can be observed. In addition to enhancing what the eye can see instrumentation embedded within the specimens can measure reinforcement strain at or near a crack.

Instrumentation was embedded into the girders before they were cast. The strain in the connection steel was of interest for these tests. By tracing the rate of change in the steel strain, the load at first crack could be identified. Beyond that, those strain values were used to identify yielding and fracture of the bars. All of the gages used on the rebar were CEA-06-125UN-350 from Micro Measurements. These gages were protected using the M Coat F Protective Kit also produced by Micro Measurements. The gages came with three preattached wires and had a gage factor of 2.11. This process is further discussed in the Construction and Processes chapter of this paper. Figure 28 and Figure 29 show the gage surface preparation and protection.

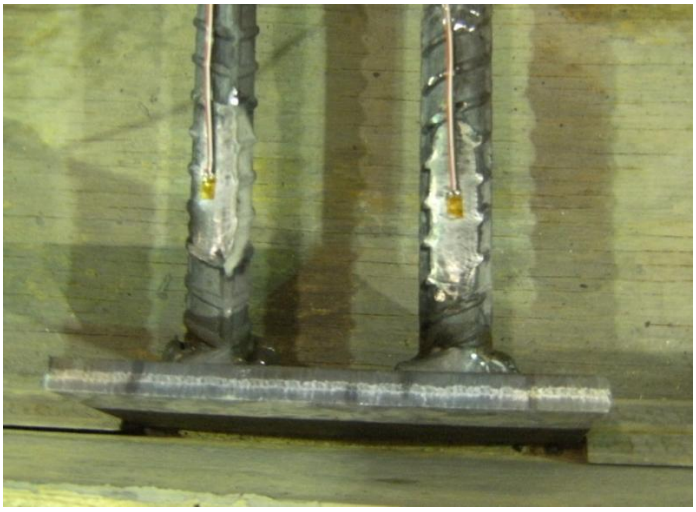

Figure 28: Strain Gages Attached to Prepared Surface of Embedded Plate Connection

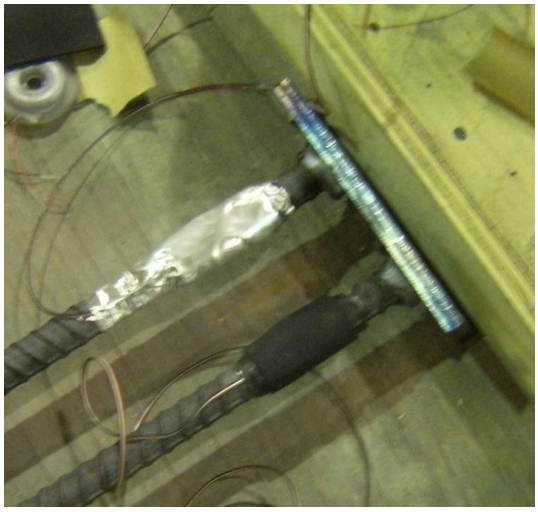

Figure 29: Protective Coating Applied to Strain Gages on Embedded Plate Connection

In addition to the strain gages applied to the rebar, embedment strain gages were also placed in a pattern throughout the CIP portion over the longitudinal joint. The gages used were 120 mm (4.72 in.) PML-120-2L concrete embedment strain gages manufactured by Tokyo Sokki Kenkyujo Co., Ltd.. The 120Ω gages had a gage factor of 2.12 and came with two preattached lead wires. The gages were placed in the CIP region of the specimens just before the closure pour was placed. In order to best capture the strain profile and propagation of cracking in the region over the longitudinal joint, the gages were placed in a uniform pattern for each of the test

specimens. Figure 30 through Figure 37 show the layout of the embedment gages. One vibrating wire gage was also inserted into each specimen at the time of deck placement to monitor shrinkage strains in the concrete. The location of this gage is shown in Figure 31. The installation of all of the strain gages is further discussed in the Construction and Processes chapter of this thesis.

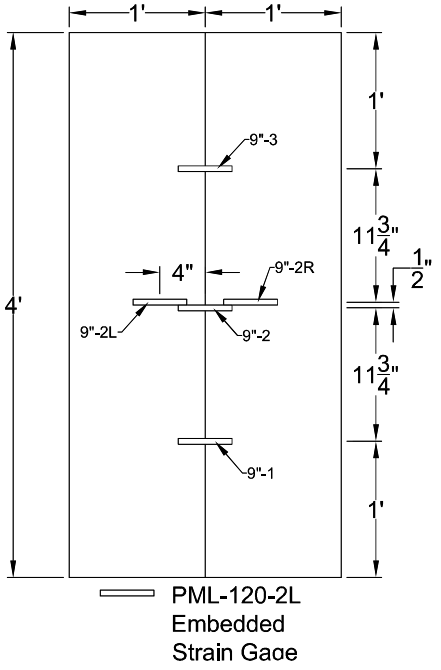

Figure 30: Plan View of Strain Gages 9 in. Above Bottom of Precast (All Specimens)

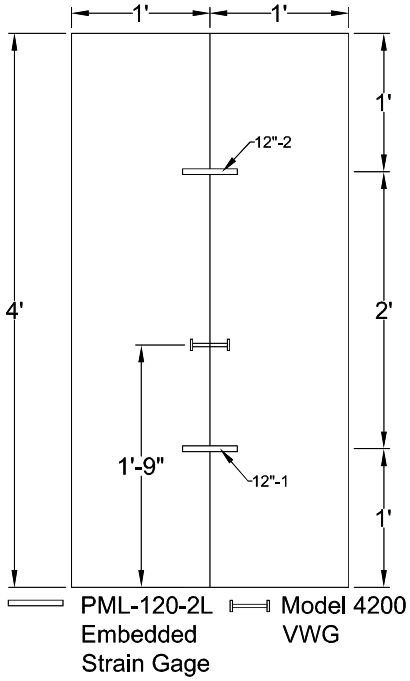

Figure 31: Plan View of Strain Gages 12 in. Above Bottom of Precast (All Specimens)

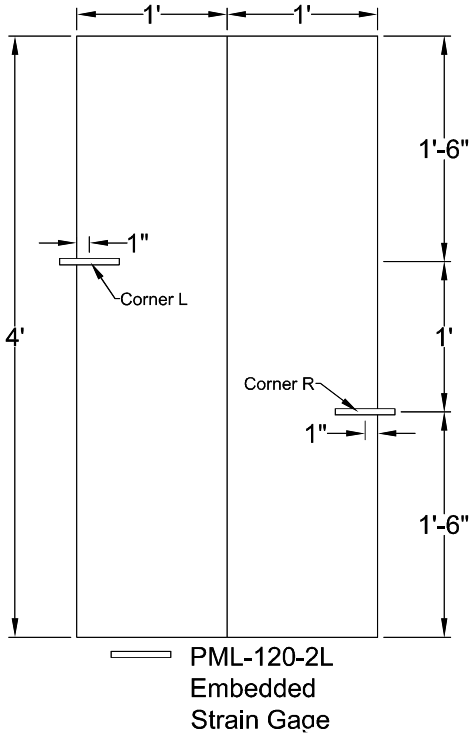

Figure 32: Plan View of Strain Gages 19 in. Above Bottom of Precast (All Specimens)

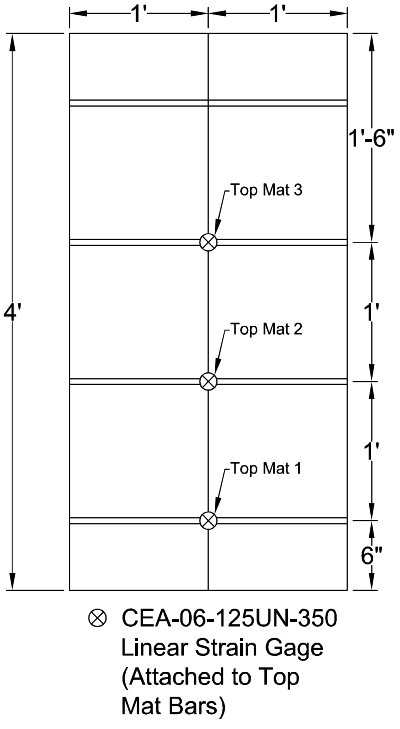

Figure 33: Plan View of Strain Gages 22.5 in. Above Bottom of Precast (All Specimens)

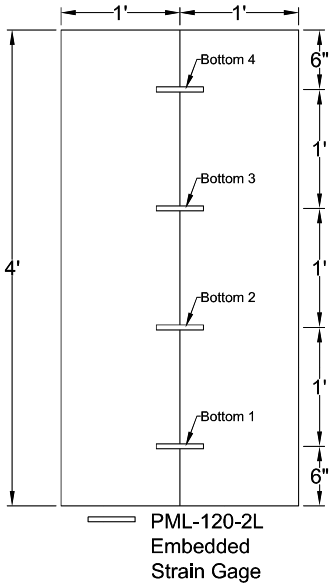

Figure 34: Plan View of Strain Gages 5 in. Above Bottom of Precast (Embedded Plate Inverted-T Only)

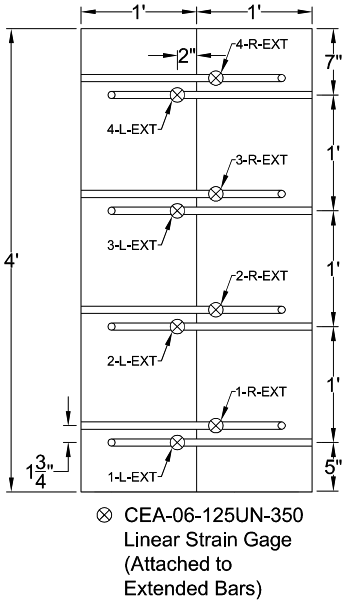

Figure 35: Plan View of Strain Gages 6 in. Above Bottom of Precast (Extended Bar Only)

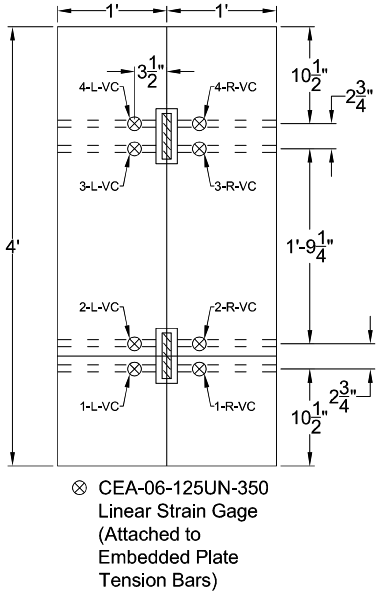

Figure 36: Plan View of Strain Gages 1.5 in. Above Bottom of Precast (Tapered and Inverted-T Embedded Plate)

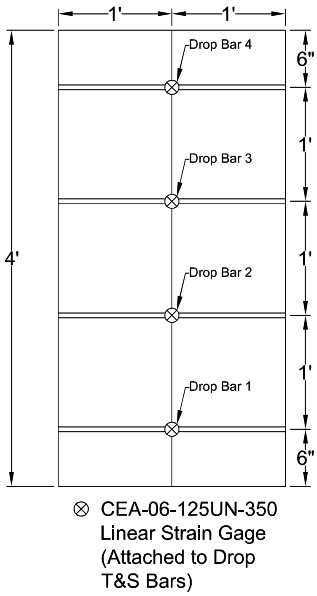

Figure 37: Plan View of Strain Gages 5 in. Above Bottom of Precast (Tapered Embedded Plate and No Connection)

In addition to the instrumentation distributed within the specimens, a series of wirepots and Linear Variable Differential Transformers (LVDTs) were placed on the exterior of each specimen. A series of wirepots were attached to the bottom of each test profile to capture the

vertical deflection of the specimens. These wirepots enabled the tracking of load versus deflection behavior during testing in order to identify the ductility of each profile. The wirepots were oriented in a pattern along the transverse direction of the test to provide a deflected shape contour. Figure 38 and Figure 39 show the orientation of the wirepots. Two wirepots were placed on either side of the joint to monitor any differential displacement where the two precast members were joined. This was intended to help to determine if any debonding was taking place between the precast girders and the CIP concrete along the top of the flange.

Figure 38: Wirepots (photo)

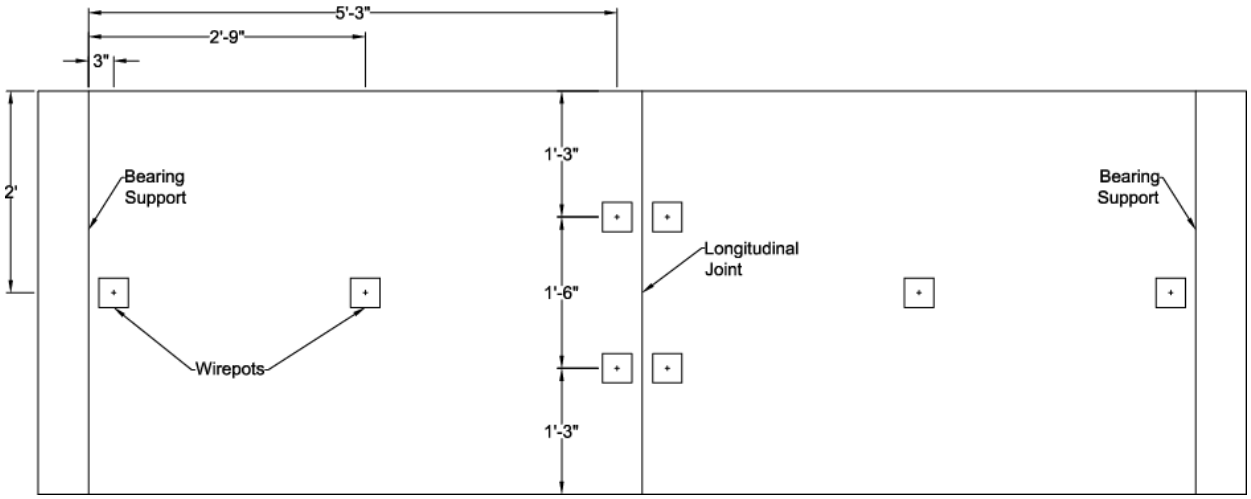

Figure 39: Plan View of Wirepot Layout

To monitor the strain profile and crack opening on the outer face of the specimens a series of LVDTs were mounted to each specimen. The four LVDTs were placed at different elevations along one external face of each specimen. Figure 40 and Figure 41 show the

orientation of the instrumentation. LVDTs 6, 8, and 9 spanned a distance of 12 in. and LVDT 7 spanned 36 in. The bottom LVDT was oriented to record the opening between the two flange tips. The LVDT above it was positioned to monitor the strain and eventual crack opening in the CIP region directly above the longitudinal joint. The third LVDT stretched three times as far as the other three and was added to capture any cracks in the vertical or tapered interface between the precast girders and the CIP deck. The fourth and final LVDT was set to record the same as the second LVDT except at a higher elevation in the CIP deck.

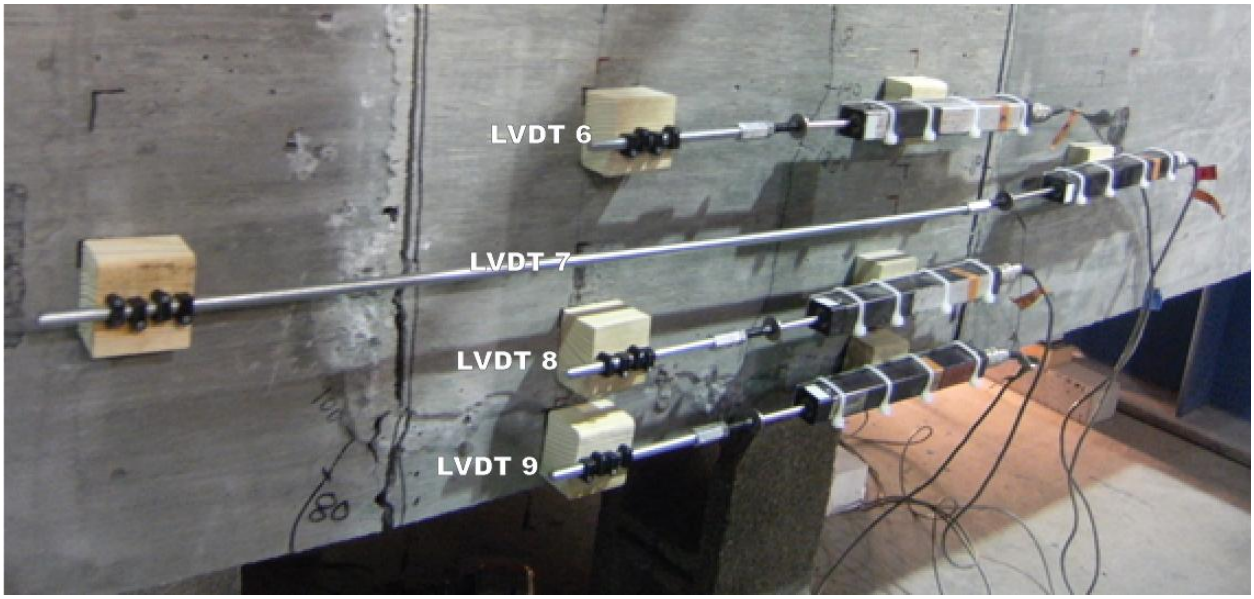

Figure 40: Photo of LVDT Layout

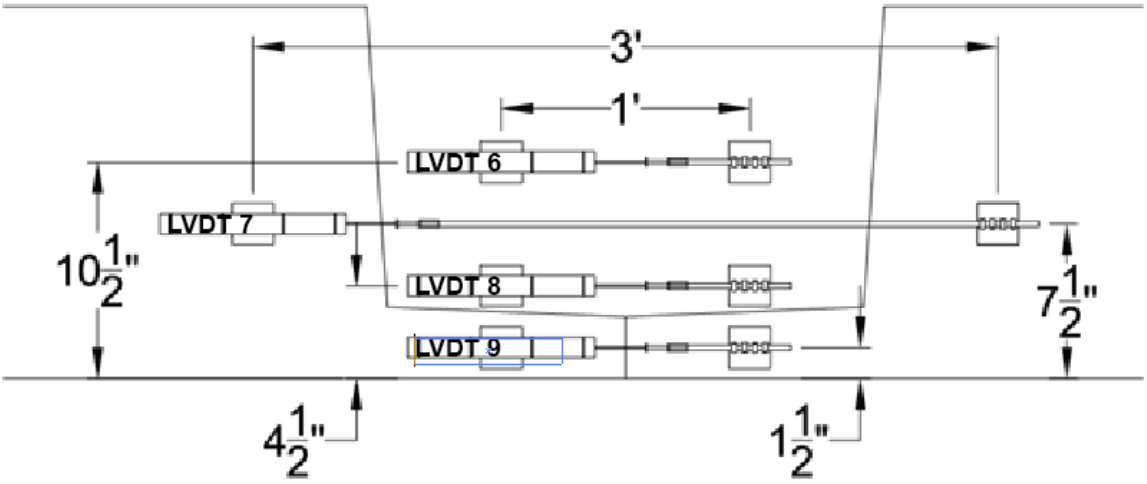

Figure 41: Layout of LVDTs

SPECIMEN CONSTRUCTION AND INSTRUMENTATION

This chapter presents the specimen construction and instrumentation methods. The specimens were fabricated in the Thomas M. Murray Structures Laboratory at Virginia Tech. The precast girder sections were formed and cast in-house and all of the material testing for the project was also conducted in-house.

Formwork Construction

In order to cast the girder sections, formwork was constructed. Four girder molds (two for the inverted-T shapes and two for the tapered shapes) were assembled to reduce cost and construction time. Each test specimen required two matching girders (total of eight was required for the four specimens) so that each mold was used twice.

The forms were constructed using plywood formboard. The forms were assembled using threaded deck screws, and reinforced with tensioned pencil rod to reduce bowing due to hydrostatic pressures. A photo of a typical form assembly can be seen in Figure 42. The side and back forms were constructed and erected atop the base. The flange face formwork was left off to allow ease of access for inserting and tying rebar. Once all of the rebar had been tied, the front face was attached and the pencil rods were inserted and tensioned. As Figure 42 shows, the form supports extended above the top of the concrete. This was done so that the form supports could be re-used for the CIP closure pour. This did add some minor inconvenience to the concrete finishing process, however, due to the extended stirrups and lifting hooks there were already major obstructions to that process.

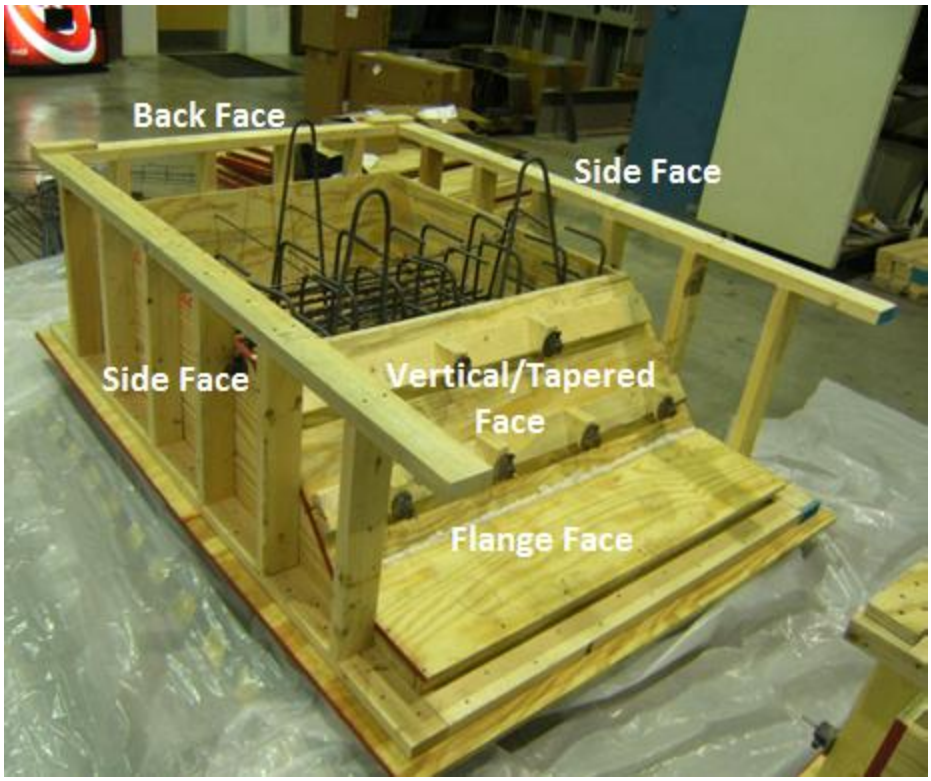

Figure 42: Formwork, Pencil Rod, and Rebar

Steel

The reinforcing steel was Grade 60 A615 steel with the exception of the tension steel for the embedded plate connection. The tension steel for the connection was A706 weldable steel to accommodate the weld to the connection plate. Grade 270, low-relaxation prestressing strand was used to represent the actual prestressing in the bridge, however, was not tensioned. Four foot lengths of Grade 270 0.6 in. diameter prestressing strand were cut and placed in the sections at the actual prestressing strand locations as determined by the preliminary bridge design. Since the sections were only 4 ft wide and the test was in the transverse direction, no significant difference in the behavior of the specimens from the prestressing strand not being tensioned was anticipated.

First Concrete Placement Attempt

The first four girder specimens cast were for the extended bar connection and the no connection tests. The concrete mix used had a 1 in. maximum course aggregate size. The

concrete for this and all other mixes was ordered from Conrock in Blacksburg, Va. In order to support the weight of the wet cast-in-place concrete, the flanges were designed with a row of No. 3 rebar running in both the transverse and longitudinal directions. Very little room was available for the 1 in. maximum course aggregate to pass through to fill the ends of the flanges as shown in Figure 43. A typical poorly consolidated flange can be seen in Figure 44.

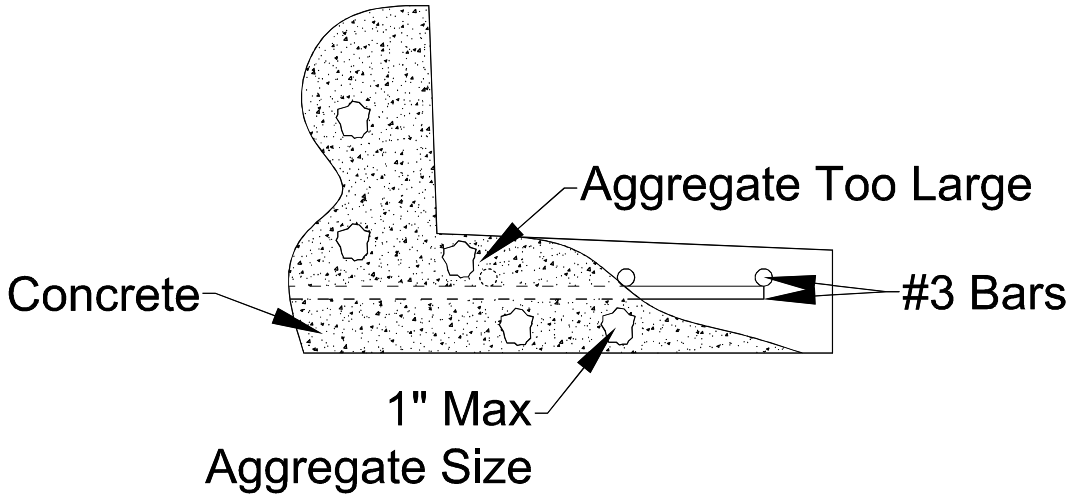

Figure 43: Flange of First Girder Placement Attempt (Drawing)

Figure 44: Flange of First Girder Placement (Photo)

The method to create the roughened surface for the first girder placement did not perform well. For this test a wire mesh was nailed to the inside of the forms. The hope was that when removed, the mesh would leave an imprint in the concrete that would create good bond with the CIP concrete. This, however, was not the case as the mesh pulled away from the forms when they were removed and stayed embedded in the concrete. The lack of roughened surface can be seen in Figure 45.

Figure 45: Poor Roughened Surface and Flanges

Due to the poor quality of the initial specimens, it was decided to test them as a trial and compare the difference between a) a smooth and a roughened surface and b) a complete and a damaged flange. The flange of one of the girders for that specimen was significantly poorer than the others and the surface was almost completely smooth. That being the case, two of the girder pieces were discarded and only a pair of damaged extended bar connection specimen was tested as a trial. Due to the poor quality of this test specimen, it was only instrumented with LVDT's and wirepots.

Girder Concrete Placement

The concrete mix and formwork design were revised to address the issues of the first placement. The second concrete mix was designed with a 1/2 in. max aggregate size and is further detailed in the Mix Design segment of this thesis. The forms were modified to ensure the concrete did completely fill the flange. This was done by leaving off the piece of formwork that covered the top of the flange during the start of the concrete placement. When the concrete reached a height of about 1 ft within the formwork, concrete was added directly into the flange tip and vibrated. The concrete in the flanges was then leveled off and the flange top form was put into place.

The means to provide a roughened surface on the girders was also modified. The mesh concept was discarded and replaced with physically altering the forms themselves. The inside faces of the forms were cut with a dado blade to create grooves. The grooves were cut 1/4 in. deep and 1/2 in. wide as shown in Figure 46 which provided a much better result as can be seen in Figure 47. This process did, however, make the form removal surface more difficult. This was anticipated and the grooved forms were heavily lubricated with both motor oil and WD-40. Even with extensive oiling, the forms were cumbersome to remove and in some cases required the use of an air chisel. This resulted in some damage to the grooves, but still left a roughened surface for the cast-in-place concrete to bond to.

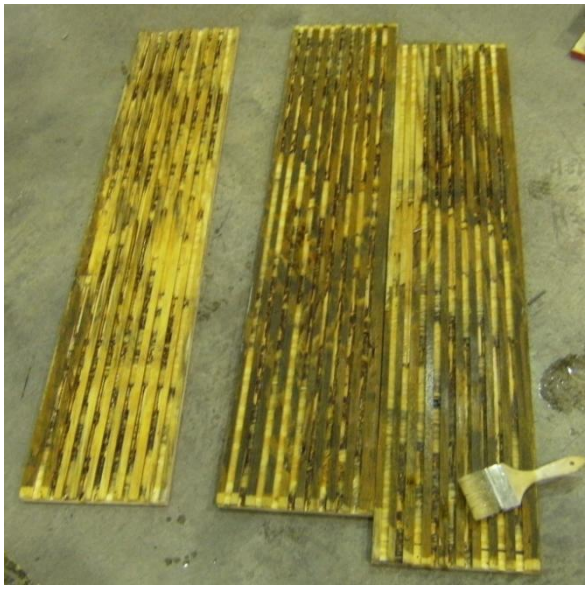

Figure 46: Grooved Formwork

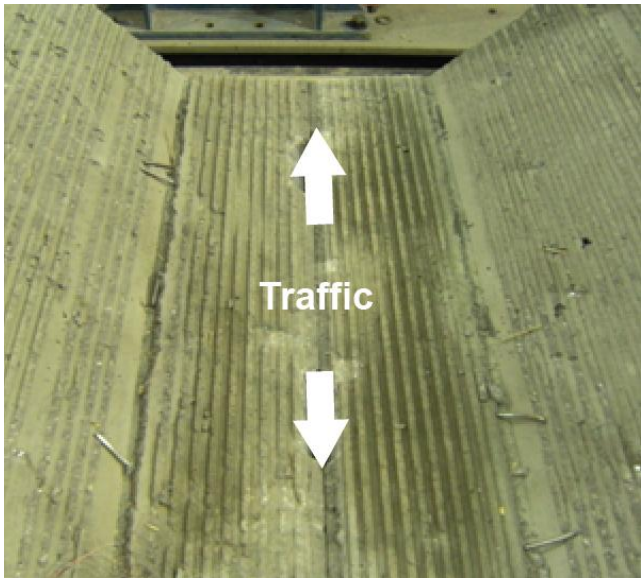

Figure 47: Roughened Surface (Flange and Tapered Face)

The top surface of the girders was given a raked finish shortly after the concrete was placed. Figure 48 shows the resultant roughened surface. The grooves for the flange and vertical/tapered face as well as the top surface were formed to run parallel with the flow of traffic on the bridge. However, for a real-life application it would be more beneficial to run the grooves perpendicular to the flow of traffic to increase the resistance to interface shear in the more pertinent longitudinal direction. This concept is further discussed in the Recommendations chapter of this thesis. The details of the surface finishing are presented in Table 2 and the properties for each girder and hw they were used are shown in Table 3.

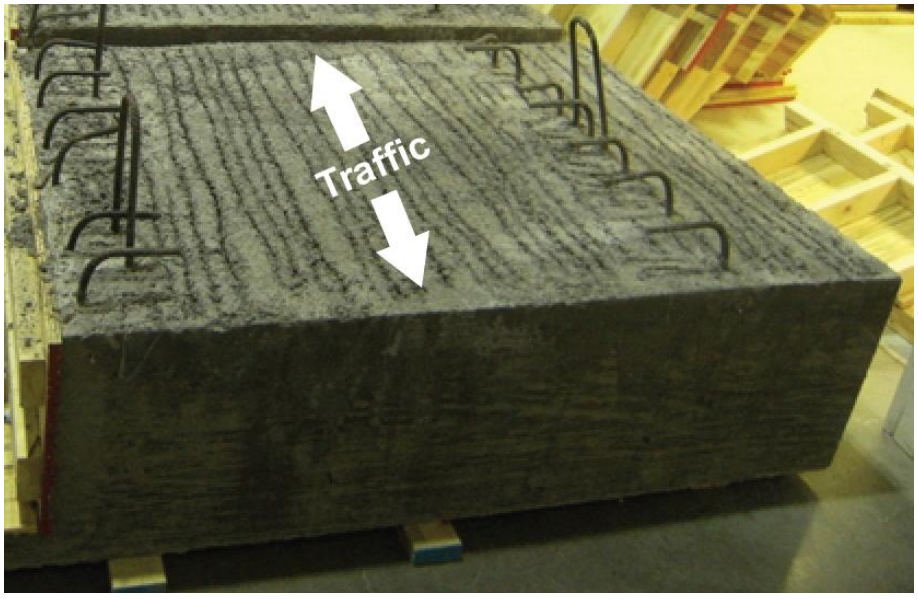

Figure 48: Roughened Surface (Top of Girder)

Table 2: Surface Conditions of Girders

Surface	Method	Direction of Roughening
Top	By Hand	Parallel to Traffic
Back	Smooth Forms	N/A
Side	Smooth Forms	N/A
Vertical/Tapered Face	Grooved Forms	Parallel to Traffic
Top of Flange	Grooved Forms	Parallel to Traffic

Table 3: Girder Uses

Pour	Geometry	Connection	Surface	Use
1	Inverted-T	Extended Bar	Smooth	Trial
1	Tapered	No Connection	Smooth	Discarded
2	Inverted-T	Embedded Plate	Roughened	Full Test
2	Tapered	Embedded Plate	Roughened	Full Test
3	Inverted-T	Extended Bar	Roughened	Full Test
3	Tapered	No Connection	Roughened	Full Test

CIP Concrete Placement

The process for the CIP placement was similar to that for the precast girder section. The forms used for the girders were modified to accommodate the differences in geometry and the steel was tied in the same manner. For each specimen two precast girders were placed flange to flange and then enclosed by the formwork as shown in Figure 49. From there, the steel was tied into place and strain gages were placed according to the layout given in the Experimental Methods chapter of this thesis. The top surface of the specimens was left smooth to provide an adequate surface for applying load.

Figure 49: Formwork for CIP Deck Concrete

Strain Gage Application

All of the strain gages used in this project were placed in a concrete environment and needed to be properly applied and protected to produce meaningful results. Electrical resistance strain gages were attached to reinforcement bars in each of the specimens. Each bar was prepared by grinding off the embossments and sanding the surface smooth. From there, the procedures set forth by the strain gage manufacturer were followed to properly adhere the gages to the steel. Since the gages were to be placed in an adverse environment, they were protected using the M-Coat F kit from Micro Measurements which is made up of soft rubber patches and neoprene pads. All protective coating was performed as prescribed by the manufacturer. The concrete embedment gages came already shielded from the concrete environment and needed no additional protection.

In order to ensure the proper location of the embedment strain gages both before and after concrete placement a secure system of mounts was provided. These mounts were formed by running additional pencil rod in the longitudinal direction and attaching the gages perpendicular to these rods. The vibrating wire gage in each specimen was installed similarly. The wires from each gage were routed along the pencil rod, grouped together, and brought out as one unit.

Timing

The timing of concrete placements and testing was planned in a way to limit the effects of differential creep and shrinkage and to better mimic field conditions. Due to time limitations of the project, providing a 90-day cure for the precast girders was not possible. Each girder was allowed to age for a minimum of 26 days before adding the CIP deck. Each deck was allowed to age a minimum of 23 days as well before testing commenced. Table 5 in the Results chapter documents the age of each girder at deck placement and each deck at time of testing.

Data Acquisition

A high speed data acquisition system was used to collect data from the strain gages, wirepots, LVDT's and load cell. A sampling rate of 1 hertz was used for each sensor. The data acquisition system was also configured so that the recording of additional readings could be

manually activated. The option to manually record was especially useful during the loading and unloading processes while conducting the cyclic tests. All data was reduced and converted into a spreadsheet document and exported to an external system for data reduction and analysis.

A datalogger was used to collect data for the vibrating wire gages. This datalogger collected information for all specimens from placement of deck concrete to the completion of testing. The recording interval ranged from once per minute in the days shortly after concrete placement to once per hour thereafter. Each instrument was calibrated before use in the tests.

Material Testing

When concrete was placed, specimens were cast for material testing. This included 4 in. x 8 in. cylinders for compressive, tensile, and modulus testing, 6 in. x 12 in. cylinders for creep and shrinkage testing, 3 in. x 3 in. x 11 in. prisms for unrestrained shrinkage testing, and 3 in. x 4 in. x 16 in. prisms for freeze-thaw testing. All test specimens were made according to (ASTM C192/C192M-09). The compressive, tensile, and modulus cylinders were tested based on the schedule presented in Table 4. These tests were conducted using the standards defined in (ASTM C39/C39M-09a), (ASTM C496/496M-04), and (ASTM C469-02) respectively. The results of these tests can be found in Appendix B.

Table 4: Material Testing Schedule

Test	Number of Tests at Each Age				
	7 days	14 days	28 days	56 days	90 days
Compressive Strength	3	3	3	3	3
Tensile strength	3	-	3	-	3
Modulus	2	2	2	2	2

The creep and shrinkage behavior of each of the concrete mixes was recorded. Unrestrained shrinkage prisms were cast and cured to the specifications set forth by (ASTM C192/C192M-09). Three prisms were cast for each concrete placement and recordings were taken on a daily basis tapering to a weekly to monthly basis as the shrinkage began to level out. Creep specimens were prepared and tested according to the guidelines set forth in (ASTM C512/C512M-02). Five 6 in. x 12 in. specimens were cast (three were loaded in a creep frame and two were left unloaded to record shrinkage). By recording the shrinkage of the unloaded

cylinders the effect of creep in the cylinders under load could be isolated. Three additional prisms were cast and cured for freeze-thaw testing. These specimens were tested by VCTIR.

Embedded Plate Connection Welds

The connections for the tapered section were welded with No. 6 reinforcement bar. For the two connections in the inverted-T profile, however, the gap was fairly large and required a No. 8 drop-in reinforcement bar. Figure 50 shows the embedded plate connection before and after the weld. The design strength of the connection was not controlled by the drop-in bar or weld size, therefore it was assumed the connections had the same tensile strength capacity.

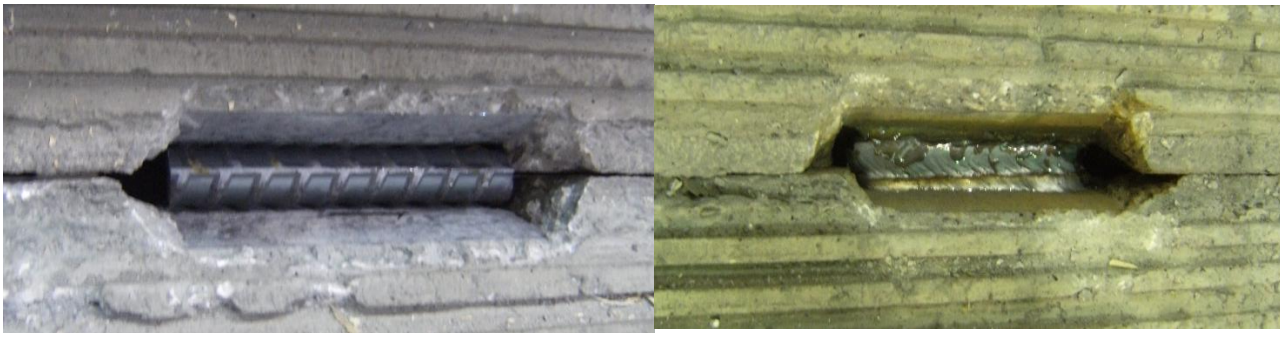

Figure 50: Embedded Plate Connection before (left) and after (right) Weld

The original idea for the welding process was to use a shielded metal arc weld (or manual stick method) to complete the connection. However, after completing two welds it became evident that a different process was needed. It was difficult to remove the built up slag from each layer of weld, which affected the quality of the weld. Also, the two connections completed with this process took almost one hour combined to complete. This was deemed to be to long for a field weld in a rapid construction application.

Switching to a gas metal arc weld (GMAW) for the remaining two connections proved to be a much better option. The two GMAW welds for the connections of the embedded plate tapered web profile took a total of ten minutes to complete. This was less than 20% of the time it took to complete the welds using the SMAW for the embedded plate inverted-T profile. Also, since there was no slag build-up, the welds were better quality. The effects of using different welds for the specimens from a research perspective are included in the Discussion chapter of this paper. An E7018 electrode was used for both welds.

Moving Specimens

Lifting hooks were embedded in the specimens for movement around the lab. Each girder section weighed between 4 and 5 kips depending on the geometry. Each full test specimen weighed approximately 15 kips. Each of the two cranes in the lab could only lift 10 kips so the system was designed to incorporate both cranes together. The hooks were placed in a manner to produce zero tension in the extreme bottom fiber as it was undesirable to expose the joint to any tensile forces before testing.

ANALYTICAL METHODS

Bridge Design

The first step of the project was to complete a structural design of the bridge super-structure for implementation of inverted-T beams. The bridges in consideration were on U.S. 360 over the Chickahominy River in the Richmond District of VDOT. (Hill & Lowe, 2010) The structures are identical 75 ft, two-span, and six lane bridges, and were designed as 19 adjacent inverted-T girders making up the 114 ft width of the bridge. A full design was performed for the candidate bridge system using AASHTO LRFD Fifth Edition (AASHTO, 2010) specifications. This design included all components of the bridge superstructure and is included in Appendix C. The design was checked and verified by Menkulasi.

Once a final design was accepted for the bridge, the sub-assemblage component was designed. The prestressing strand, mild steel, concrete, etc. needed for each specimen to best simulate real life conditions was established. The Test Specimens chapter of this thesis presents further detail of the process of how the specimens were sized and placed within the test setup. The work done in Minnesota (French et al., 2011) was identified as the state-of-the-art design practice for this type of bridge system. For that reason the control design closely resembled the recommendations set forth by the University of Minnesota. The other proposed specimens were designed similarly to the control sub-assemblage with minor differences to investigate potential improved performance parameters. The goal of this work was to improve upon the existing system, not completely change it.

Finite Element Models

Prior to testing, two finite element models were developed. The first was of the candidate VDOT bridges for implementation of inverted-T beams. The second was of the sub-assemblage test specimens. Both were used to aid in the design of the sub-assemblage test specimens as well as develop testing protocols. Finite element modeling was performed by Fatmir Menkulasi (Ph.D candidate, Virginia Tech). A dissertation containing more details of this work will be completed by Menkulasi in the future.

According to ACI (ACI-318, 2008) a deep beam is defined as (a) clear spans equal to or less than four times the overall member depth; or (b) regions with concentrated loads within twice the member depth from the face of the support. The sub-assemblage test specimen is characterized as a deep beam because the distance from the applied load to the face of the support is 1.2 times the depth of the member. This arrangement is shown in Figure 51. Simple beam mechanics do not completely apply to the system and a more in depth analysis must be done. For this reason the test setup was modeled using the finite element method.

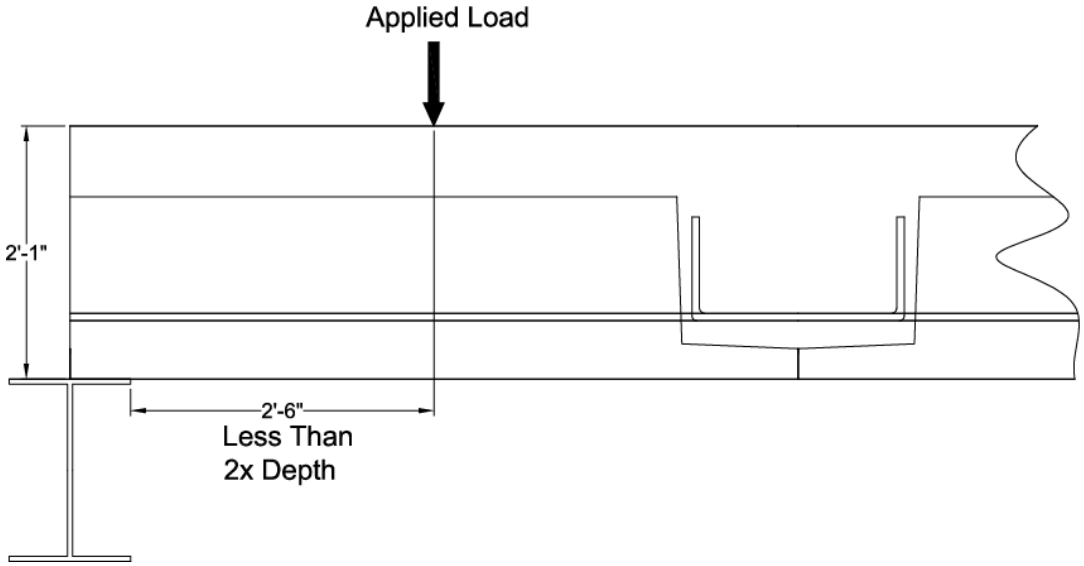

Figure 51: Deep Beam Categorization of Test Setup

The goal of sub-assemblage testing was to develop inverted-T connection details that resulted in no cracking at the inverted-T beam-to-beam interface under service load. Therefore, one component to validating the sub-assemblage test was identifying the service level stress in the candidate bridge and relating that to the sub-assemblage test specimens. In order to find this stress a preliminary finite element model of the candidate bridge was created. The model was based on the full-scale finalized bridge design. The system as modeled with a pin support across the middle pier with roller supports at the outer piers. All elements used were shells and analyzed as such. Since the main interest was identifying the flexural and shear stress in the transverse direction, the effect of prestressing was ignored and therefore not modeled. To simplify the model further, no mild steel was included in the model. The model consisted of two sets of 19 adjacent inverted-T girders (one set for each span) that were made composite via a CIP deck. The deck-girder interface was assumed to be fully bonded.

The dead loads were assumed to not contribute to transverse flexural stress. This is due to the fact that transverse stresses will only develop between girders once the CIP deck hardens and a composite section is created. This does not apply to superimposed dead loads such as barriers or a wearing surface. For this reason the superimposed dead load was added to the model as uniform distributed load in addition to the AASHTO uniform lane loads. (AASHTO, 2010) Other conditions such as differential shrinkage were not considered in lieu of keeping the preliminary model simple and time spent modeling at a minimum. A more detailed model will be completed after sub-assemblage testing is completed.

The anticipated service level transverse stress was identified by placing AASHTO specified truck and tandem loads over the bridge deck surface and recording the worst-case stress scenario. This was done by shifting the location of the AASHTO truck and tandem loads and recording the resulting maximum stress. Figure 52 and Figure 53 show the deflected shape of the bridge under two loading configurations (tandem and lane). Through this process it was identified that minimal transverse shear stress was developed across the sub-assemblages. This is logical as there are no supports along the sides of the bridge and the primary load path is to the abutments. The study also showed that the worst-case transverse flexural stress was approximately 0.18 ksi. Several loading combinations and configurations were analyzed with the finite element model. The stress of 0.18 ksi was obtained by combining the effects of lane loading and a tandem load with dynamic load allowances in the outermost lane with the wheel loads positioned directly over the longitudinal joints as shown in Figure 54.

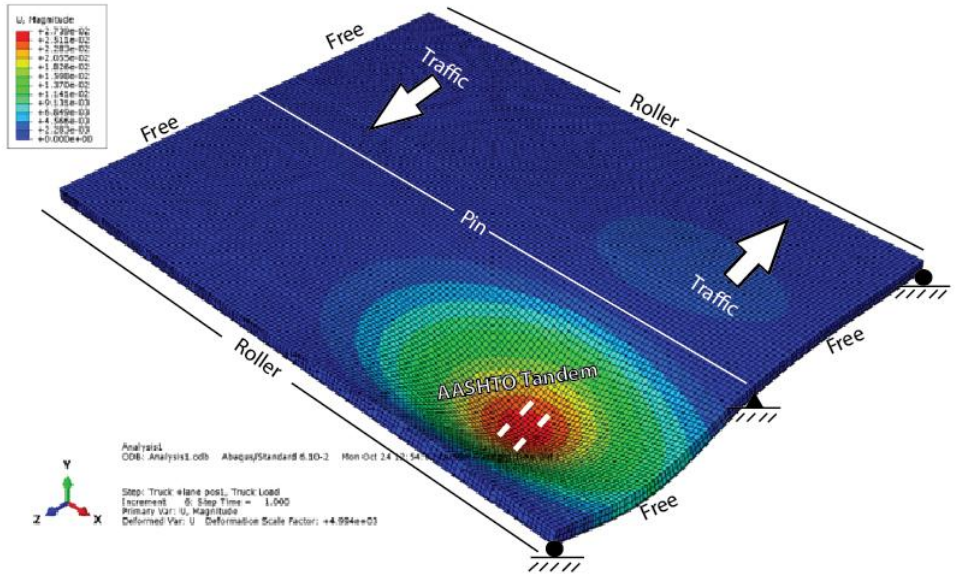

Figure 52: Deformed Shape under Tandem Load on the First Span

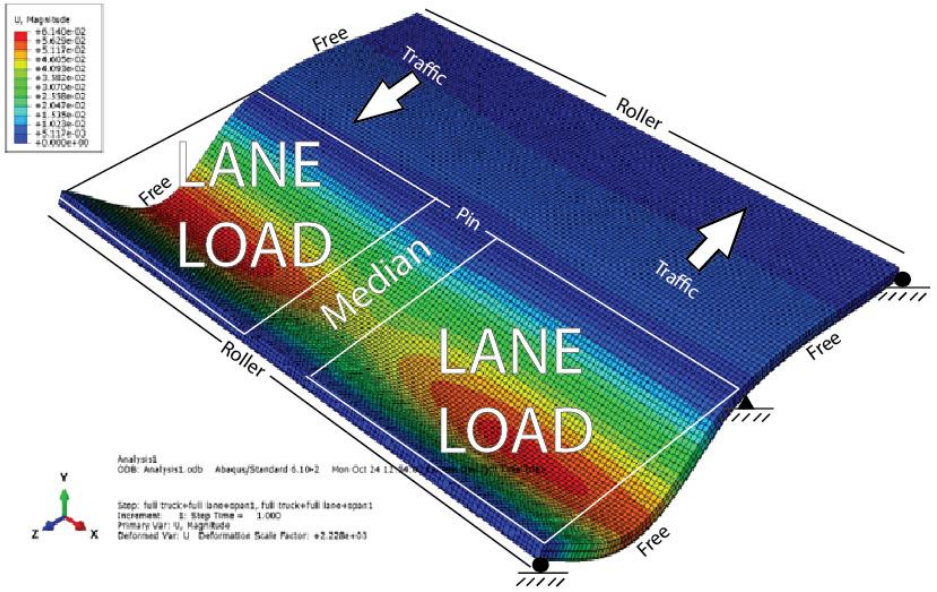

Figure 53: Deformed Shape under Lane Loading on the First Span

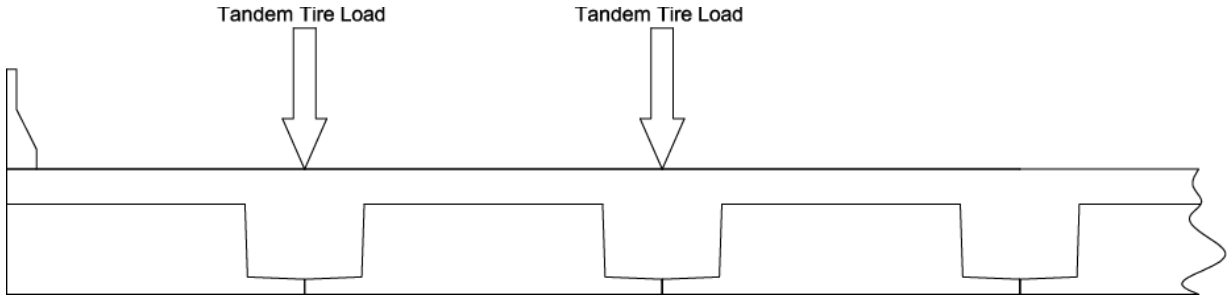

Figure 54: Position of Tandem Tire Loads For Worst-Case Transverse Bending Stress

The geometry of the U.S. 360 bridge is unusual in that its width is greater than its span. This creates interesting behavior that is not found in all inverted-T applications. A short, wide bridge has higher transverse shears and lower transverse load distribution than a more narrow structure. The load spreads out more and has a less direct route to the support. It is for this reason that the given full-scale model provides conservative results in comparisons to narrower bridge systems.

As discussed in the Experimental Methods chapter of this thesis a four point loading system was used to achieve uniform flexural stress and minimal shear stress across the region of interest in the specimen. In order to best recreate the stress effects in the region of interest a variety of load orientations were modeled using a finite element model of the sub-assemblage test specimens. The stress at the joint and interface was best approximated using two point loads with each applied three feet from each end of the specimen. Achieving the target flexural stress (0.18 ksi) required a total applied load of 25 kips. Figure 55 and Figure 56 show the transverse stresses from the finite element model in two different orientations with two point loads applied three feet from the edge of each specimen. Figure 57 shows the stresses in the full-scale model for comparison against the model of the test specimen. Note the similarity of stresses at the longitudinal joint.

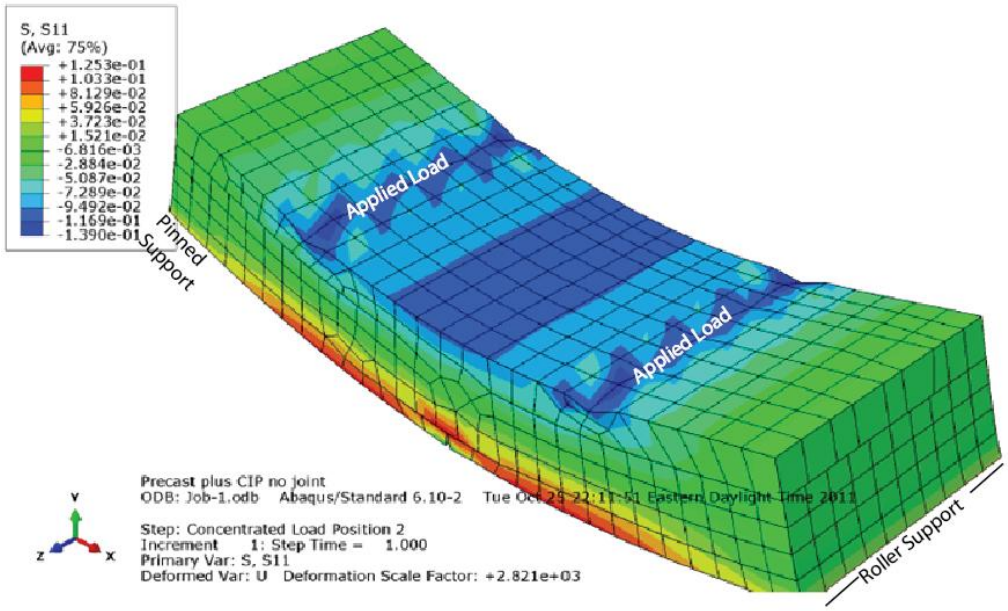

Figure 55: Isometric View of Transverse Stress in Test Specimen (Shown Applied as Line Loads - Actually Modeled as Point Loads)

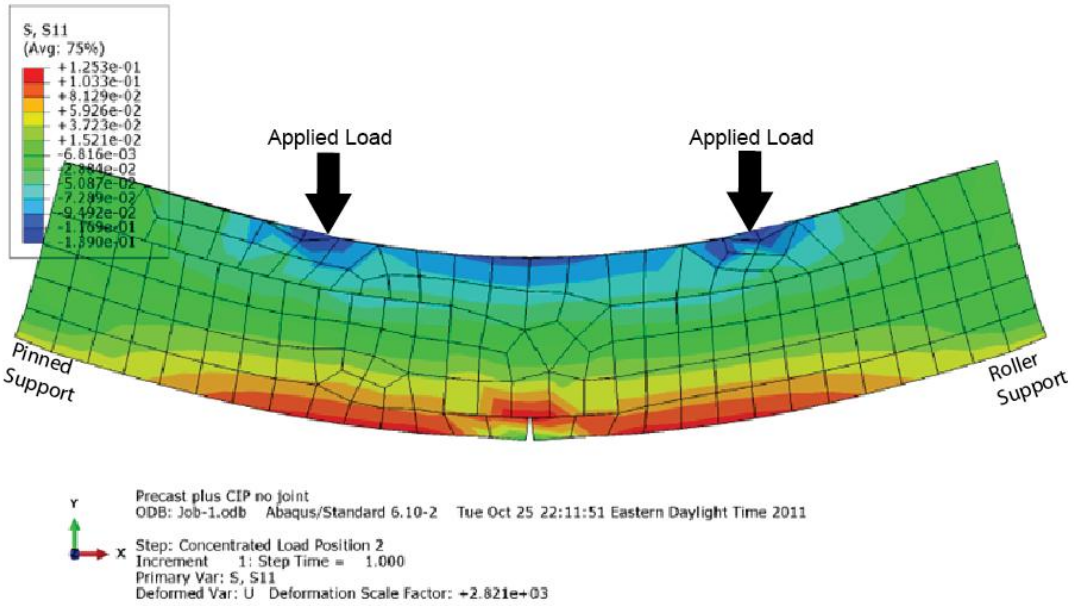

Figure 56: Profile View of Transverse Stress in Test Specimen with Load Applied 3 Feet from Each Edge of Specimen

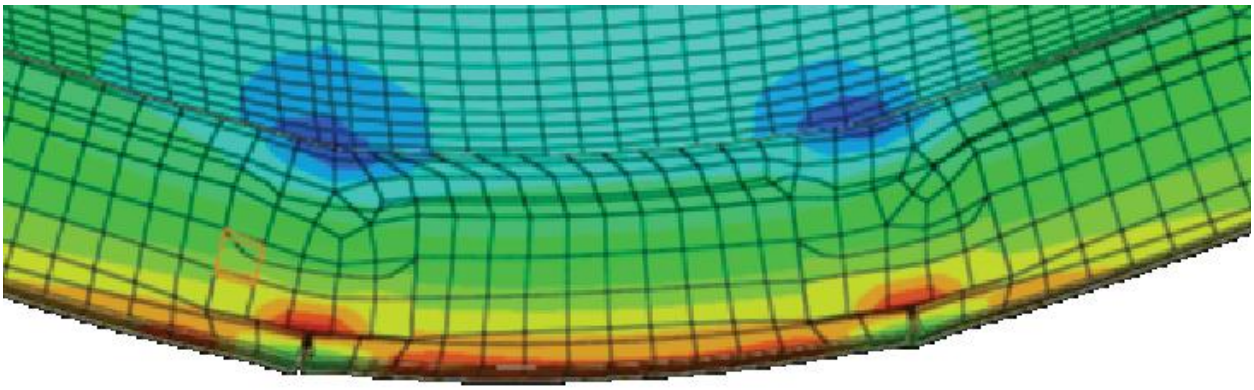

Figure 57: Stresses in Full-Scale Model

The load to induce a stress of 0.18 ksi in the sub-assemblage at the longitudinal joint was first calculated in the finite element model since the sub-assemblage test specimens exhibit deep beam behavior. The service level load was also calculated with classical beam behavior and compared to the finite element model. The differences in the two methods were negligible.

All of the assessments done within the finite element program were conducted using a linear-elastic analysis. This characterizes the type of behavior expected in the range of loads that represent service level stresses up to cracking. Under service level loads the concrete is not expected to crack and is therefore assumed to remain linear-elastic. The results of the laboratory test support this assumption.

RESULTS

This chapter presents the results from testing the sub-assemblage specimens. Five specimens were tested, the first with limited instrumentation, which was used as an instrumentation and testing protocol trial. The other four were fully instrumented and provided the basis for the conclusions and recommendations at the end of this thesis.

Material Testing

When concrete was placed, samples were cast for material property verification testing. Of major interest were the compressive strength, tensile strength, and modulus of elasticity. These values, with linear interpolations to the time of testing, are listed in Table 5. The 28 day design compressive strengths for the deck and precast mixes were 4 ksi and 8 ksi, respectively. More detailed material test results can be found in Appendix B.

Table 5: Interpolated Concrete Strength Values

Specimen	Cast-in-Place Deck				Precast Inverted-Ts			
	Age at Testing	f'_c	f_t	E	Age at Testing	f'_c	f_t	E
	(days)	*(psi)*	*(psi)*	*(ksi)*	*(days)*	*(psi)*	*(psi)*	*(ksi)*
Extended Bar	28	3380	360	3110	54	8820	750	5510
Embedded Plate Inverted-T	24	3680	420	3900	66	9390	820	5720
Embedded Plate Tapered	28	3810	430	4190	70	9380	804	5730
No Connection	23	3400	340	3280	49	8985	740	5530

Visual Documentation

At each load step visual cracks were marked. Propagation height and width of the largest overall crack and the crack over the joint were also recorded. This information is presented for the four (trial specimen not included) test specimens in Appendix D. Photographs were also taken during each test to document crack propagation in each specimen. The end of each crack was marked with the load that propagated the crack to that point. These photos are given in Figure 58 through Figure 61.

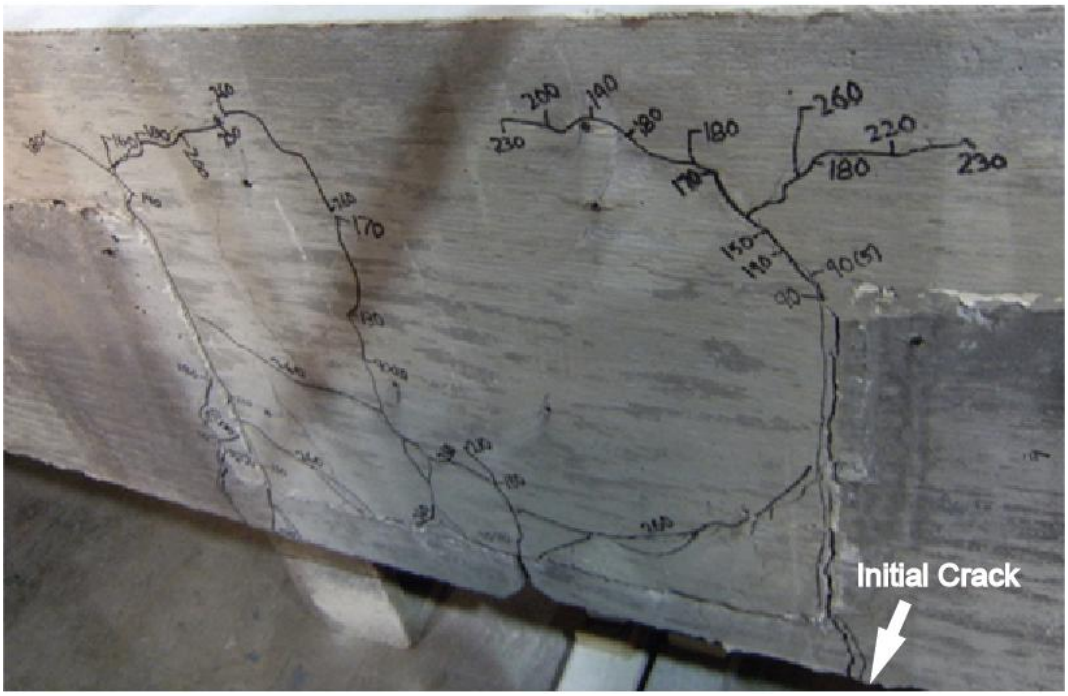

Figure 58: Cracks on Extended Bar Specimen (photo)

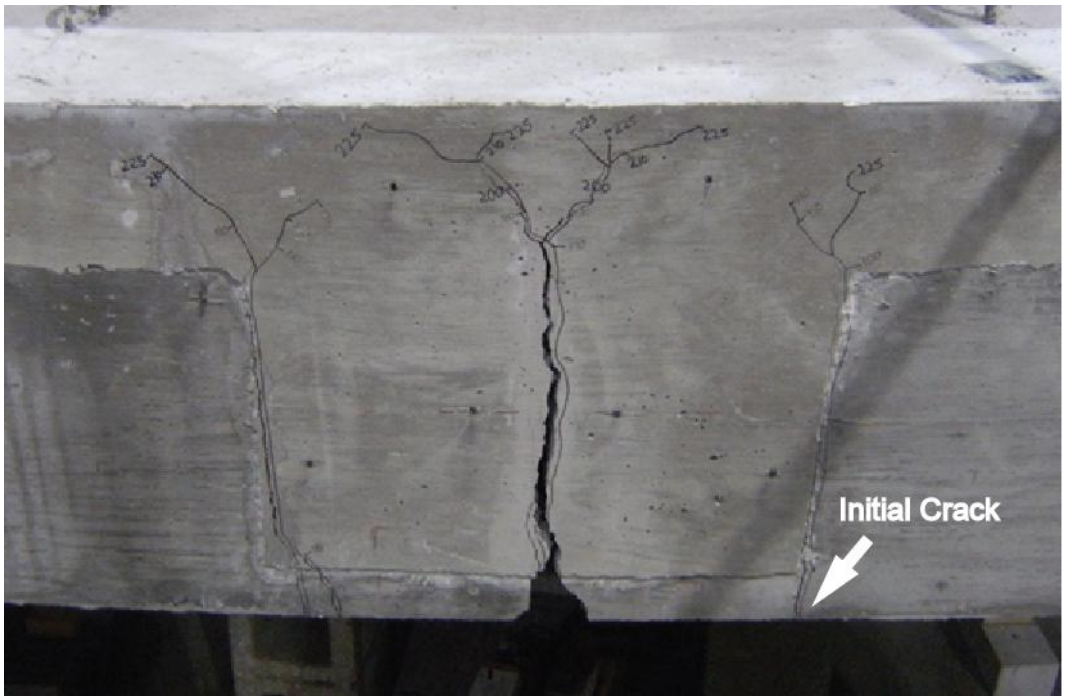

Figure 59: Cracks on Embedded Plate Inverted-T Specimen (photo)

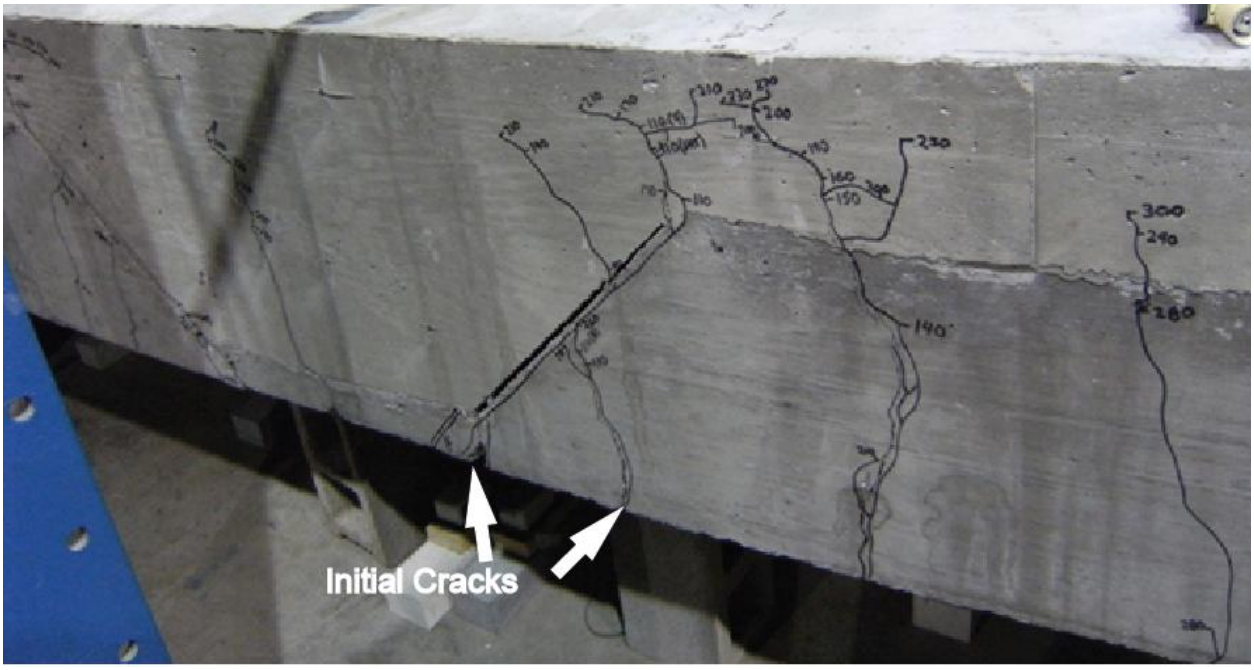

Figure 60: Cracks on Embedded Plate Tapered Specimen (photo)

Figure 61: Cracks on No Connection Specimen (photo)

Deformed Shapes Under Load

One indicator of the relative performance of the different specimens is bending behavior. Specifically, the presence or absence of a plastic hinge was noted using deflected shape plots. An illustration of bending versus hinging behavior is shown in Figure 62. Plastic hinging refers to

the deformation of a section of a beam where steel has yielded. Before a hinge is formed, the system undergoes distributed bending (no yielding). If a hinge forms, however, large rotations occur at the location of the plastic hinge which can cause the formation of large cracks. From a service load perspective the formation of a hinge is undesirable. Under service load conditions, the entire system should remain linear-elastic. From a strength perspective the formation of a plastic hinge is expected as the bending moment reaches the first yield moment. Figure 63 through Figure 66 show that none of the specimens formed plastic hinges at the service load and that deflections at that load were small. Some of the specimens did develop plastic hinges near the ultimate load as the applied moment approached yield. This, however, is not a concern for serviceability.

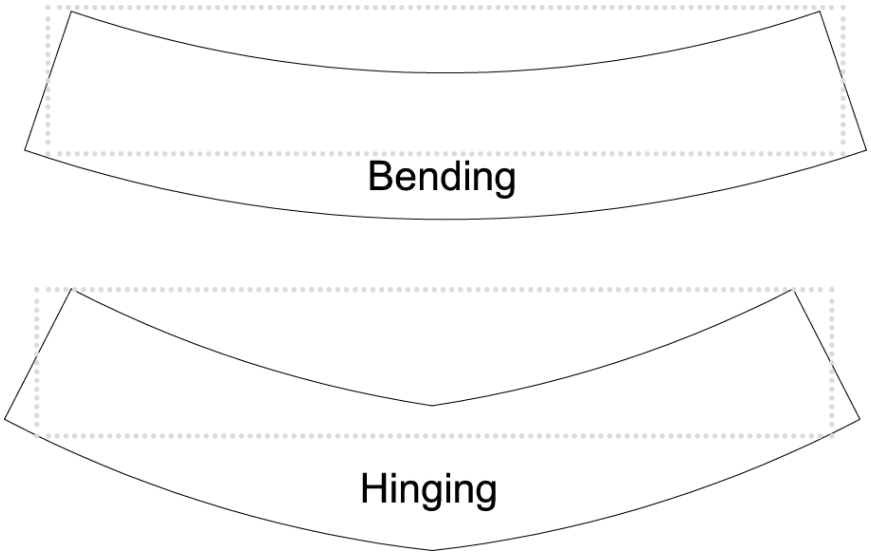

Figure 62: Bending vs. Hinging Behavior

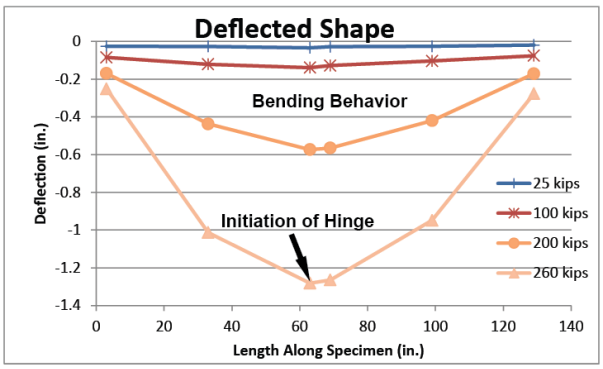

Figure 63: Deflected Shape for Extended Bar Specimen

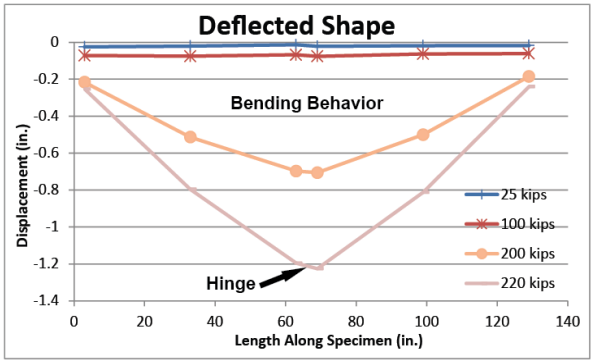

Figure 64: Deflected Shape for Embedded Plate Inverted-T Specimen

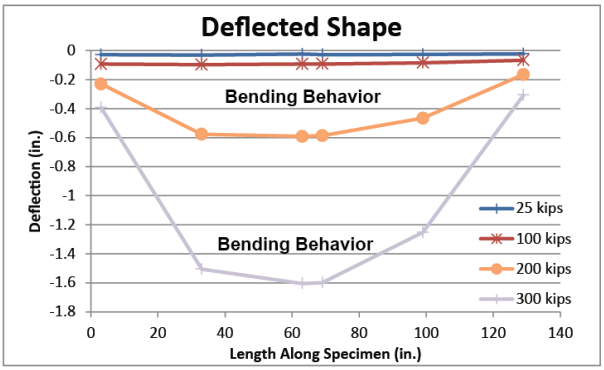

Figure 65: Deflected Shape for Embedded Plate Tapered Specimen

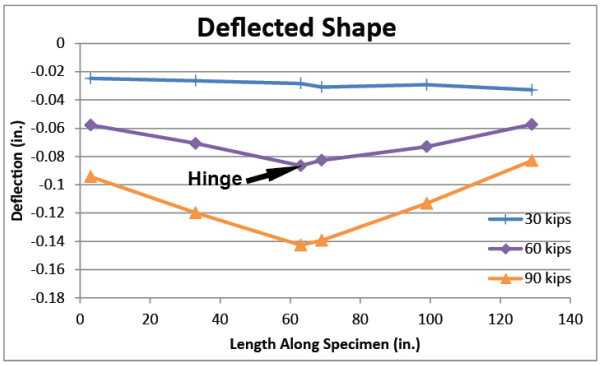

Figure 66: Deflected Shape for No Connection Specimen

Load Versus Deflection Behavior

Some of the fundamental indicators of the performance of each connection-geometry combination are elasticity and ductility. It is beneficial for a system to remain linear-elastic for service loads. Any load that causes plastic behavior creates permanent damage to the system and compromises the future behavior of the bridge. It is, therefore, desirable for a specimen to remain linear-elastic under service loads.

As a bridge approaches failure it is beneficial to have some degree of warning. It is for that reason that connection ductility was suggested as important criteria in making a system recommendation. The load deflection behavior for the four specimens tested can be found superimposed in Figure 67 and Figure 68. The stiffness and ductility of each specimen is addressed in the Discussion chapter of this thesis.

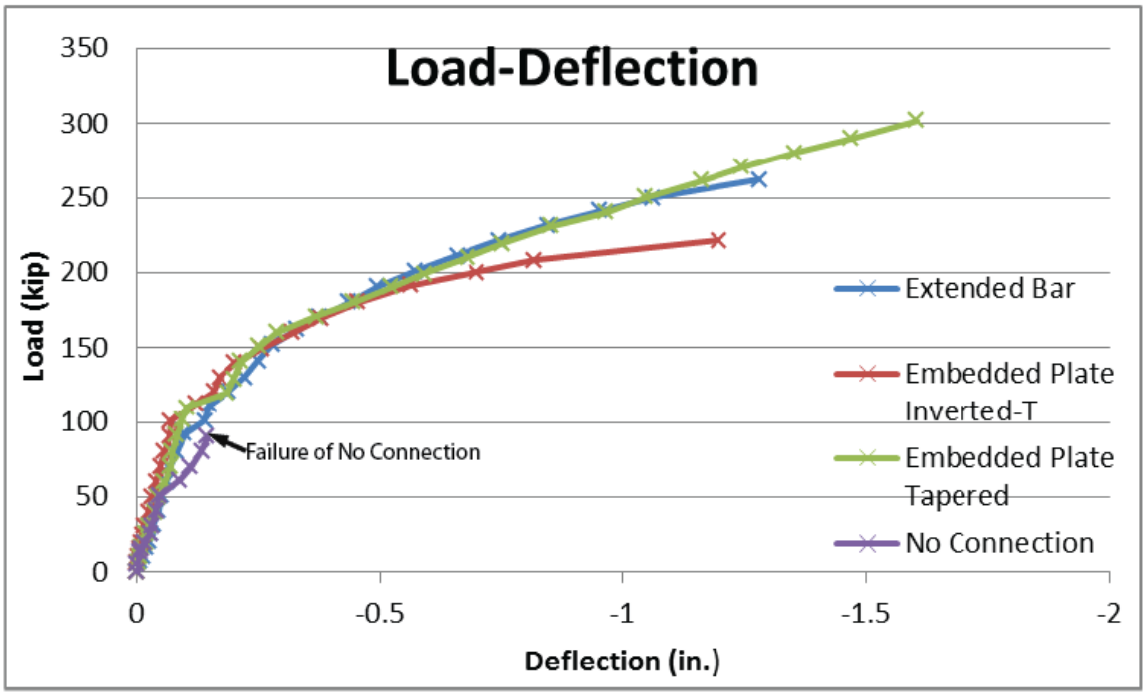

Figure 67: Load-Deflection Behavior for Entire Range of Load

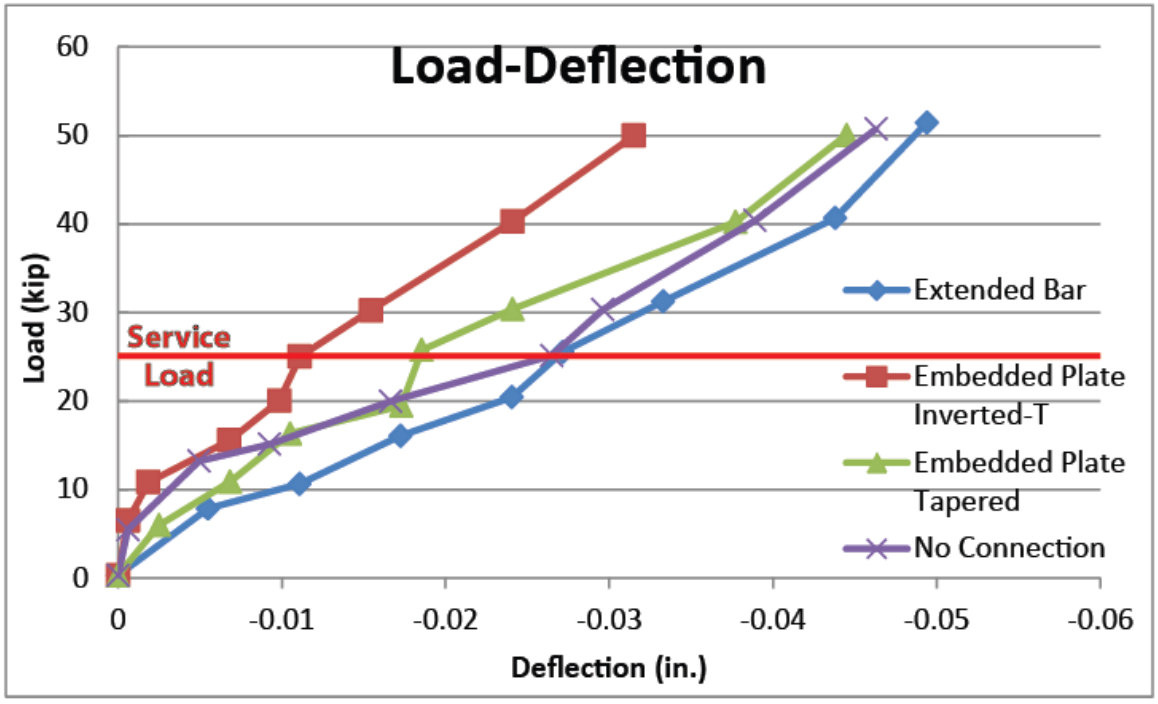

Figure 68: Load Deflection Behavior for up to 50 kips

Strain Gage Results

Strain gages were used as documented in the Experimental Methods chapter of this thesis. The recorded strains were graphed against their corresponding loads and used to develop a strain profile for each specimen. The gages attached to the steel within the specimens provided valuable information about the loads at which reinforcement yielding occurred. Both the linear strain gages attached to the steel and the embedment gages placed in the concrete provided information on cracking loads. Spikes in the strain graphs indicated the initiation of cracking near the gage. This data provided insight to what was happening inside of the specimens. Table 6 shows the applied load that caused the initial crack at the location of the connection steel. These were taken as the extended bars for the extended bar test, the tension rebar behind the embedded plate in the embedded plate tests, and the drop bars in the no connection test. The notation for the gages is illustrated in Figure 69. The load that caused the steel to yield is also included. Table 7 shows the loads that caused cracking in the CIP region over the longitudinal joint.

Table 6: First Crack and Connection First Yield Loads

Connection Steel Member	Extended Bars		Embedded Straight		Embedded Tapered		No Connection	
	EMB-L (1-4)		*EXT-L (1-4)*		*EMB-L (1-4)*		*Drop Bar 1-4*	
	First Crack	Yield	First Crack	Yield	First Crack	Yield	First Crack	Yield
	(kips)	*(kips)*	*(kips)*	*(kips)*	*(kips)*	*(kips)*	*(kips)*	*(kips)*
Near	90	160	110	140	120	170	60	80
Near-Middle	80	160	110	140	120	160	60	90
Far-Middle	80	190	110	140	120	170	60	80
Far	80	150	110	140	120	180	60	90

Figure 69: Documentation of Connection Steel

Table 7: Cracking Loads at Gages Located 9 in. and 12 in. Above Bottom of Precast

Gage	Extended Bars	Embedded Straight	Embedded Tapered	No Connection
	Initial Crack	Initial Crack	Initial Crack	Initial Crack
	(kips)	*(kips)*	*(kips)*	*(kips)*
9"-1	90	110	120	60
9"-2L	100	No Crack	100	70
9"-2	100	110	120	60
9"-2R	110	No Crack	150	No Crack
9"-3	80	120	120	**
12"-1	90	120	120	60
12"-2	90	140	160	60

** - Too difficult to identify

The strain gages reinforced what was observed visually. Almost all of the strain gages indicated the first crack in the specimen at the same load that was visually determined. Strain gages 3-R-EMB (gage attached to one of the tension rebar on the welded plate connection on the right precast girder) and 9”-2L (embedment gage located 9 in. above bottom of precast, midway through the section, and on the left side of the joint) on the embedded plate tapered specimen, however, indicated first crack at 100 kips instead of the first visually identified crack at 110 kips. All other gages were consistent with what was identified visually.

Extended Bar

Two plots are included to show the development of strain at key points in the specimen. Figure 70 shows the strain in the extended bars on the right side of the specimen throughout the range of applied load. This figure shows the even distribution of strain across those bars, which corresponds to an even distribution of stress. Figure 71 shows the strain in the gages attached to the top mat of temperature and shrinkage steel. This figure shows the shift of the compression zone in the top of the specimen. As the applied load approaches about 160 kips the steel becomes less compressive. At a load of about 260 kips the steel in this region goes into tension. All of these figures are explained further in the Discussion chapter.

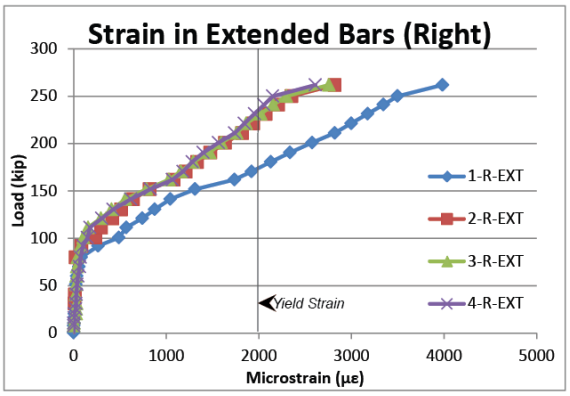

Figure 70: Strain in Extended Bar Steel (Right Side) (6 in. Above Bottom of Precast) Similar to Left Side

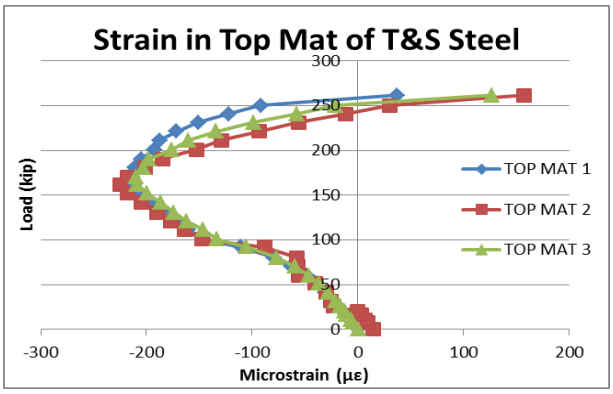

Figure 71: Strain in Gages Attached to Top Mat of T&S Steel (22.5 in. Above Bottom of Precast)

Embedded Plate Inverted-T

Four graphs are included and described to show the behavior of the specimen and applicability of the results for the embedded plate inverted-T test. These plots are further discussed in the following chapter. Figure 72 shows the strain in tension steel behind the embedded plate connection and how the stress in those bars was distributed. The spike in the data is most likely due to a loss of bond between the strain gages and steel so all data after around 180 kips of applied load should be disregarded. Figure 73 shows the development of cracking along the longitudinal joint and the lack of such to the left and right of it. Figure 74 shows the development of cracking directly above the vertical precast to CIP interface. This graph shows that though there was no cracking directly left or right of the inverted-T to inverted-T joint there was other cracking in the constant moment region other than at the joint. Figure 75

shows the strain in the top mat of steel. Like in the extended bar specimen, this plot shows the change from compression to tension of the top mat of steel with the onset of cracking. This graph also reinforces the equal distribution of stresses across the member under service load conditions.

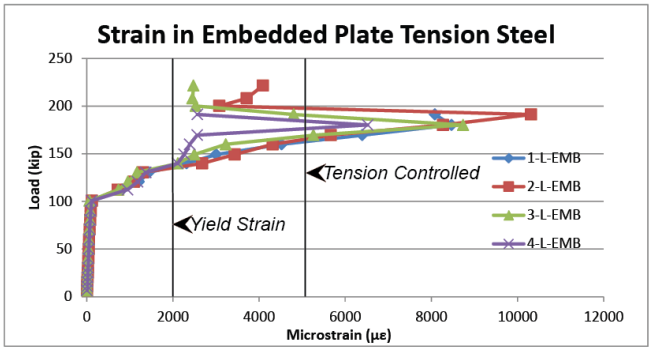

Figure 72: Strain in Embedded Plate Tension Steel (Left Side) (1.5 in. Above Bottom of Precast)

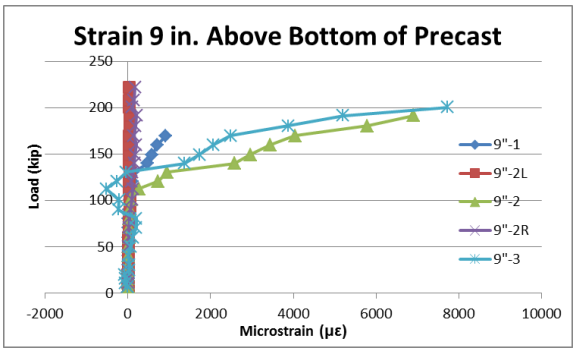

Figure 73: Strain in Row of Gages 9 in. Above Bottom of Precast

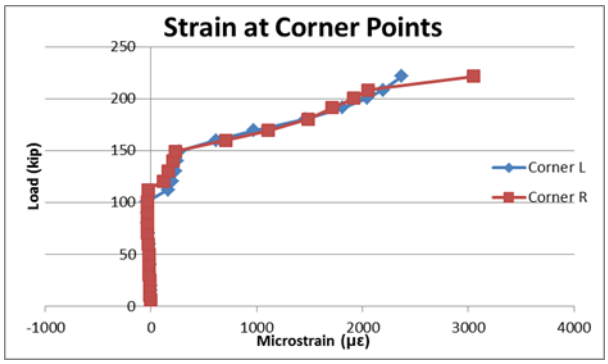

Figure 74: Strain in Two Gages at Corner Points of Interface (19 in. Above Bottom of Precast)

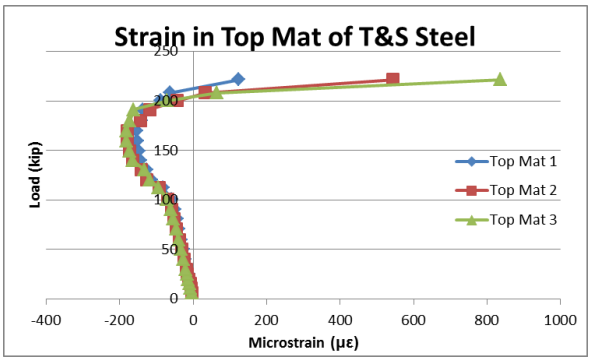

Figure 75: Strain in Gages Attached to Top Mat of T&S Steel (22.5 in. Above Bottom of Precast)

Embedded Plate Tapered

Three plots are included to show the development of strain in the embedded plate tapered test specimen. Figure 76 shows the strain in tension steel behind the embedded plate connection and how the stress in those bars was distributed. Like in the embedded plate inverted-T plot of the same connection the data after the spike at around 220 kips should be neglected as those values represent what the gages recorded after debonding from the steel. Figure 77 shows the development of cracking along the longitudinal joint and the inclusion of cracking both to the left and right of it. This shows that this specimen had a greater distribution of cracking throughout the CIP region above the joint. Figure 78 shows the strain in the top mat of T&S steel. In this case the rebar remained increasingly compressive throughout loading. This indicates

that the neutral axis did not approach this region during this test. More advanced analysis is included in the Discussion chapter.

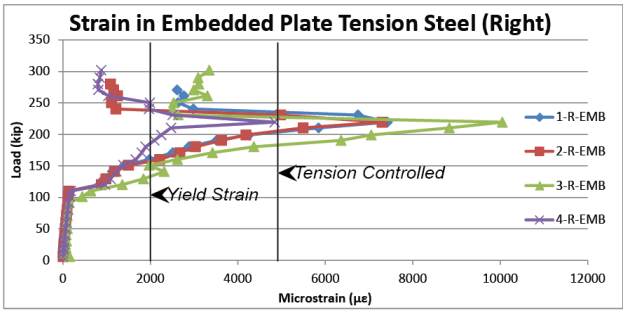

Figure 76: Strain in Embedded Plate Tension Steel (Right Side) (1.5 in. Above Bottom of Precast)

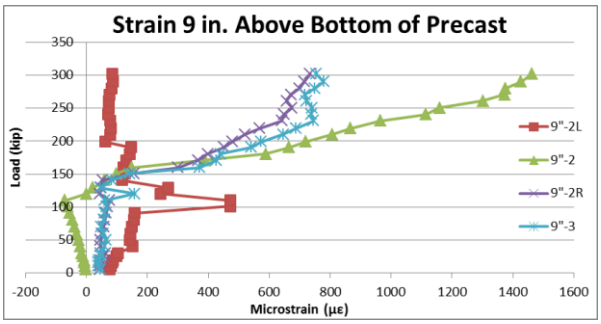

Figure 77: Strain in Row of Gages 9 in. Above Bottom of Precast

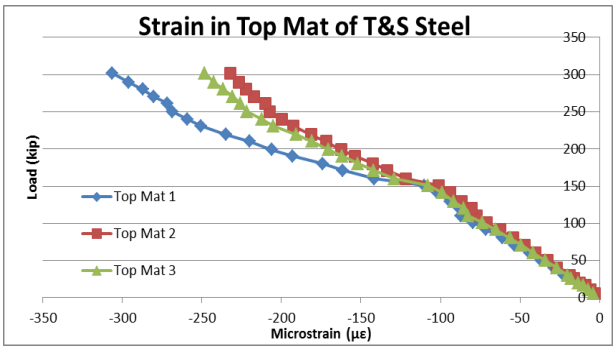

Figure 78: Strain in Gages Attached to Top Mat of T&S Steel (22.5 in. Above Bottom of Precast)

No Connection

Four plots are included to show the unique behavior of the no connection test specimen. Figure 79 shows the development of cracks in the concrete nine inches above the bottom of precast. It indicates cracking along the near side of the longitudinal joint and not on the far side or to the left or the right. (Disregard the stray point for gage 9”-2L) Figure 80 again shows the development of cracks 3 in. above Figure 79. This graph reinforces the development of cracks along the near side of the joint but not the far. Figure 81 shows the strain in the drop bars that were designed to carry the tensile force across the joint. The plot indicates even distribution of strain in the bars. Figure 82 shows the strain in the top mat of temperature and shrinkage reinforcement. This figure shows increasingly compressive strain throughout the range of loading. This suggests that the neutral axis did not approach the top mat of steel in this test.

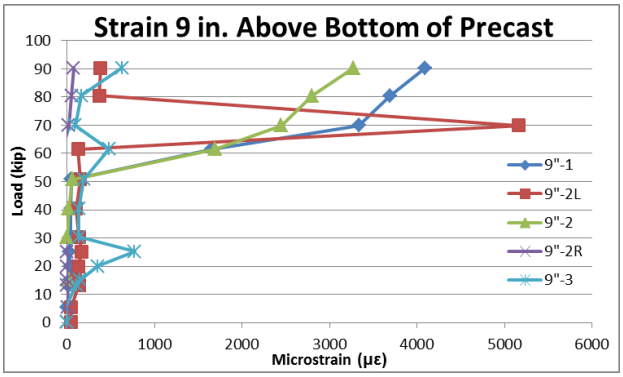

Figure 79: Strain in Row of Gages 9 in. Above Bottom of Precast

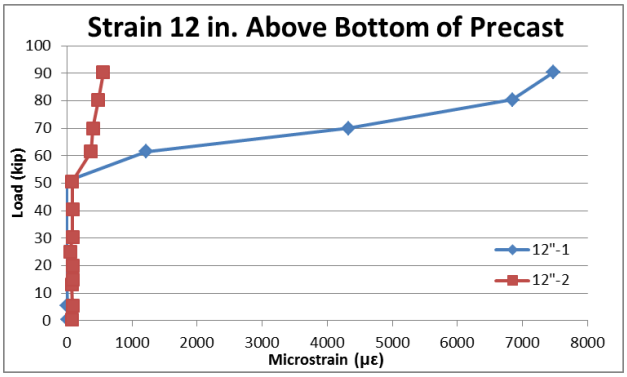

Figure 80: Strain in Two Gages 12 in. Above Bottom of Precast

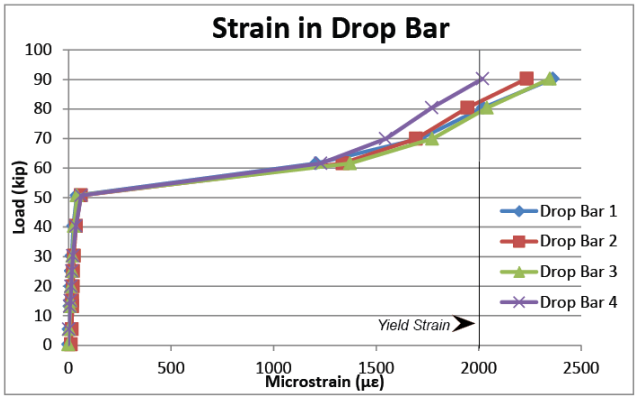

Figure 81: Strain in Drop Bar (5 in. Above Bottom of Precast)

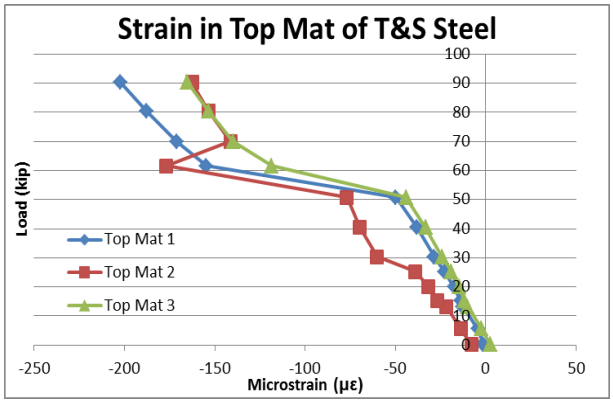

Figure 82: Strain in Gages Attached to Top Mat of T&S Steel (22.5 in. Above Bottom of Precast)

Comparisons

Every specimen had five gages located 9 in. above the bottom of the precast girder as shown in Figure 30 in the Experimental Methods chapter of this thesis. In the center of that pattern was gage 9”-2. Figure 83 provides a direct comparison of the strain of each of the four specimens tested at the same location.

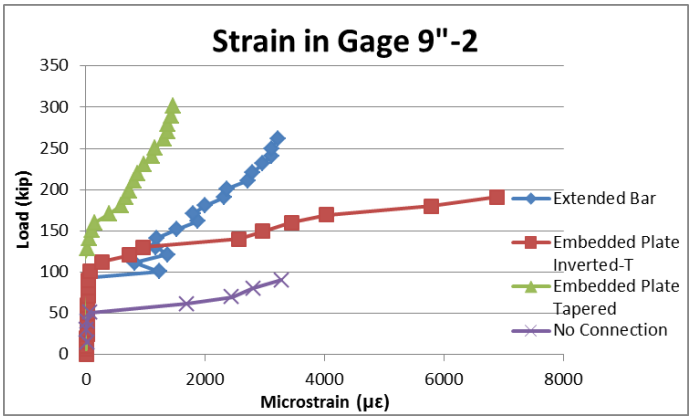

Figure 83: Comparison of 9"-2 Gages in Each Specimen

The load vs. strain graphs for each specimen in Figure A-7 through Figure A-17 of Appendix E show the strain development at the various other locations where gages were placed, but not included in the discussion. The installation of strain gages at different elevations throughout the specimens provided a strain profile for each test. Figure 84 shows the strain profiles for each respective test. This figure represents the strain slope in each specimen in the linear-elastic range at a load of 30 kips.

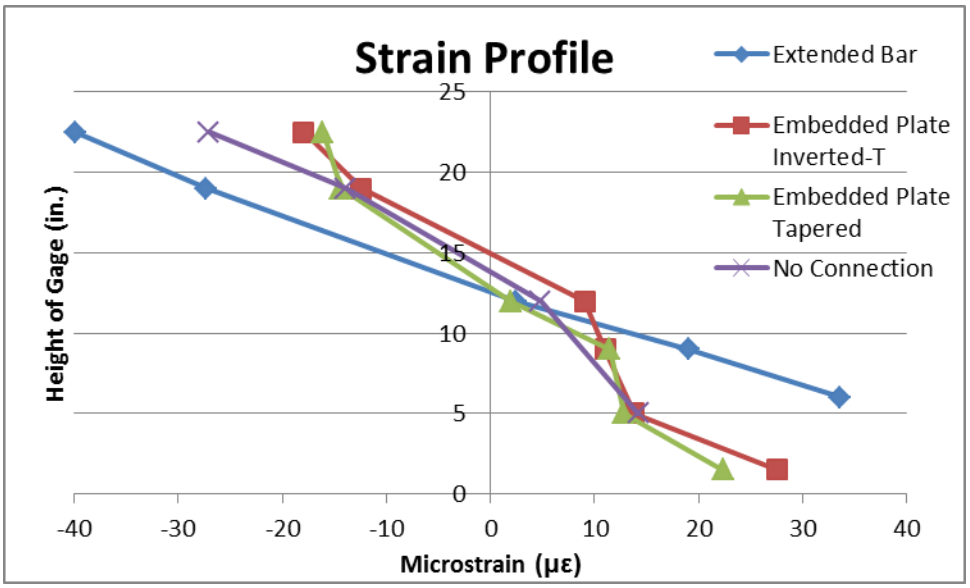

Figure 84: Strain in Each Specimen at an Applied Load of 30 kips

Vibrating Wire Gages

Vibrating wire gages were inserted into each specimen at the time of deck placement to monitor shrinkage strains in the concrete. Figure 85 shows the raw strain data without temperature correction for each of the specimens tested. The specimens exhibited similar behavior with strain magnitudes consistent with one another. Though there was some variance in the strain of each test, the difference is small and strain in the system before testing can be eliminated as a variable between specimens.

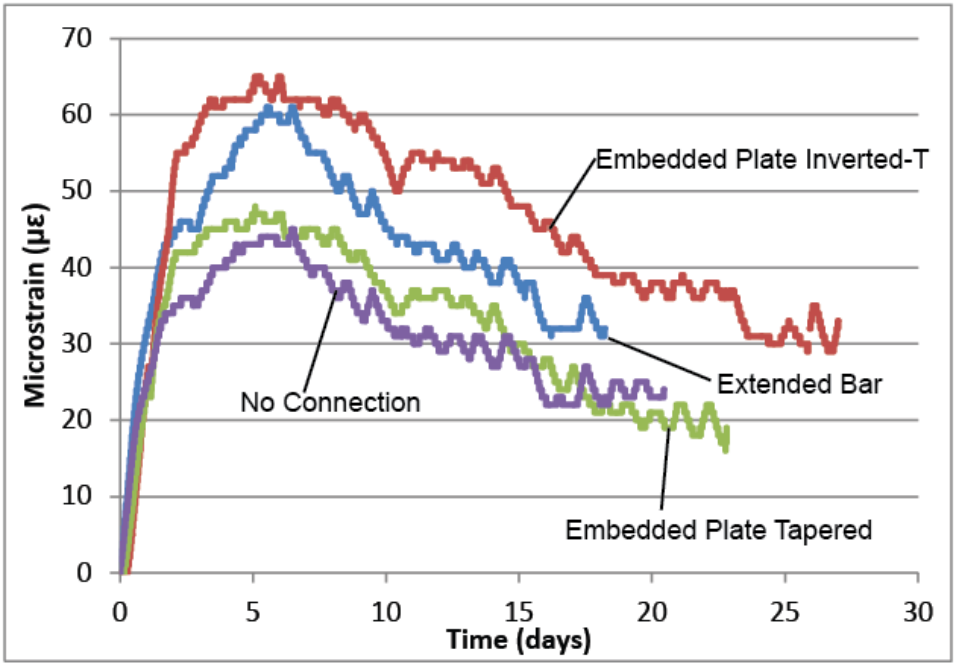

Figure 85: Strain Recorded From VWGs from Time of Deck Placement

LVDT Results

LVDTs were attached to one side of each specimen as documented in the Experimental Methods chapter of this thesis. These gages were attached to identify first cracking and to provide a strain profile. The performance of the LVDTs was poorer than expected. While the LVDTs were able to indicate a load at first cracking across the interface and at the girder-to-girder joint, there was no trend to the data to help indicate a strain profile throughout the depth of the specimens. Also, the loads indicated for the onset of cracking were not consistent with the

strain gages and visual observation. Moreover, one of the four LVDTs failed to record reliable data for two of the tests.

DISCUSSION

Comparison to Work Done at the University of Minnesota

The framework of this research was based on the NCHRP (National Cooperative Highway Research Program) Project 10-71 completed by members of the University of Minnesota. (French et al., 2011) The sub-assemblage test setup was based off of similar work done as part of that project. Both projects involved testing two girder sections (with outer flanges removed) cast together with a deck topping that was simply supported with an applied vertical load. The instrumentation configuration used in Minnesota produced favorable results and was therefore closely imitated in this project.

Though similar, there were differences that made this research unique from what had previously been conducted. The most discernible difference was the connection and geometry variation in this project. For the NCHRP project the only variation between tests was the size and spacing of the extended bars and reinforcing cage and size of the precast members. This project expanded the inverted-T concept to consider two different connection types and investigate varying the geometry of the precast elements.

After examining the results of the tests in Minnesota it was decided to also vary the loading regimen and configuration. The results from the NCHRP publication indicated that the fatigue loading of several thousand load cycles at various load steps had negligible effect on the cracking behavior of the specimens. For that reason it was decided to simplify the fatigue testing to what was defined in the Experimental Methods chapter of this paper.

The specimens were tested by applying two point loads at the quarter points opposed to one line load along the inverted-T to inverted-T joint. The consensus was that the four-point loading better simulated the full-scale stress states that were calculated in the finite element model. The clamping assembly used in Minnesota was disregarded since it also did not properly simulate expected behavior.

Material Testing

While the mixes for the precast inverted-T sections met or exceeded the desired strength neither of the two deck mixes met their design 28 day strength values. A table of this data can be found in the Results chapter of this thesis.

To accommodate the designed casting sequence two separate pours were made for the four specimens. The two embedded plate precast sections were cast first and had a 28 day compressive of 8670 psi which was 8% greater than the design f'_c of 8000 psi. The extended bar and no connection inverted-T sections tested at 9680 psi at 28 days which was 21% greater than designed. The tensile strengths and modulus of elasticity of the inverted-T girders were also higher than designed. The design for the tensile strength was taken as $7.5\sqrt{f'c}$ and the modulus of elasticity was taken as $57\sqrt{f'c}$. Table 8 shows the difference between the design and recorded concrete strength.

Table 8: Difference in Recorded and Designed Concrete Strength of Girder Mixes at 28 Days

Concrete	Girder Mix 1			Girder Mix 2		
Strength	Measured	Design	% Difference	Measured	Design	% Difference
f'_c - *(psi)*	8670	8000	8%	9680	8000	21%
f'_t - *(psi)*	910	671	36%	700	671	4%
E - *(ksi)*	5380	5098	6%	5710	5098	12%

The critical tensile stress for the sub-assemblage tests occurs at or immediately above the inverted-T-to-inverted-T joint. It is the strength of the concrete at this location that is of importance. Like the girders, the CIP pours were done in two separate placements. The first of these, which acted as the topping for the embedded plate specimens had a tested 28 day compressive strength of 3810 psi, which is approximately 5% less than the design f'_c of 4000 psi. The deck concrete for the extended bar and no connection specimens had a tested compressive strength of 3380 psi at 28 days, which was approximately 16% below what was designed. The tensile strengths and modulus of elasticity values generally tested lower than designed. Table 9 shows the difference between the calculated and recorded concrete strength values.

Table 9: Difference in Recorded and Designed Concrete Strength of Deck Mixes at 28 Days

Concrete	Deck Mix 1			Deck Mix 2		
Strength	Measured	Design	% Difference	Measured	Design	% Difference
f'_c - *(psi)*	3810	4000	-5%	3380	4000	-16%
f'_t - *(psi)*	430	474	-9%	360	474	-24%
E - *(ksi)*	4190	3605	16%	3110	3605	-14%

The lack of quality of the mixes creates the issue of hindering the performance of the specimens and perhaps allows the onset of cracking at lower loads. However, since the cast-in-place concrete in all sub-assemblages was below the design compressive strength of 4000 psi, the tests results should be conservative.

Applicability of Loads

Considering existing stresses in the specimens caused by self-weight and weight of the spreader bar, the applied load determined by the finite element model to induce service level stress (0.18 ksi) at the joint is 25 kips. This corresponds to the transverse stress induced from AASHTO tandem and lane loadings. Table 10 shows the ratio of the transverse stress caused at each load step to the service level stress. (Note: These stresses only apply up until the onset of cracking.) The service load is the load that induces service load stresses. P_{cr} is the theoretical load at which cracking should occur based on the tensile strength of the concrete.

Table 10: Applied Load to Service Stress Relationship

Applied Load (kip)	Stress (ksi)	Applied Stress/ Service Stress	
5	0.09	0.51	
10	0.11	0.63	
15	0.13	0.76	
20	0.15	0.88	
25	0.17	1	← Service Load
30	0.19	1.13	
40	0.24	1.37	
50	0.28	1.62	
60	0.32	1.87	
70	0.37	2.11	
80	0.41	2.36	
90	0.45	2.6	← P_{CR}
100	0.49	2.85	
110	0.54	3.1	
120	0.58	3.34	

The ratio of applied stress to service stress in Table 1 can be somewhat deceiving. For instance, an applied load of 25 kips has a ratio of 1.0 while double that load (50 kips) has a ratio of 1.62 instead of 2.0. This is due to the effect of the self-weight of the specimen and the spreader beam. This self-weight contributes a larger percentage of the total load at lower levels than it does when the applied loads get larger. These calculations are included in Appendix F. These calculations are made based on classical beam theory. The finite element model of the test setup supported those calculations for loads within the linear-elastic range.

Comparison of Calculated and Tested Values

The design nominal strengths and cracking loads were not the same for all of the specimens. These values were calculated by taking the smallest value from the following section analyses 1) over the longitudinal joint, 2) at the vertical (or tapered) precast to CIP interface, and 3) at the minimum depth of CIP concrete. The design nominal strengths and cracking loads are displayed in Table 11 and are compared to the results from the laboratory tests. All design values are based off of nominal strength values of the steel and concrete. Bold values indicate the

controlling factors for nominal moment capacity. Calculations for the data in Table 11 are included in Appendix G.

Table 11: Comparison of Design Nominal and Cracking Loads to Test Results

Nominal & Cracking Loads	Extended Bar	Embedded Plate Inverted-T	Embedded Plate Tapered	No Connection
Design $\mathbf{M_n}$ Over Longitudinal Joint *(kip-in)*	4110	**2740**	3510	2310
Design $\mathbf{M_n}$ At Vertical/Tapered Interface *(kip-in)*	**2270**	**2740**	3510	2600
Design $\mathbf{M_n}$ At Min. Depth of CIP Concrete *(kip-in)*	**2270**	**2740**	**2740**	**1070**
Design Applied Load $\mathbf{P_n}$ *(kip)*	123	151	151	50
Actual Applied Load at Strength *(kip)*	260	225	300	90
(Actual/Design)	2.11	1.49	1.99	1.80
Design $\mathbf{M_{cr}}$ *(kip-in)*	1890	1930	1930	1890
Design Applied Load $\mathbf{P_{cr}}$ *(kip)*	100	102	102	100
Actual Applied Load at Crack *(kip)*	90	100	110	60
(Actual/Design)	0.90	0.98	1.08	0.60

In all four cases the test specimens exceeded their design nominal load capacity. The strength was over-predicted for all four tests by 49% to 111%.

The cracking load prediction was within 10% of the tested results for the extended bar and two embedded plate specimens. Any lack of conservatism is most likely due to the lower than desired strength of concrete in the CIP deck. The CIP deck had a corresponding lower tensile strength concrete, which would cause the specimens to crack at lower tensile stresses. It is interesting to note that for the no connection specimen the design cracking moment (1890 kip-in.) exceeded the design nominal moment (1070 kip-in.). This is due to the fact that the minimum reinforcing prescribed by AASHTO was not provided. This same relationship is seen with the extended bar connection as well since the design nominal moment (2270 kip-in) does not exceed 1.2 times the cracking moment (2270 kip-in.) as prescribed by AASHTO (AASHTO, 2010). For this reason additional testing should be conducted to further examine this behavior and perhaps design the extended bar and no connection specimens to meet minimum reinforcing requirements.

Validation of Finite Element Models

The finite element models for both the full bridge and the test specimens were created based on several assumptions. Both models were designed entirely of concrete with all inverted-T girder geometries and did not consider the effects of steel. The stress profiles for the model full-scale bridge under AASHTO loading conditions and the model test specimen with simply supported boundary conditions and a 25 kip load split evenly between the two quarter point loads were almost identical.

The strain profiles of all of the test specimens could not be obtained at the service load of 25 kips due to irregularity in the strain gage results. For that reason, the strain profile from the finite element models is compared to the test specimen strain profiles of the next largest load increment (30 kips). This comparison is shown in Figure 86. Both finite element models had a tensile stress of approximately 0.18 ksi directly above the longitudinal joint and a compressive stress of approximately 0.16 ksi at the extreme compression fiber with a linear trend between those points. Adjusting those stresses to a 30 kip load and using Hooke's Law and the design modulus elasticity of 3600 ksi converts those stresses to strains of 55 με and -50 με respectively. (The design modulus of elasticity closely represents the average recorded modulus of elasticity of 3620 ksi for the four test specimens.) The 30 kip load step is within the linear elastic range for the models and the test specimens.

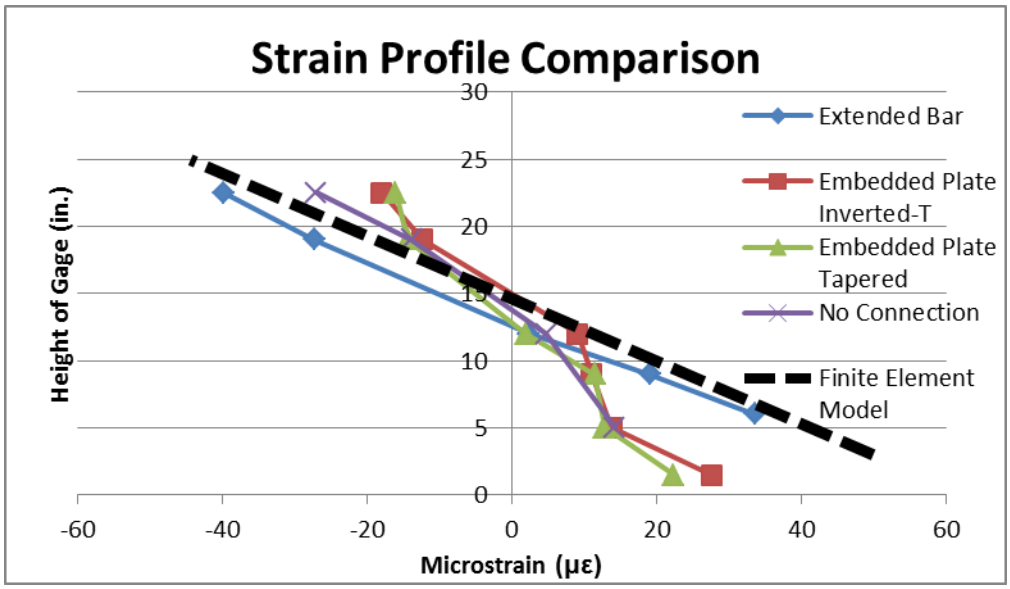

Figure 86: Comparison of Strain Profiles of Test Specimens to the Finite Element Models at an Applied Load of 30 kips

As Figure 86 shows, the slope of the strain profile of the finite element model replicates the behavior of the test specimens. The extended bar specimen experienced larger strains while the other three specimens experienced smaller strains than predicted. The generally conservative nature of the models is most likely due to the fact that the effects of reinforcement, which stiffen the test specimens, were not considered in the models. The lack of conservatism in the extended bar connection is most likely due to the low modulus of elasticity of deck concrete in that specimen. Table 5 shows the concrete strength values. Though the comparison is not direct it can still be seen that the assumptions of the model do represent the actual behavior of the tests at a load close to service level.

Comparison of Specimens

It is insufficient to compare the ultimate and cracking loads of the specimens as the only means to evaluate relative performance. The service level stress is a key aspect to consider. Since the daily demand on the bridge system falls into this classification it is beneficial to identify how each connection and geometry behaves under these stress conditions. There is also benefit in comparing the specimens from a relative performance standpoint. Identifying the maximum capacity of each specimen indicates how it might behave under ultimate or over-loading conditions. In addition to these qualities the durability and constructability of each connection are also of importance. Following are sections discussing these and other considerations.

Service Level Load Behavior

One of the primary goals of this research was to develop an inverted-T to inverted-T connection with good resistance to reflective cracking. The stress corresponding to crack initiation in each specimen was compared directly to the applied load causing the first crack. For applied loads up to the design service load of 25 kips none of the specimens cracked. It wasn't until well above this value that the no connection specimen cracked. The other three specimens first cracked at larger loads as shown in Table 12. This table also shows the stiffness of each specimen throughout the linear-elastic range up to a load of 50 kips. This data is derived from Figure 68 in the Results chapter. The stiffness values are relatively similar to one another which

indicates that each of the specimens is behaving linear-elastically and offering similar resistance to the applied force. From a service level perspective all specimens behaved adequately and would be suitable for implementation.

Table 12: Comparison of Service Load Behavior

Specimen	Cracking Load	Load Ratio	Stiffness
	(kips)	*(Cracking Load/ Service Load)*	*(kip/in)*
Extended Bar	90	2.60	970
Embedded Plate Inverted-T	100	2.85	1460
Embedded Plate Tapered	110	3.10	1050
No Connection	60	1.87	940

Relative Strength and Ductility

From a strength standpoint the embedded plate tapered section behaved the best of all of the sections tested. It was the only connection and geometry combination that could not be tested to failure since its capacity exceeded that of the loading frame. The extended bar and embedded plate inverted-T specimens failed at similar loads (260 kips and 225 kips, respectively). The no connection specimen, as expected, had the lowest load at first cracking and at failure.
Ductility is the ability of a section to deform beyond its yield point without significant strength loss. (Wight and MacGregor, 2009) Table 13 shows the ultimate load and deflection ductility of each specimen. The ductility was calculated by dividing the measured specimen deflection just before failure by the deflection at yielding of the steel. (Park and Paulay, 1975) This table shows that the extended bar and two embedded plate connection specimens gave an indication of failure and therefore better ductile performance while the no connection specimen did not. The justification for the poor behavior in the no connection specimen is discussed later in this chapter.

Table 13: Comparison of Nominal Load and Ductility

Specimen	Strength (kips)	Ductility (Ultimate Deflection/ Yield Deflection)
Extended Bar	260	3.4
Embedded Plate Inverted-T	225	6.0
Embedded Plate Tapered	*300	*7.4
No Connection	90	1.1

* - Test Setup Limited Maximum Load to 300 kips
(Embedded Plate Tapered Specimen did not fail)

The deflection ductility ratio is based on the midspan deflection of the specimen at the largest recorded load step before failure divided by the midspan deflection of the specimen at the yielding of the connection steel. Connection steel yielding was determined from the strain gage readings in the Results chapter.

A tension-controlled section has a tension-reinforcement area such that when the beam reaches its nominal flexural strength, the net tensile strain in the extreme layer of tensile steel is greater than or equal to 0.005. If the net tensile strain is less than the yield strain of steel of 0.002 the section is considered compression-controlled. A net tensile strain between 0.002 and 0.005 is considered a transition-zone section. Appropriate φ factors are assigned based on the amount of strain exhibited in the extreme tension steel. (Wight and MacGregor, 2009) Figure 72 and Figure 76 in the Results chapter show that the tension steel in the embedded plate specimens exceeded 0.005 and both are therefore tension-controlled and can use the full φ factor for flexure of 0.9. Figure 70 and Figure 81 indicate that the tension steel in the extended bar and no connection specimens reached a strain of 0.002, but did not reach 0.005. Based on this data and according to ACI-318 these specimens are in the transitional region and should therefore have a reduced φ factor. (ACI-318, 2008) The plots for the extended bar and no connection specimens, however, are based off of the strain from only one location on each bar. It is possible that other locations experienced larger strains than what was captured by the strain gages.

A section analysis of each specimen indicated that all four tests were designed to be tension-controlled. This design can be found in Appendix G. Moreover, there was no observed crushing in the compression zone during testing. A more likely explanation is that the high, ductile strains of the extended bar and no connection specimens were localized away from where the strain gages were installed. This is reinforced by the fact that the significant crack opening,

and therefore high concentration of stress in the steel, occurred at locations away from the strain gages for both the extended bar and no connection specimens.

Durability

Each test specimen was subjected to cyclic loading after first cracking. This test protocol is detailed in the Experimental Methods chapter of this thesis. For each cyclic load test the number of cracks and crack lengths stabilized after a few cycles of load.

Assuming an uncracked connection area at service loads, the extended bar and no connection details will not be particularly susceptible to chloride ingress. The tension rebar above the joint for these two specimens have at least 2 in. of clear cover from the top of the exposed joint as per AASHTO bridge design guidelines. The same cannot be said for the two embedded plate connections. For those details the inclined plates and portions of the tension rebar attached to those plates are directly exposed to the elements as shown in Figure 87.

Figure 87: Plates Exposed to Elements

This exposure means that the welded connection attaching the precast members will be directly exposed to corrosion inducing chemicals. The onset of corrosion will likely cause concrete spalling above the connection and possibly reduce the service life of the system.

Constructability

Since the inverted-T bridge system was developed for rapid construction implementations it is desirable to optimize the system so that it is easy to fabricate, ship, and assemble the precast

elements. One key factor in the rapid construction concept is to minimize the impact of the construction sequence on traffic. There are three key points to consider for each specimen 1) cost of precast element fabrication, 2) ease of shipping, and 3) ease of assembly in field.

Constructability issues with the extended bar connection were part of the reason for this research. The extended bars created issues during fabrication, transportation, and installation. From a fabrication standpoint the extended bars made constructing and removing formwork a challenge. Complicated formwork was required to accommodate the bent bars that protruded from the girder's side. The bars also created issues during transportation as they would often get bent while in transit or during loading or unloading. In addition, the bars made placing the girders onsite a meticulous operation. On the positive side, the extended bar connection requires little work in the field if the bars arrive and can be installed undamaged. Workers simply install the shear cage into the region over the joint, tie the steel in the deck, and place concrete.

The two embedded plate connection details present similar issues. From a constructability perspective the geometry of the girders makes very little difference other than the forms for the tapered section are easier to remove. In either case there are no major modifications that need to be done to the formwork like for the extended bar girders. There are also no concerns with shipping the embedded plate girders since they don't have any protruding elements. The welded connection does, however, require additional in-field labor. With the current design, an in-field weld must be performed on 2 ft intervals along each longitudinal joint between adjacent girders. The practicality of such work is currently unknown. The details of the welding process are included in the Construction and Processes chapter and further discussions of this topic are included in the Conclusions chapter of this thesis.

The no connection detail was by far the simplest design tested. There are no special accommodations that need to be considered by either the precaster or the contractor. The precast girders are simply cast, shipped, and then positioned onsite. There are no connections that need to be constructed and standard tapered forms can be used with no slots or holes.

Geometry

The introduction of a tapered profile to the inverted-T concept produced some promising results. In the case of the direct comparison between the two embedded plate connections the specimen with the tapered profile required the application of 10 more kips to crack. It also

exceeded the 300 kip capacity of the frame, whereas the inverted-T profile failed at a load of 225 kips. Furthermore, the type of cracking in the tapered section was more desirable. See Figure 59 and Figure 60 in the Results chapter of this paper. The inverted-T profile failed at the joint which opened up dramatically at the failure load. The tapered specimen showed little damage at the joint, but rather had more crack distribution with the majority of the opening at the tapered interface between precast and CIP concrete.

Though it is difficult to directly compare, since one specimen failed and the other did not, the load-deflection behavior indicates that the tapered profile showed much better ductility than the inverted-T specimen. Figure 67 in the Results chapter illustrates this behavior. The load-deflection relationship in the two specimens was very similar up to a load of 190 kips. From that point the inverted-T profile deflected significantly with each additional load step while the tapered profile showed more linear behavior to the point of maximum load frame capacity.

Crack Control

The introduction of reflective cracking reduces the effective moment of inertia and in turn reduces the strength of the system. Reflective cracks also provide a path for chlorides to the interior steel of the members which can cause corrosion and shorter service life. Limiting the initiation of reflective cracking and controlling crack widths is a desirable quality for the inverted-T to inverted-T connection. Figure 88 shows the height of the highest crack in the specimen at each load step. Figure 89 shows the height of the crack at the inverted-T to inverted-T joint. These graphs are based on the data presented in Appendix D. The vertical origin for both plots is defined as the bottom of the specimen.

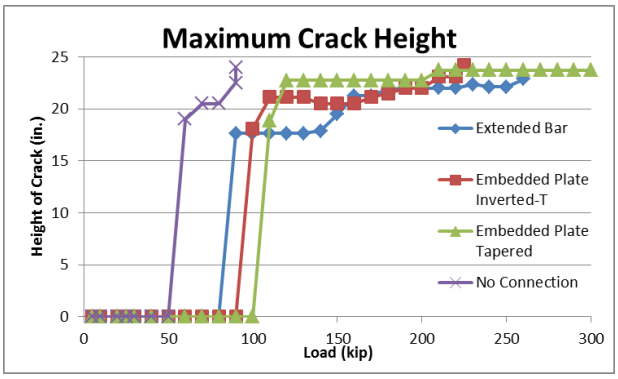

Figure 88: Maximum Crack Propagation Height in Each Specimen

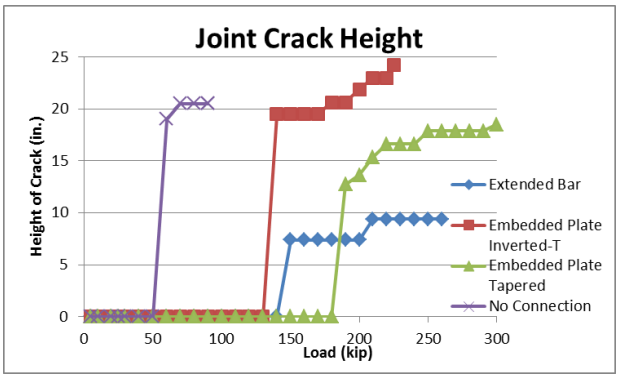

Figure 89: Crack Propagation Height at Joint in Each Specimen

Figure 88 shows that, in all cases, the first crack extended several inches vertically at initiation. Additionally, in all cases except the extended bar connection the cracks propagated to approximately their final height shortly after the formation of the first crack. Most of the additional cracking that took place after the formation of the first crack was in the form of new cracks not the propagation of the existing ones. As the specimens cracked, the neutral axis shifted up. This concentrated the compression force over a smaller area. Figure 89 shows behavior similar to that in Figure 88. The difference in Figure 89 is that for the two embedded plate connections the cracks did not extend vertically nearly as much at first crack. This indicates that the embedded plate connection possessed some crack arresting properties that the other two connections did not.

According to ACI standards, the maximum allowable crack width for dry air conditions is 0.016 in. This value reduces to 0.012 in. for humid, moist air and to 0.007 in. for conditions where deicing chemicals are used. (ACI-318, 2008) For a bridge to meet service requirements, the maximum crack width should not exceed these values where appropriate. Figure 90 shows the maximum crack widths recorded in each specimen throughout the loading process. Figure 91 shows the maximum crack widths up to the ACI limit for dry conditions. (Note the difference in scale of the two plots.) These figures are based on the visual crack documentation in Appendix D.

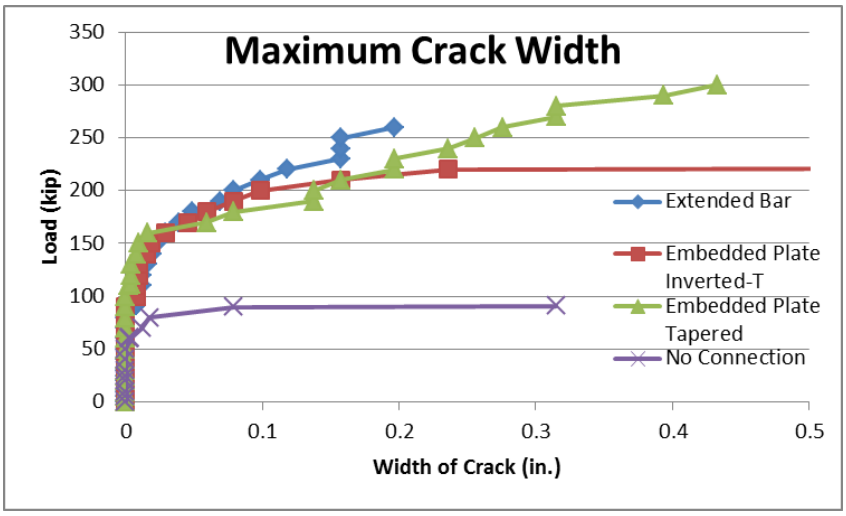

Figure 90: Maximum Crack Width in Each Specimen through Full Range of Applied Load

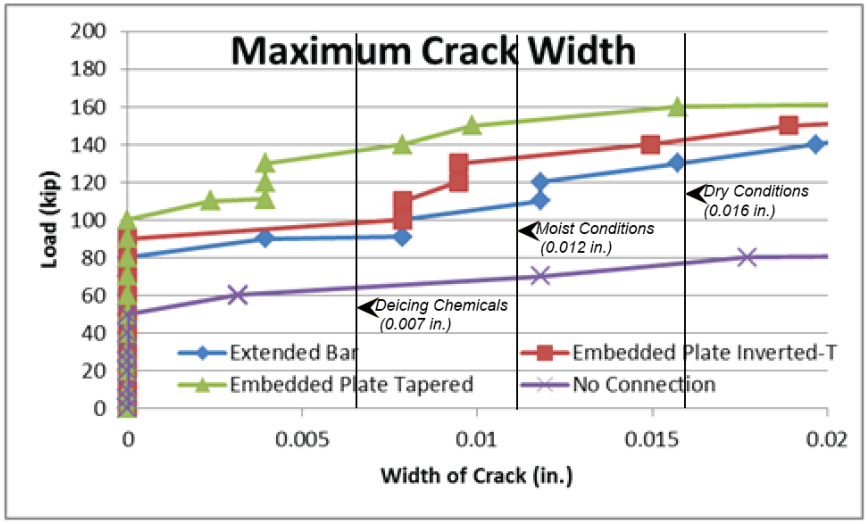

Figure 91: Maximum Crack Width in Each Specimen up to ACI Crack Width Limit

None of the specimens tested cracked under service load conditions. It was not until the loads presented in Table 14 that the specimens exceeded the ACI limits for maximum crack width under different conditions. This confirms that crack widths are not a serviceability issue for any of the specimens tested.

Table 14: Loads at Which Each Specimen No Longer Meets Service Requirements for Crack Width

Environment	Extended Bar	Embedded Plate Inverted-T	Embedded Plate Tapered	No Connection
	(kip)	*(kip)*	*(kip)*	*(kip)*
Dry	130	140	160	70
Moist	100	130	150	60
Deicing Chemicals	90	90	130	60

Cracking in the Extended Bar Specimen

The extended bar connection exhibited cracking during testing above the inverted-T to inverted-T joint as can be seen in Figure 58 in the Results chapter. The largest cracks were located at the vertical interface between precast and CIP concrete. The cracks did not propagate vertically as fast for this test as the other three. There was minimal cracking over the joint for this test. A small crack did initiate at the joint, but was arrested at the approximate location of the extended bars and then extended horizontally as the failure load approached. The instrumentation

attached to the extended bars showed no signs of rebar failure during any point of the loading regimen, even at failure of the specimen.

The lack of cracking over the joint indicates that the increased steel in that region due to overlap of extended bars prevented cracking. Figure 11 in the Specimen chapter of this paper shows this overlap. The majority of the cracking occurred at the interface where only one set of extended bars spanned. The cracking in this region also could suggest a loss of bond between the precast and CIP concrete.

Cracking in the Embedded Plate Inverted-T Specimen

Though cracking initiated at the vertical interface between precast and CIP concrete, the failure crack occurred directly through and above the inverted-T to inverted-T joint. The failure crack was a large crack that limited the strength of the specimen at ultimate load. By comparing cracking at the joint and the data from the strain gages attached to the tension bars welded to the embedded plates, it can be deduced that the significant crack opening over the joint was a direct result of the yielding of the tension connection steel. The strain gages in Figure 72 indicated that the tension steel attached to the embedded plates yielded at a load of about 140 kips. Shortly after this load the crack over the joint showed significant growth while the load deflection curve leveled out. Further discussion of the connection yielding is discussed in the Connection section of this chapter.

Cracking in the Embedded Plate Tapered Section

Cracking in the tapered section with embedded plate connectors initiated at the interface between precast and CIP concrete. This interface also had the largest crack during testing of the specimen. As stated before, this specimen did not fail under the maximum load applied. It is interesting to note, however, that the strains shown in Figure 76 indicated that the tension rebar attached to the embedded plates yielded in all connections between 140 and 190 kips. This is much different than the inverted-T test with the same connection which failed not long after the tension bars yielded. This indicates that either the geometry of the specimen or the inclusion of the drop T&S rebar had some effect in extending the capacity of the specimen.

Though none of the cracks opened to the extent of the joint crack in the embedded plate inverted-T specimen it is worth noting that the embedded plate tapered section did possess many more cracks, especially away from the longitudinal joint near the application of the two point loads. This indicates that the tapered profile better distributed the transverse strain throughout the specimen than the inverted-T design which simply opened up at one point to form a hinge. The tapered section exhibited no hinging, but instead demonstrated beam bending behavior throughout testing. Figure 65 illustrate this behavior.

Cracking in the No Connection Specimen

The specimen with a tapered geometry and no connection cracked at a lower applied load than the other tests. The first crack initiated at the inverted-T to inverted-T joint where there was the least effective moment of inertia. The crack that showed the greatest opening, however, formed through the thickest portion of the precast element. This is a result of the limited amount of tension steel in the precast girder in the transverse direction. In the three other cases the connection steel passed through the bottom of the precast girder to develop the tensile strength of the connection. In this specimen, however, since there was no connection steel to develop, the bottom row of steel across the girder was designed only to support the weight of wet CIP concrete on the flange. This is detailed in Figure 25 in the Test Specimens chapter of this thesis. The only steel running transversely across the bottom of the precast girder was #3 rebar spaced 18 in. on center. That limited amount of steel could not carry the tensile force that developed across the bottom of the specimen and the result was a large failure crack forming at a load of 90 kips. This is supported by the nature of the failure which occurred through the precast section of the test specimen. This behavior is discussed further in the next section. It is interesting to note that while the specimen failed at a low load it exhibited behavior similar to the other tests up until that point. There was very little ductility in the failure, which does raise some concern from a safety perspective.

Failure Modes

Structural failure refers to loss of the load-carrying capacity of structure or an individual component within a structure. Structural failure is initiated when the material is stressed to its

strength limit, thus causing fracture or excessive deformations. (Wight and MacGregor, 2009) For this project failure was determined at the point in which the test specimen could no longer carry additional applied load.

Extended Bar Connection Failure

The extended bar connection failed as a result of a large crack at the vertical interface between precast and CIP concrete. As mentioned before, this behavior is most likely due to the lesser amount of connection steel at that location in comparison to the other regions of the CIP portion or a bond failure at the interface.

Embedded Plate Connection Failure

The tension steel yielded for both specimens tested with embedded plate connections. In the case of the straight web inverted-T profile the bars yielded at 140 kips as shown in Figure 72. The rebar in the tapered section yielded between 140 and 190 kips as shown in Figure 76. The point of rupture for both of the connections in the inverted-T profile was in the tension rebar just behind the embedded plate. Figure 92 shows a close-up view of the fracture. There was no rupture in the tapered profile test.

Figure 92: Embedded Plate Inverted-T Connection Failure (photo)

The weld attaching the drop-in bar between the two plates held for all of the connections. This weld was designed to be the strongest point in the connection. This eliminated any variability that might have come from using different sized drop-in bars and welding processes. The reason that the bars in the inverted-T profile ruptured and the ones in the tapered profile didn't is most likely a result of strain distribution. As discussed earlier, the strain was more equally distributed through multiple cracks in the tapered section profile. In the inverted-T test all of the strain was localized at the joint and thus at the weakest point in the embedded plate connection. The weakest point of the connection happened to be in the tension bar directly behind the plate. The weld between that bar and the plate was completed as a full-penetration weld and had a higher capacity than the tension bars. Initial inspection indicated that the connection had failed at the weld, but upon further investigation the shape of the bar at failure indicated the location of rupture.

No Connection Failure

The performance of the no connection specimen was satisfactory from a service level perspective, yet the failure behavior was unsettling. The design of the transverse bottom layer of steel in the precast girder was under designed as an oversight. The drop bar could not carry the transverse tensile force once the bar bent upwards along the tapered face of the precast girder because of the reduced depth of the force couple. This made the tensile force shift to the transverse bottom layer of steel in the girder. The #3 bars at 18 in. spacing were not designed to carry such force. This resulted in the failure of the specimen through the girder section. This oversight limited what conclusions could be drawn about this system. If bars had been designed to carry that force it is likely that the ultimate capacity of the specimen would have been much higher. By any respect it would have been more beneficial to force the failure to occur near the joint to more directly compare this configuration to the others tested. This idea is discussed further in the Conclusions and Recommendations Chapters of this thesis.

Strain Gage Results

The strain gages placed within the specimens both reinforced the visual observations made during testing and provided new information about the behavior of the profiles under loading. The cracking loads indicated by the gages in the lower elevation regions of the specimens closely reflected the loads at which cracks were first visually identified.

Extended Bar

The strain gages in the extended bar connection indicated cracking at a load 10 kips less than what was identified visually. Figure 70 shows that three of the gages attached to the extended bars on the left specimen indicated cracking at 80 kips. A gage located 9 in. above the bottom of the precast in location 9”-3 captured this behavior as well. As Figure 70 in the Results chapter indicates the strain in each of the extended bars was similar. This shows that there was good distribution of stress across the bottom of the section and that each of the extended bars was carrying a fairly equal share of the tensile force. This behavior is favorable to a situation

where one side of the specimen strains significantly more than the other due to an unbalanced load distribution.

Figure 71 shows the shift of the compression zone in the top of the specimen. The gages in that plot were positioned 22.5 in. above the bottom of the precast section. Up to a load of around 160 kips all of the gages were in compression. As the cracks began to propagate through the section the neutral axis moved upward. At 160 kips the neutral axis shifted to a point that resulted in a decrease in compression in the top mat of T&S steel. At a load of around 250 kips, just before failure, the neutral axis passed above that region and the bars went into tension. This indicates that even though the top mat of reinforcing steel was in tension the specimen was still able to support the applied load.

Embedded Plate Inverted-T

The gages for the embedded plate inverted-T test produced the most concise results with the fewest scatter of all of tests performed. The biggest issue with the gages in this test was that the four gages attached to the tension rebar on the right side of the welded connection were destroyed when the girders were cast. The gages attached to the tension rebar behind the embedded plates on the left side, however, did capture some interesting behavior in the specimen.

As Figure 72 shows all four gages indicated cracking at the same point at around 110 kips. From that point the four gages indicated different magnitudes of strain up to a load of around 180 kips. It is at that load that the gages all show a drop in strain. Initial observation of this behavior suggested that the bars have ruptured at this load. This, however, is not the case as the specimen was able to carry an additional 45 kips of load. A more likely inference is that at the load of around 180 kips the bond between the strain gages and the rebar failed. Debonding of the gages from the rebar creates an immediate drop in strain reading in the gages. By this reasoning any behavior indicated beyond 180 kips in Figure 72 should be ignored.

The gages located 9 in. above bottom of precast in Figure 73 show that the crack remained almost exclusively along the longitudinal joint. The three gages (9”-1, 9”-2, and 9”-3) that were located along the center of the section all indicate cracking while the two offset gages (9”-2L and 9”-R) show no variance in strain. Though most of the cracking in the CIP region was

limited to the area directly over the joint this does not mean that there was no other cracking in the constant moment region. The two gages in Figure 74 that were located above the interface indicate that cracking did occur there between 110 and 120 kips. This is supported by the photo in Figure 59. The behavior of the top mat of T&S steel displayed in Figure 75 is similar to that of the extended bar connection. This region shows initial compression followed by a shift towards extreme tension near the failure load.

Embedded Plate Tapered

The gages attached to the tension steel behind the embedded plate connection in the tapered embedded plate test in Figure 76 showed behavior similar in nature to that of the inverted-T geometry test of the same connection. Like in the inverted-T profile all strain data beyond where the gages indicate debonding should be ignored.

Unlike the inverted-T test the tapered profile did crack in more than one place in the CIP region. Figure 77 indicates that all five locations along the 9 in. elevation cracked. This signifies that the use of the tapered profile helped spread the strain throughout that region more effectively. In the inverted-T profile all of the strain was concentrated in one large crack directly over the joint. In the tapered profile, however, the one large and eventual failure crack was replaced by a series of smaller cracks throughout the CIP region over the flanges. Moreover, the vertical shift of the neutral axis was limited in this test. As Figure 78 shows the strain in the top mat of T&S steel remained increasingly compressive throughout the 300 kips of applied load. This indicates that the distribution of stress helped the specimen maintain strength.

No Connection

The responses of some of the gages in the no connection test are erratic and may not appropriately describe the behavior of the test. First off, the behavior of the 9”-2L gage in Figure 79 does not seem consistent with what would be expected in this region. It is believed that the large spike in data is effectively an error in the gage as it does not describe anything the specimen actually exhibited and the data points before and after that point report data similar to one another. Regardless of that odd point the rest of the gages do suggest that the majority of cracking in the CIP region occurred directly over the girder to girder joint. With the exception of

the one outlier point shown in Figure 79: Strain in Row of Gages 9 in. Above Bottom of PrecastFigure 79, neither of the two offset gages indicated cracking. There is also indication that one transverse face of the specimen experienced more cracking than the other. The gage labeled 9”-3 shows little strain by comparison to the two gages across the joint. This behavior is supported at the level 12 in. above the bottom of precast by Figure 80. In this figure gage 12”-1 indicates significantly more strain than gage 12”-2. This signifies that the specimen did not equally distribute the load in the longitudinal direction. This is peculiar because Figure 81 shows the gages in the drop bars that were designed to carry the tension force in this specimen all show similar values of strain. Since the drop bars are all the same size and material this strain relationship indicates that they are under the same stress and thus carrying the same tensile force. The behavior of the gages in the top mat of T&S steel in Figure 82 indicates that the neutral axis never approached that layer of steel in this test.

Comparisons

Every specimen had a layer of five gages located nine inches above the bottom of the precast girder as shown in Figure 30 in the Experimental Methods chapter of this thesis. In the center of that pattern was gage 9”-2. Figure 83 shows the amount of strain directly over the longitudinal joint in the center of the specimen. This gage shows the inability of the embedded plate inverted-T specimen to distribute stresses compared to the other three. Looking at the slopes of the regions of the graphs after cracking provides insight to the ability of the geometry and connection combination to arrest cracks once they form. The embedded plate tapered section cracked at a similar load to the embedded plate inverted-T specimen, but was better able to restrain that crack from opening. The extended bar connection also did a better job of arresting the crack width opening in the region over the inverted-T to inverted-T joint. Much like what the other instrumentation indicated, after the formation of the first crack, the no connection detail showed significant crack growth with each additional load step. All of this behavior did, however, occur at loads well above the service level and should be considered as such.

Figure 84 shows the strain profile for each specimen at a load of 30 kips. The selected load is an arbitrary point within the linear-elastic range that exceeds the service level load. This plot shows that the strain profile for each of the systems is on the same magnitude and that the

specimens behaved similarly. The linearity of the strain indicates monolithic behavior of all of the specimens before cracking. This supports the assumptions made in design and in the finite element model.

Extended Bar Trial Specimen

As noted in the Construction and Processes chapter of this thesis a trial specimen was created because a mistake made in the girder casting process. This specimen was instrumented with only LVDTs and wirepots and was used primarily as a practice to work out any issues in the testing process. The specimen was put through the same loading regimen as the other tests and external cracking was documented accordingly. The primary differences between this specimen and the other extended bar test were the concrete mix and quality of flanges and roughened surfaces. From a testing perspective the only real difference was the absence of strain gages on the interior of the specimen.

The results of the trial specimen were surprising and if nothing else created many more questions about the behavior of the transverse sub-assemblage connections. Despite the poor quality of the exterior of the girder components the entire specimen actually showed better performance than the supposedly better quality specimen. The trial specimen's capacity exceeded what the frame could apply. The extended bar specimen, however, could not carry any load past 260 kips. This is counterintuitive on a few levels. First of all, the trial specimen experienced its first crack at a load 10 kips below the extended bar test. In addition, the extended bar failed at the vertical interface between the precast girder and the CIP deck. It is logical that that the extended bar specimen with its roughened surface would have better bond at this interface and thus better resistance to separation. The trial specimen showed significant crack opening at that interface, but such opening did not restrict the specimen from carrying more load through the 300 kip range tested. As Figure 93 shows the two specimens behaved almost identically up until a load of 200 kips. They maintained similar behavior to 260 kips until the extended bar specimen failed.

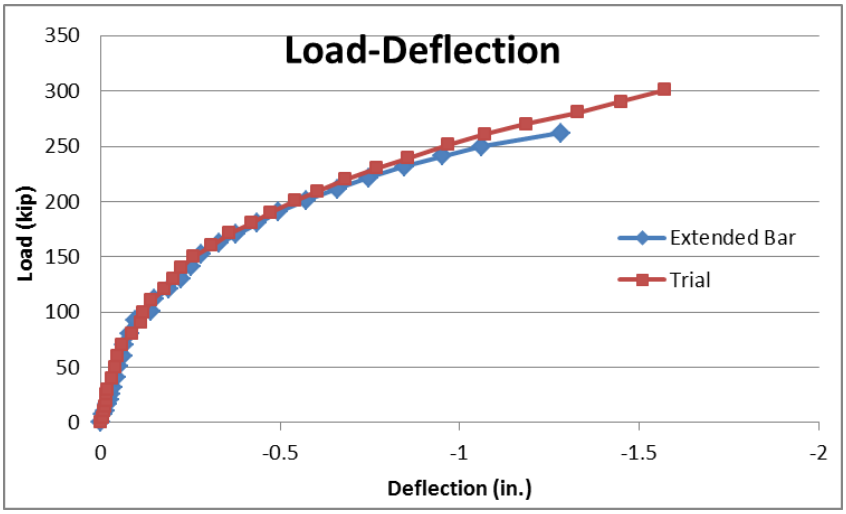

Figure 93: Comparison of Load-Deflection Behavior between Extended Bar and Trial Specimens

The one advantage the trial specimen possessed over the extended bar specimen was a stronger deck concrete mix. The CIP portion of the trial specimen was cast with the two embedded plate specimens. The strengths of this mix are listed in Table 5 in the Results chapter of this paper. The behavior of the cracking at failure of the extended bar connection indicates that deck concrete strength could have been the controlling factor for capacity. As the extended bar specimen approached failure, the deck concrete over the joint exhibited a web-like pattern of cracking. At that load, cracks extended in all directions throughout the CIP concrete. These cracks did not extend into the precast girder. This indicates that the concrete in that region did not have the tensile strength to handle the applied stress at that load.

The comparison of behavior of the deck concrete in those two tests raises some questions concerning the applicability of the other tests run in this research. If the deck concrete strength is such a crucial component then the reasonableness of comparing specimens with different deck strengths becomes questionable. This result indicates that it is possible that the extended bar and no connection specimens might have behaved better than recorded if the deck concrete mix had reached its proposed strength. This notion, however, most likely applies to the extended bar connection due to the fact that the no connection specimen failed in the precast girder. Though it is possible that increasing the strength of the deck concrete would have increased the load that first induced cracking, it is doubtful that it would have added any ultimate capacity to the no connection test.

The difference in capacity between the trial and extended bar specimens indicates one of two things. The first being the differences in the specimens discussed in the segment above and the second being variance of specimens. In every case only one test of each profile was completed. The limited sample size leaves the tests susceptible to unidentified variance. It is possible that any of the profiles could have tested stronger or weaker on average than what was recorded as part of this research.

Summary

The objective of this research is to recommend an improved inverted-T system for sub-assemblage and full-scale testing. The data and discussions presented show the benefits and detriments of each geometry-connection combination. Table 15 includes a qualitative summary of each of the specimens for each of the critical system characteristics. A rating of Acceptable means that the specimen met the requirements for the given characteristic. A rating of Poor designates that the specimen did not meet requirements or expectations. A rating of Questionable indicates that further study must be completed to provide a suitable evaluation of the given characteristic.

Table 15: Evaluation of Each Specimen

Characteristic	Extended Bar	Embedded Plate Inverted-T	Embedded Plate Tapered	No Connection
Service Load Behavior	Acceptable	Acceptable	Acceptable	Acceptable
Strength	Acceptable	Acceptable	Acceptable	Acceptable
Ductility	Acceptable	Acceptable	Acceptable	Questionable
Durability	Acceptable	Questionable	Questionable	Acceptable
Constructability	Poor	Questionable	Questionable	Acceptable

Table 15 shows a comparison of each of the specimens based on how each one can meet the needs of the bridge system. The extended bar specimen was deemed acceptable for everything except constructability. The poor constructability of this system was known before any testing was conducted, but it was beneficial to include this specimen as a control to represent the current state of the inverted-T system.

Despite the several advantages of the tapered profile, the two embedded plate specimens are equally applicable for implementation based on their similar weaknesses. Both tests

performed much better than needed from a service and ultimate load standpoint that the advantages of the tapered profile are relatively insignificant compared to the inverted-T. The uncertainty that comes with the embedded plate connection limits the applicability of either of these systems. As discussed earlier in this chapter, the exposed steel of the connection raises concerns in terms of durability. Also, the feasibility of performing the in-field welds in a timely manner is questionable.

Although it had the lowest ultimate strength, the no connection test was strong enough to be acceptable for both service load and ultimate conditions. The 60 kip cracking load is well beyond the 25 kip service load. There was little ductility in the system and this is a concern. However, the main cause of the low ductility lies in the nature of the failure. The reason for the failure was due to an oversight in the design. By adjusting the design to meet the demands of the system the likelihood of increasing both the ultimate capacity and ductility is great. Since this system is by far the easiest to construct, further testing of this system is recommended. The goal of the further testing will be to improve the ultimate strength and ductility by increasing the amount of steel in the bottom layer of transverse reinforcement. By adding steel to this region the specimen should better be able to carry the tensile force and prevent the failure crack from forming through the precast section. This should allow the specimen to carry additional load until it fails in the region over the longitudinal joint like in the other specimens of this testing.

CONCLUSIONS

The objective of this research was to develop an improved inverted-T to inverted connection. Based on the analysis of the results from the sub-assemblage tests, the following conclusions are drawn.

- Small to medium size course aggregates and a high concrete slump are required to properly form the flanges of the precast girders. In addition, consolidation of the concrete in the flange can be improved by using open formwork at the flange tip and installing the formwork when the concrete is properly consolidated in the flange.
- All of the specimens tested met the service load requirements for lane, tandem, and truck loads set forth by AASHTO.
- The embedded plate inverted-T specimen performed similarly to the extended bar specimen. The embedded plate connection is a pursuable option for further study and implementation into the inverted-T bridge system. However, durability and constructability of the embedded plate connection needs further evaluation.
- The embedded plate tapered profile generally performed better than the embedded plate inverted-T profile and is an acceptable alternative to the non-tapered system.
- The strength of the no connection system was controlled by the small amount of reinforcement in the bottom of the precast section, not by the strength at the inverted-T to inverted-T joint. The strength of the no connection system can be significantly improved by increasing the amount of reinforcement in the bottom of the precast section.
- All connections displayed acceptable performance under the post-cracking repeated load regime.

RECOMMENDATIONS

Based on the analysis of the results from the sub-assemblage tests, the following recommendations are made

1. Concrete quality should be closely monitored and controlled. Maximum aggregate sizes greater than 1/2 in. should not be used for the precast girders.
2. Any implementation of the current system of extended bar connections include the use of a tapered section geometry.
3. The no connection concept should be considered for use in the U.S. 360 bridge. Additional testing and modification to the detail, however, should be completed before implementation. The under design of the transverse tension steel, however, raised some concerns from an ultimate strength and ductility perspective. A few practical options exist for further testing. Based off calculations made to resist the transverse tensile force these options include #4 bars at 6 in. spacing, #5 bars at 8 in. spacing, or #6 bars at 12 in. spacing. These options should be considered to optimize the transfer of the tensile force across the bottom of the section.
4. Testing should be conducted to monitor the behavior of the no connection sub-assemblage under conditions that include shear. Though the finite element model indicated negligible worst-case shear for the system there would be value in documenting the behavior of a transverse sub-assemblage connection under both service level and ultimate shear stresses.
5. Future studies should consider hollow core beams. The self-weight of the girder section adds a significant amount of stress to the system. The inclusion of holes in the web region of the girders would reduce the self-weight and the stresses associated with that weight.

REFERENCES

American Association of State Highway Transportation Officials (AASHTO). *AASHTO LRFD Bridge Design Specifications, Fifth Edition*. Washington, D.C.: 2010.

ASTM C39/39M-09a,"Standard Test Method for Compressive Strength of Cylindrical Concrete Specimens", ASTM International, West Conshohocken, PA, 2009.

ASTM C192/C192M-09,"Standard Practice for Making and Curing Concrete Test Specimens in the Laboratory", ASTM International, West Conshohocken, PA, 2009.

ASTM C469-02,"Standard Test Method for Static Modulus of Elasticity and Poisson's Ratio of Concrete in Compression", ASTM International, West Conshohocken, PA, 2002.

ASTM C496/C496M-04,"Standard Test Method for Splitting Tensile Strength of Cylindrical Concrete Specimens", ASTM International, West Conshohocken, PA, 2004.

ASTM C512/C512M-10,"Standard Test Method for Creep of Concrete in Compression", ASTM International, West Conshohocken, PA, 2010.

Bell, Charles M., Catherine F. French, and Carol K. Shield. *Application of Precast Decks and Other Elements to Bridge Structures*. Rep. St. Paul MN: Mn/DOT, 2006. Print. MN/RC-2006-37.

Building Code Requirements for Structural Concrete (ACI 318-08) and Commentary. Second Printing ed. Farmington Hills, MI: American Concrete Institute, 2008. Print.

Culmo, Michael P. *Accelerated Bridge Construction - Experience in Design, Fabrication and Erection of Prefabricated Bridge Elements and Systems*. Rep. McLean, VA: FHWA, 2011. Print. FHWA-HIP-12-013.

Culmo, Michael P. *Connection Details for Prefabricated Bridge Elements and Systems*. Tech. Mclean, VA: FHWA, 2009. Print. FHWA-IF-09-010.

French, C. E., C. K. Shield, D. Klaseus, M. Smith, and W. Eriksson. *Cast-In-Place Concrete Connections for Precast Deck Systems*. Rep. NCHRP, 2011. Web-Only Document 173.

Gonzalez, David. *Contract Employees Lower a Pre-fab Bridge Beam into Place on the Hwy 72 Bridge in District 2.* 2005. Photograph. Minnesota. *Newsline*. Mn/DOT, 5 Oct. 2005. Web. 1 May 2012.

Hill, Jeffrey C., and Christopher M. Lowe. *Route 360 Over Chickahominy River Bridge Replacements*. Rep. Richmond: Central Office Structure & Bridge Division, 2010.

Park, R. and Ruitong, D., 1988. *Ductility of Doubly Reinforced Concrete Beam Section, ACI Structural Journal* 85: 217-225.

Park, R., and T. Paulay. *Reinforced Concrete Structures*. New York: Wiley, 1975. Print.

Ralls, Mary Lou. "Framework for Prefabricated Bridge Elements and Systems (PBES) Decision-Making." *FHWA* Spring (2006). Print.

Ralls, Mary Lou, Ronald D. Medlock and Sharon Slagle. "Prefabricated Bridge National Implementation Initiative." *2002 Concrete Bridge Conference*.

Ralls, Mary L., Michael D. Hyzak, Ronald D. Medlock, and Lloyd M. Wolf. *Prefabricated Bridges - Current U.S. Practice and Issues*. Rep. New Brunswick, NJ, 2004. Print. FHWA/AASHTO Second National Prefabricated Bridge Elements & Systems Workshop.

Russell, Henry, Mary Ralls, and Benjamin Tang. "Part 3: Concrete Bridges: Prefabricated Bridge Elements and Systems in Japan and Europe." *Transportation Research Record* 1928.1 (2005): 101-09. Print.

Smith, Matthew, Whitney Eriksson, Carol Shield, and Catherine French. *Monitoring and Analysis of Mn/DOT Precast Composite Slab Span System (PCSSS)*. Rep. St. Paul, MN: Mn/DOT, 2008. Print. MN/RC 2008-41.

Wight, James K., and James G. MacGregor. *Reinforced Concrete Mechanics and Design*. Fifth ed. Upper Saddle River, NJ: Pearson Prentice Hall, 2009. Print.

APPENDIX A - SUB-ASSEMBLAGE REINFORCEMENT DETAILS

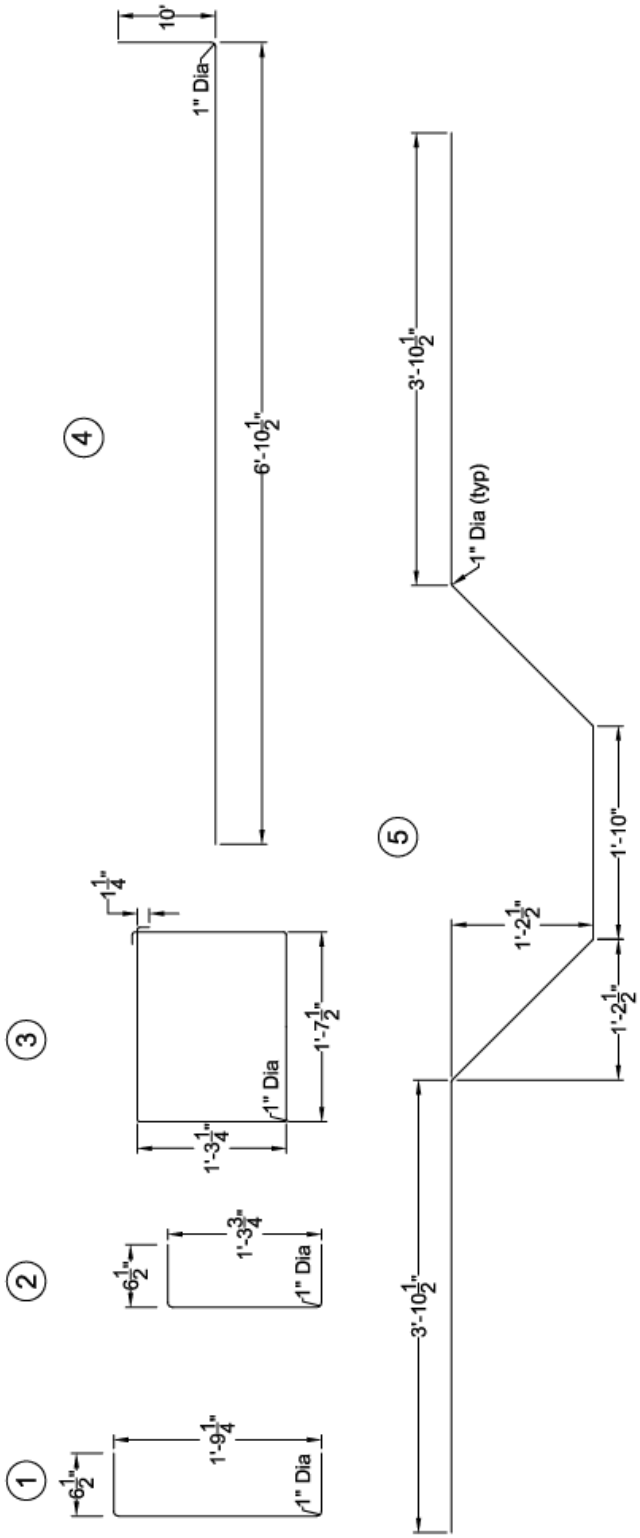

Figure A-1: Detail of Bent Rebar Shapes

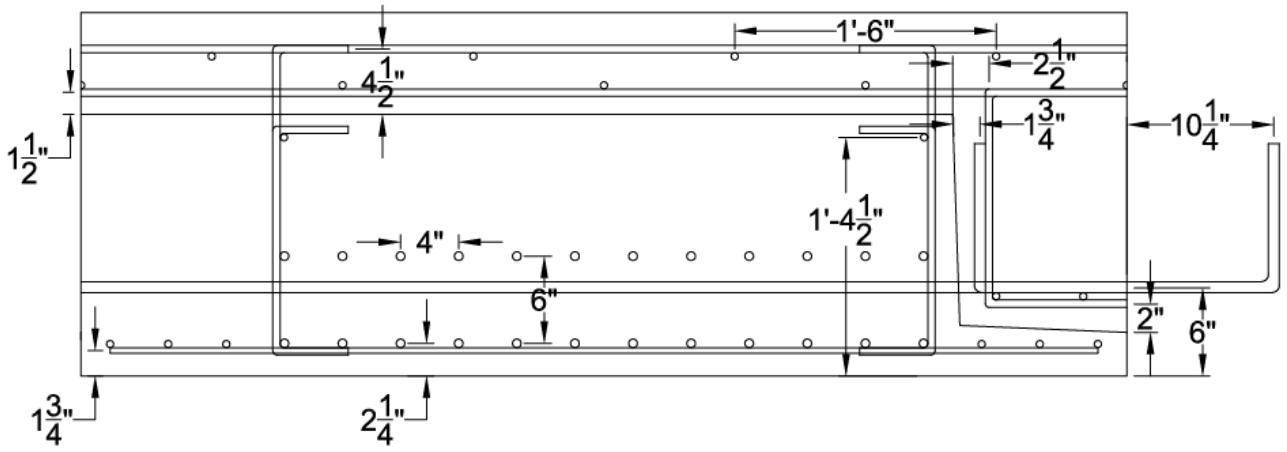

Figure A-2: Steel Location for Extended Bar Specimen

Table A-1: Rebar Schedule for Extended Bar Specimen

Description	BAR	NO.	SIZE	TYPE	LENGTH (in)	WEIGHT (lbs)
T&S (Transverse)	A	8	#4	STR.	142	7.9
T&S (Longitudinal)	B	20	#4	STR.	46	2.6
Tall Shear Stirrups	C	28	#4	1	35	1.9
Short Shear Stirrups	D	28	#4	2	29.5	1.6
Flange Steel (Longitudinal)	E	12	#4	STR.	46	2.6
Flange Steel (Transverse)	F	6	#3	STR.	68	2.1
Cage	G	4	#4	3	74	4.1
Lifting Hooks	H	6	#4	STR.	46	2.6
Minnesota Connection	I	8	#6	4	92.5	11.6

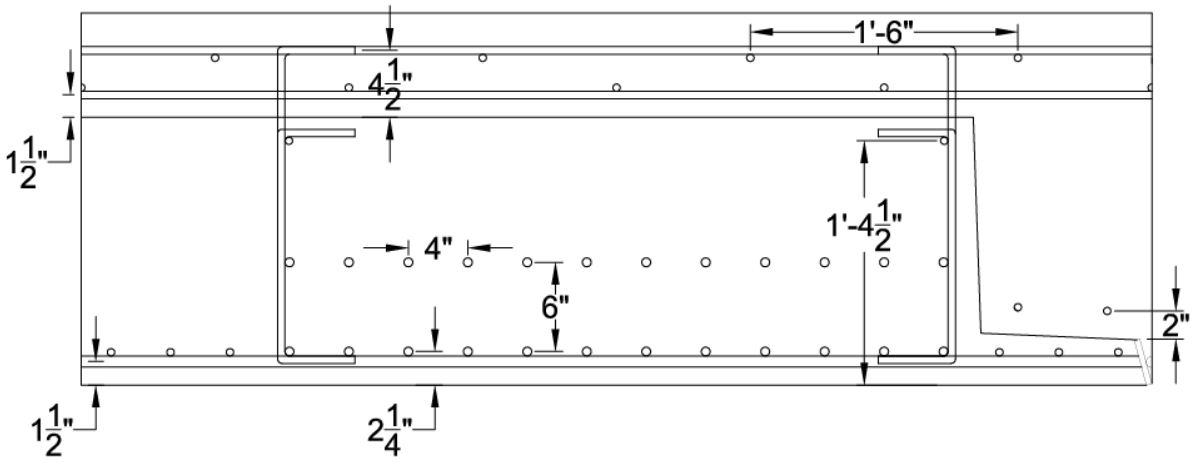

FigureA-3: Steel Location for Embedded Plate Inverted-T Specimen

Table A-2: Rebar Schedule for Embedded Plate Inverted-T Specimen

Description	BAR	NO.	SIZE	TYPE	LENGTH (in)	WEIGHT (lbs)
T&S (Transverse)	A	8	#4	STR.	142	7.9
T&S (Longitudinal)	B	20	#4	STR.	46	2.6
Tall Shear Stirrups	C	28	#4	1	35	1.9
Short Shear Stirrups	D	28	#4	2	29.5	1.6
Flange Steel (Longitudinal)	E	12	#4	STR.	46	2.6
Lifting Hooks	F	6	#4	STR.	46	2.6
Flange Steel (Transverse)	G	6	#3	STR.	68	2.1
Vector Connector Tie (A706 Steel)	H	8	#6	STR.	70	8.8

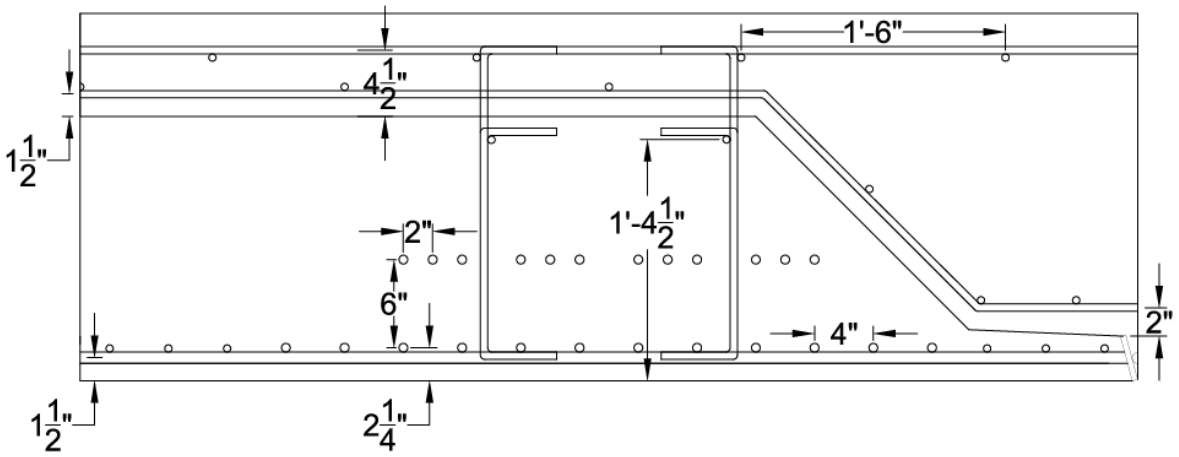

Figure A-4: Steel Location for Embedded Plate Tapered Specimen

Table A-3: Rebar Schedule for Embedded Plate Tapered Specimen

Description	BAR	NO.	SIZE	TYPE	LENGTH (in)	WEIGHT (lbs)
T&S (Transverse)	A	4	#4	STR.	142	7.9
T&S (Longitudinal)	B	20	#4	STR.	46	2.6
Tall Shear Stirrups	C	28	#4	1	35	1.9
Short Shear Stirrups	D	28	#4	2	29.5	1.6
Flange Steel (Longitudinal)	E	12	#4	STR.	46	2.6
Flange Steel (Transverse)	F	6	#3	STR.	68	2.1
Lifting Hooks	G	6	#4	STR.	46	2.6
Vector Connector Tie (A706 Steel)	H	8	#6	STR.	70	8.8
Bent T&S (Transverse)	I	4	#4	5	156	8.7

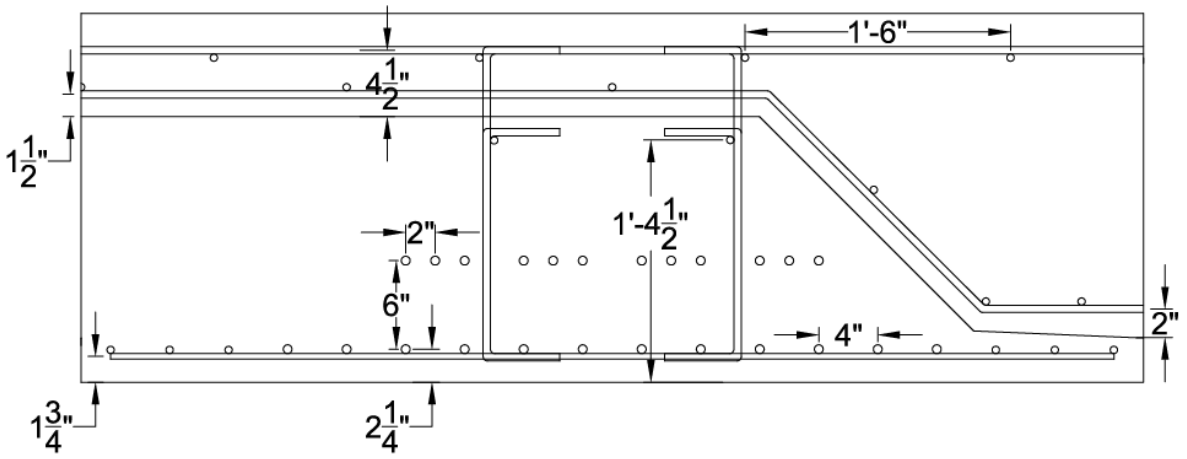

Figure A-5: Steel Location for No Connection Specimen

Table A-4: Rebar Schedule for No Connection Specimen

Description	BAR	NO.	SIZE	TYPE	LENGTH (in)	WEIGHT (lbs)
T&S (Transverse)	A	8	#4	STR.	142	7.9
T&S (Longitudinal)	B	20	#4	STR.	46	2.6
Tall Shear Stirrups	C	28	#4	1	35	1.9
Short Shear Stirrups	D	28	#4	2	29.5	1.6
Flange Steel (Longitudinal)	E	12	#4	STR.	46	2.6
Lifting Hooks	F	6	#4	STR.	46	2.6
Flange Steel (Transverse)	G	6	#3	STR.	68	2.1
Bent T&S (Transverse)	H	4	#6	5	156	19.5

Note: Each specimen contains 48 – 46 in. long cut pieces of 0.6 in. prestressing strand. (24 per girder)

APPENDIX B - CONCRETE MIXTURE DESIGN

CIP Deck Concrete Mix

The concrete mix for the CIP deck was based off of studies done in the summer of 2011. During that time four different mixes were proposed for investigation. Each of the test mixes were designed for a compressive strength of 4,000 psi. The goal of this testing was to identify a mix that produced minimal shrinkage and maximum creep. Minimal shrinkage was desirable to reduce any cracking in the CIP section as a result of differential shrinkage. Since the girder sections were to be aged before the placement of the deck the majority of the shrinkage in the girders would have already occurred. Any shrinkage in the deck creates tensile stress in the deck which can lead to cracking. Since completely eliminating the differential shrinkage issue is not possible, there is benefit in providing a mix that allows for high levels of creep. If the mix can creep under the internal forces caused by the differential shrinkage the tensile stress in the deck can be somewhat relieved. Alleviating this stress reduces the likelihood and magnitude of any cracks from differential shrinkage.

From the testing performed on the deck mixes, which is further detailed in a paper by Achmaa Vaanjilnorov (unpublished data). The design that provided the best properties from that study for this application was the VDOT standard A-4 mix. This mix is detailed in Table A-5.

Table A-5: Mix Proportions for CIP Deck

Material	Quantity per yd^3
#57 Stone	1853 lbs
Nat. Sand	1168 lbs
Cement	533 lbs
Fly Ash	133 lbs
Water	250 lbs
Water Reducer 161	34 oz
Midrange Water Reducer	13 oz
Water/Cement Ratio	0.38

Precast Girder Concrete Mix

The mix design for the girders was selected based on previous research conducted at Virginia Tech. The mix is detailed in Table A-6.

Table A-6: Mix Proportions for Precast Girders

Material	Quantity per yd^3
#78 Stone	1544 lbs
Nat. Sand	1502 lbs
Cement	675 lbs
Water	267 lbs
Microsilica	54 lbs
SIKA 2100	27 oz
Retarder	24 oz
Water/Cement Ratio	0.36

Concrete Strengths

Girder Mix 1 and Deck Mix 1 apply to the two embedded plate specimens and Girder Mix 2 and Deck Mix 2 apply to the extended bar and no connection specimens.

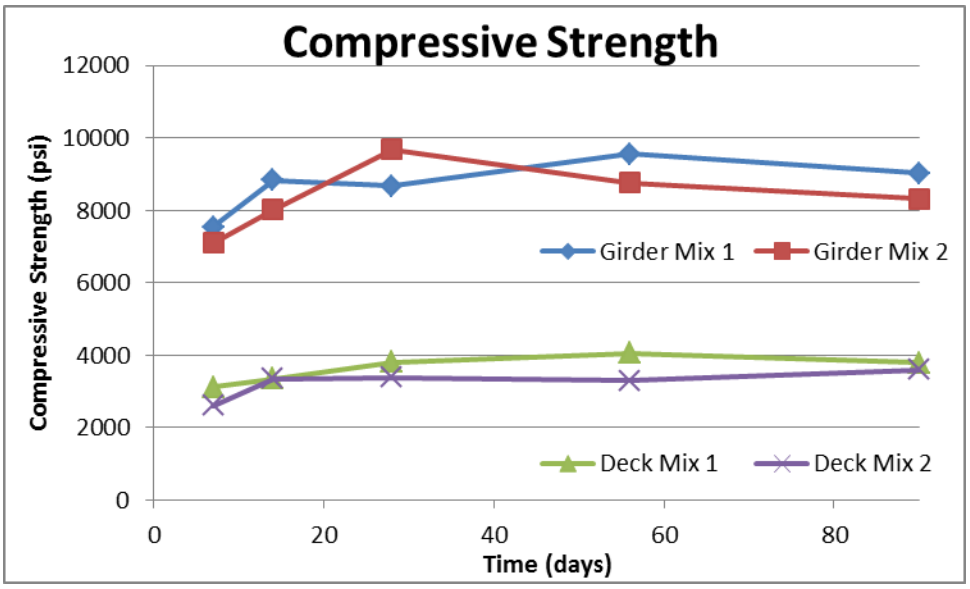

Figure A-6: Compressive Strength Gain with Time

Table A-7: Concrete Compressive Strengths

Day	Girder Mix		Deck Mix	
	1	2	1	2
	(psi)	*(psi)*	*(psi)*	*(psi)*
7	7530	7100	3110	2610
14	8830	8010	3340	3340
28	8670	9680	3810	3380
56	9550	8750	4050	3300
90	9020	8310	3780	3590

Table A-8: Concrete Modulus of Elasticity Values

Day	Girder Mix		Deck Mix	
	1	2	1	2
	(ksi)	*(ksi)*	*(ksi)*	*(ksi)*
7	5090	4860	4120	3110
14	5250	5370	3150	3710
28	5380	5600	4190	3110
56	5810	5510	4390	3360
90	5980	5710	5080	3370

Table A-9: Concrete Tensile Strengths

Day	Girder Mix		Deck Mix	
	1	2	1	2
	(psi)	*(psi)*	*(psi)*	*(psi)*
7	730	718	360	280
28	910	700	430	360
90	750	830	410	340

APPENDIX C - U.S. 360 SUPER-STRUCTURE DESIGN

1. Introduction

2. Materials, Geometry, Loading information and Load Factors

3. Loads

4. Moments and Shears

5. Restraint Moments and Losses

6. Flexural Stress Check

7. Prestress Losses

8. Stresses Due to Prestress

9. Service Stress Check

10. Flexural Strength Check

11. Vertical Shear Design

12. Longitudinal Reinforcement Check

13. Interface Shear Design

14. Spalling Forces

15. Transverse Load Distribution

16. Reflective Crack Control

17. Bottom Flange Reinforcement

1. Introduction:

This worksheet serves as the preliminary design of Route 360 over the Chickahominy River bridge replacements. All calculations are based on the two bridges that were part of a study done at Virginia Tech. The format of this worksheet is based on work done at the University of Minnesota for work done on NCHRP Project 10-71.

2. Materials, Geometry, Loading information and Load Factors:

Materials:

Concrete:

$f_{c\_b} := 8ksi$ *Compressive strength of precast prestressed inverted T-beam at 28 days*

$f_{ci\_b} := 5ksi$ *Compressive strength of precast prestressed inverted T- beam at transfer of prestressing force*

$\gamma_b := 0.150\frac{kip}{ft^3}$ *Unit weight of precast prestressed Inverted T-beams in kips per cubic feet*

$f_{c\_d} := 4ksi$ *Compressive strength of CIP concrete at 28 days (d for deck)*

$\gamma_d := 0.150\frac{kip}{ft^3}$ *Unit weight of CIP concrete in kips per cubic feet*

$K1 := 1.0$ *Correction factor for source of aggregate*

$E_b := 33000K1\cdot\left(\frac{\gamma_b}{\frac{kip}{ft^3}}\right)^{1.5}\cdot\sqrt{f_{c\_b}\cdot ksi} = 5422.5ksi$ *28 day modulus of elasticity of precast concrete*

$E_{bi} := 33000K1\cdot\left(\frac{\gamma_b}{\frac{kip}{ft^3}}\right)^{1.5}\cdot\sqrt{f_{ci\_b}\cdot ksi} = 4286.8ksi$ *Modulus of elasticity of precast concrete at transfer*

$E_d := 33000K1\cdot\left(\frac{\gamma_d}{\frac{kip}{ft^3}}\right)^{1.5}\cdot\sqrt{f_{c\_d}\cdot ksi} = 3834.3ksi$ *Modulus of elasticity of CIP concrete*

$H := 70$ *Average ambient relative humidity*

$\phi_u := 2.1$ *Ultimate creep coefficient*

$\varepsilon_{sh\_b} := 0.0005$ *Ultimate shrinkage strain in precast concrete*

$\varepsilon_{sh\_d} := 0.0006$ *Ultimate shrinkage strain in CIP concrete*

$\alpha := 0.00000$ *Coefficient of thermal expansion /degree F*

Strand:

$Num_{layers} := 2$ *Number of layers of strands*

$Num_{strands\_1} := 12$ *Number of strands in layer one of beam*

$Num_{strands\_2} := 12$ *Number of strands in layer two of beam*

$Num_{strands} := Num_{strands\_1} + Num_{strands\_2}$

$Num_{strands} = 24$ *Total number of strands*

$cover_{bot} := 2in$ *Required cover for bottom of precast beam*

$d_v := 0.5in$ *Diameter of shear steel (stirrups)*

$A_p := 0.215in^2$ *Area of one prestressing strand*

$A_{ps} := A_p \cdot Num_{strands} = 0.036ft^2$ *Total area of prestressing steel*

$d_b := 0.6in$ *Nominal diameter of one prestressed strand*

$d_{layer1} := cover_{bot} + d_v + \frac{d_b}{2} = 2.8in$ *Distance between centerline of strands in layer 1 to bottom of Inverted T:*

$d_{layers1and2} := 3in$ *Distance between centerline of strands in layers 1 and 2:*

$f_{pu} := 270ksi$ *Tensile strength of prestressing steel*

$E_p := 28500ksi$ *Modulus of elasticity of prestressing steel*

$f_{py} := 0.9 \cdot f_{pu}$ *Yield strength of prestressing steel*

$f_{pj} := 0.75 \cdot f_{pu}$ *Jacking force (initially applied force)*

$t := 18$ *Time from tensioning to detensioning of strands (hours)*

Rebar:

$f_y := 60ksi$ *Yield stress of mild reinforcing*

$E_s := 29000ksi$ *Modulus of elasticity of mild steel*

$A_{bar} := 0.79in^2$ *Number 8 bars*

$Num_{bars} := 0$ *Number of bars of mild steel (no mild steel included)*

$A_s := A_{bar} \cdot Num_{bars}$

$A_s = 0 \cdot in^2$ *Area of mild steel*

$A_{bar\_d} := 0.44in^2$ *Number 6 bars*

$D_{bar\_d} := 0.5in$ *Diameter of number 4 bars*

$cover_d := 1in$ *Cover over steel in deck*

$Num_{bars\_d} := 8$ Number of bars of mild steel in slab

$A_{s\_d} := A_{bar\_d} \cdot Num_{bars\_d}$

$A_{s\_d} = 3.52 \cdot in^2$ *Longitudinal rebar in slab*

$A_{shearbar} := 0.2in^2$ *Number 4 bars*

Geometry:

$h_b := 18in$ *Height of precast inverted T (from bottom of flange to top of web)*

$h_{fl} := 3in$ *Thickness of flange*

$b_b := 72in$ *Width of bottom of beam*

$b_{fl} := 12in$ *Width of one flange*

$h_{web} := h_b - h_{fl} = 15 \cdot in$ *Height of web*

$b_{web} := b_b - 2 \cdot b_{fl} = 48 \cdot in$ *Width of web*

$b_v := 72in$ *Shear width of the precast section (web and longitudinal trough width)*

$A_c := h_{fl} \cdot b_b + \left(\frac{h_b}{2} - h_{fl} \right) \cdot b_{web} = 504 \cdot in^2$ *Area of concrete on flexural tension side of member (see LRFD B5.2-3)*

Slab:

$h_d := 7in$ *Thickness of the CIP topping above the web of the inverted T*

$b_d := 24in$ *Width of the CIP region between the precast units*

$h_{ws} := 0in$ *Thickness of the CIP slab assumed to be wear*

$h_c := h_b + h_d$ *Total thickness of composite beam and slab (does not include wearing surface)*

Span:

$L := 37.5ft$ *Centerline of pier to centerline of pier dimension*

$Pier_{offset} := 6in$ *Distance from centerline of pier to end of beam*

$L_b := L - Pier_{offset} = 37 \cdot ft$ *Overall length of the precast section*

$L_{pad} := 12in$ *Length of bearing pad*

$Bearing_{offset} := 6in$ *Distance from end of beam to centerline of bearing*

$L_{des} := L_b - 2 \cdot Bearing_{offset} = 36 \cdot ft$ *Design span of the precast section*

$$VtoS_b := \frac{\left(h_{fl} \cdot b_b + b_{web} \cdot h_{web}\right) \cdot L_b}{2 \cdot \left(h_{fl} \cdot b_b + b_{web} \cdot h_{web}\right) + b_b \cdot L_b + b_{web} \cdot L_b + 2 \cdot h_{web} \cdot L_b + 2 \cdot b_{fl} \cdot L_b + 2 \cdot h_{fl} \cdot L_b}$$

$VtoS_b = 5.081 \cdot in$ *Volume to surface ratio of the precast section*

$$VtoS_d := \frac{\left(h_d \cdot b_b + 2 \cdot b_{fl} \cdot h_{web}\right) \cdot L_b}{b_b \cdot L_b + 2 \cdot L_b \cdot \left(h_d + h_{web}\right) + 2 \cdot b_{fl} \cdot L_b + 2 \cdot h_{web} \cdot L_b + b_{web} \cdot L_b}$$

$VtoS_d = 3.963 \cdot in$

Bridge:

$S := 6ft$ *Beam spacing*

$Num_b := 19$ *Number of the precast section in the bridge cross-section*

$width_{tot} := 114ft$ *Overall width of bridge*

$width_{ctoc} := 110ft$ *Curb to curb width of bridge*

$Num_{lanes} := 6$ *Number of lanes*

Loads:

Dead:

$Num_{barriers} := 4$ *Number of barriers*

$w_{barrier} := 0.3 \frac{kip}{ft}$ *Weight of single barrier*

$w_{ws\_future} := 0.025 \frac{kip}{ft^2}$ *Weight of future wearing surface*

Live:

$w_{lane} := 0.64 \frac{kip}{ft}$ *Design lane load*

HL-93 *Notional live load per LRFD specs*

Construction Timing:

$t_{trans} := 1$ *Time from tensioning of strands to release of prestress (days)*

$t_{age} := 90$ *Time from transfer to deck placement*

$t_{deck} := 97$ *Time when continuity is established (days)*

$t_{final} := 20000$ *Assumed end of service life of bridge (days)*

Load and Resistance Factors:

$\phi_v := 0.9$ *Resistance factor for shear*

$DLA := 0.33$ *Dynamic load allowance (LRFD 3.6.2.1-1)*

Non-composite Section Properties:

Area of Inverted T-Beam:

$A_b := h_b \cdot b_b - 2 \cdot h_{web} \cdot b_{fl} = 936 \cdot in^2$

Centroid of the Inverted T from the Bottom of the Flange:

$$y_b := \frac{h_b \cdot b_b \cdot \frac{h_b}{2} - 2 \cdot h_{web} \cdot b_{fl} \cdot \left(h_{fl} + \frac{h_{web}}{2} \right)}{A_b} = 8.423 in$$

Moment of Inertia of the Precast Inverted T about x-axis:

$$I_b := \frac{b_b \cdot h_b^3}{12} + b_b \cdot h_b \cdot \left(\frac{h_b}{2} - y_b \right)^2 - 2 \cdot \left[\frac{b_{fl} \cdot h_{web}^3}{12} + b_{fl} \cdot h_{web} \cdot \left(h_{fl} + \frac{h_{web}}{2} - y_b \right)^2 \right]$$

$I_b = 27120 in^4$

Section Moduli (Top and Bottom):

$$S_b := \frac{I_b}{y_b} = 3220 in^3$$

$$S_t := \frac{I_b}{h_b - y_b} = 2832 in^3$$

Strand Pattern Properties:

$$y_{bar\_strands} := \frac{Num_{strands\_1} \cdot d_{layer1} + Num_{strands\_2} \cdot \left(d_{layer1} + d_{layers1and2} \right)}{Num_{strands\_1} + Num_{strands\_2}}$$

$y_{bar\_strands} = 4.3 \cdot in$

$ecc := y_b - y_{bar\_strands} = 4.123 in$

Area of CIP Portion over each Inverted T-Beam:

$A_d := h_d \cdot b_b + 2 \cdot h_{web} \cdot b_{fl} = 864 \cdot in^2$

Composite Section Properties:

Effective width:

$$b := \begin{pmatrix} \frac{1}{4} \cdot L \\ 6 ft \\ 16 \cdot h_d + b_b \end{pmatrix}$$

$b_{eff} := \min(b)$ $b_{eff} = 6 \cdot ft$ *This includes all area above precast beam*

Transformed Section Analysis:

$$\eta := \frac{33 \cdot 150^{1.5} \cdot \sqrt{f_{c\_d}}}{33 \cdot 150^{1.5} \cdot \sqrt{f_{c\_b}}} = 0.707$$

$b_{trans} := \eta \cdot b_{eff} = 50.912\,in$

Gross Area:

$$A_g := A_b + b_{eff} \cdot \eta \cdot h_d + 2 \cdot b_{fl} \cdot \eta \cdot h_{web}$$

$A_g = 1546.9\,in^2$

Gross Centroid:

$$y_g := \frac{A_b \cdot y_b + b_{eff} \cdot \eta \cdot h_d \cdot \left(h_b + \frac{h_d}{2} \right) + 2 \cdot b_{fl} \cdot \eta \cdot h_{web} \cdot \left(\frac{h_{web}}{2} + h_{fl} \right)}{A_g}$$

$y_g = 11.777\,in$

$y_{g\_top} := h_b + h_d - y_g = 13.223\,in$ *Centroid from top of CIP*

Gross Moment of Inertia:

$$I_{g1} := I_b + A_b \cdot \left(y_g - y_b \right)^2 + \frac{1}{12} \cdot b_{eff} \cdot \eta \cdot h_d^{\,3} + \left(b_{eff} \cdot \eta \cdot h_d \right) \cdot \left(h_b + \frac{h_d}{2} - y_g \right)^2$$

$$I_{g2} := 2 \cdot \left[\frac{1}{12} \cdot b_{fl} \cdot \eta \cdot h_{web}^{\,3} + b_{fl} \cdot \eta \cdot h_{web} \cdot \left(\frac{h_{web}}{2} + h_{fl} - y_g \right)^2 \right]$$

$I_g := I_{g1} + I_{g2}$ *Broken apart to fit on page*

$I_g = 77984\,in^4$ *Gross moment of inertia of composite section*

Gross Section Moduli:

$S_{g\_b} := \frac{I_g}{y_g} = 6621.4\,in^3$ *Taken from bottom of Inverted T-Beam*

$S_{g\_t} := \frac{I_g}{h_b - y_g} = 12532.5\,in^3$ *Taken from top of inverted T-Beam*

$S_{g\_d} := \frac{I_g}{y_{g\_top}} = 5897.8\,in^3$ *Taken from top of CIP concrete*

Deck Properties:

$$y_d := \frac{b_{trans} \cdot h_d \cdot \left(h_b + \frac{h_d}{2} \right) + \eta \cdot 2 \cdot b_{fl} \cdot h_{web} \cdot \left(h_{fl} + \frac{h_{web}}{2} \right)}{b_{trans} \cdot h_d + \eta \cdot 2 \cdot b_{fl} \cdot h_{web}}$$

$y_d = 16.917\,in$ *Centroid of deck measured from bottom of precast girder*

$e_d := y_d - y_g = 5.139\,in$ *Distance between centroid of deck and centroid of gross composite section*

3. Loads

Self-weight of the Inverted T's:

$$weight_b := A_b \cdot \gamma_b = 0.975 \frac{kip}{ft}$$

Weight of the CIP portion over each inverted T beam:

$$weight_d := A_d \cdot \gamma_d = 0.9 \frac{kip}{ft}$$

Future wearing surface:

$$weight_{ws} := w_{ws\_future} \cdot \frac{width_{ctoc}}{Num_b} = 0.145 \frac{kip}{ft}$$ *per beam*

Barrier Loads:

$$weight_{barrierperbeam} := \frac{Num_{barriers} \cdot w_{barrier}}{Num_b} = 0.063 \frac{kip}{ft}$$ *per beam*

Live Loads:

Distribution Factors:

Following provisions set forth by LRFD 4.6.2.3 under the assumption that the superstructure acts like a slab-type bridge.

Single Lane Loading:

$$L_1 := \begin{cases} L_{des} & \text{if } L_{des} < 60ft \\ 60ft & \text{otherwise} \end{cases}$$ *Modified span length taken equal to the lesser of the actual span or 60'*

$L_1 = 36ft$

$$W_{1\_1} := \begin{cases} width_{tot} & \text{if } width_{tot} < 30ft \\ 30ft & \text{otherwise} \end{cases}$$ *Modified edge-to-edge width of bridge taken to be equal to the lesser of the actual width or 60' for multilane loading, or 30' for single-lane loading*

$W_{1\_1} = 30ft$

The equivalent width of longitudinal strips per lane for both shear and moment with one lane, i.e, two lines of wheels, loaded

$$E_{strip1} := 10in + 5in \cdot \sqrt{\frac{L_1}{ft} \cdot \frac{W_{1\_1}}{ft}}$$ *Already factors in 1.20 to account for the multiple presence effect*

$E_{strip1} = 14.526ft$

$$DF_1 := \frac{b_b}{E_{strip1}} = 0.413$$ *In terms of fraction of one lane to be distributed to one precast member*

Double Lane Loading:

$$W_{1\_2} := \begin{cases} width_{tot} & \text{if } width_{tot} < 60ft \\ 60ft & \text{otherwise} \end{cases}$$

$W_{1\_2} = 60ft$

The equivalent width of longitudinal strips per lane for both shear and moment with more than one lane loaded

$$E_{strip2} := \begin{cases} 84in + 1.44in \cdot \sqrt{\frac{L_1}{ft} \cdot \frac{W_{1\_2}}{ft}} & \text{if } 84in + 1.44in \cdot \sqrt{\frac{L_1}{ft} \cdot \frac{W_{1\_2}}{ft}} < \frac{12 width_{tot}}{Num_b} \\ \frac{12 width_{tot}}{Num_b} & \text{otherwise} \end{cases}$$

$E_{strip2} = 12.577 \cdot ft$

$DF_2 := \frac{b_b}{E_{strip2}} = 0.477$ *In terms of fraction of one lane to be distributed to one precast member*

Governing Case:

$$DF := \begin{cases} DF_1 & \text{if } DF_1 > DF_2 \\ DF_2 & \text{otherwise} \end{cases}$$

$DF = 0.477$ *In terms of fraction of one lane to be distributed to one precast member (Applicable to both shear and moment)*

4. Moments and Shears

At release the structure will behave as two simply supported beams in the longitudinal direction. There are two points of interest at this point of time which include:

$L_t := 60 \cdot d_b$ *Transfer point of strands*

$midspan := \frac{L_{des}}{2}$ *Midspan of beam*

$x_r := \begin{pmatrix} L_t \\ midspan \end{pmatrix}$ *Matrix of points of interest at release*

$x_r^T = (3 \quad 18)\, ft$

At final conditions the structure will behave as a composite system. Some of the loads, such as beam and CIP concrete self-weight will act on the simple span system while superimposed loads applied after continuity is established will act on the continuous system. These effects can be superimposed to produce shears, moments, and stresses that properly mimic the bridge system. The composite system has five points of interest which include:

$x_{f_1} := 0ft$ *Centerline of left bearing*

$x_{f_2} := L_t - \frac{L_b - L_{des}}{2}$ *Left transfer point of strands*

$x_{f_3} := 0.72 h_c + \frac{L_{pad}}{2}$ *Left critical section for shear*

The critical section for shear is d_v from the face of the support. This can be conservatively assumed to be 0.72h

$x_{f_4} := \frac{L_{des}}{2}$ *Midspan of beam*

$x_{f_5} := 0.375 L_{des}$ *Point of max moment from uniformly applied distributed load on both spans*

$x_f^T = (0 \;\; 2.5 \;\; 2 \;\; 18 \;\; 13.5)\,\text{ft}$ *Matrix of points of interest at final conditions*

$x_{fc} :=$ for $n \in 1..11$: $x_{fc_n} \leftarrow \frac{n-1}{10} \cdot L$; x_{fc}

Matrix that displays points of interest (tenth points) along Span 1 ranging from the centerline of the left pier to the centerline of the center pier

$x_{fc}^T = (0 \;\; 3.75 \;\; 7.5 \;\; 11.25 \;\; 15 \;\; 18.75 \;\; 22.5 \;\; 26.25 \;\; 30 \;\; 33.75 \;\; 37.5)\,\text{ft}$

For beam design itself, the results of the continuous structure must be mapped onto the checkpoints of the beam. The following function maps the results from the continuous beam analysis to the beam check points at final using linear interpolation

$Map(PO, BO, x_f, x_{fc}, MVc) :=$

$j_{max} \leftarrow last(x_{fc})$

for $i \in 1..last(x_f)$

$j \leftarrow 1$

while $(PO + BO + x_{f_i}) > x_{fc_j}$

$j \leftarrow j + 1$

break if $j > j_{max}$

$C \leftarrow \frac{PO + BO + x_{f_i} - x_{fc_{j-1}}}{x_{fc_j} - x_{fc_{j-1}}}$

$MV_i \leftarrow MVc_{j-1} + C \cdot (MVc_j - MVc_{j-1})$

MV

The moments and shears shown below were manually entered into this template. They represent 10th-point values of the left span that were generated by a 2-D continuous beam program (RISA 3-D). All similarly highlighted regions represent manually entered values that were generated in a similar fashion.

Future Wearing Surface:

$$M_{fws\_c} := \begin{pmatrix} 0 \\ 6.6 \\ 11.2 \\ 13.8 \\ 14.3 \\ 12.7 \\ 9.2 \\ 3.6 \\ -4.1 \\ -13.8 \\ -25.5 \end{pmatrix} \cdot kip \cdot ft \qquad V_{fws\_c} := \begin{pmatrix} 2 \\ 1.5 \\ 1 \\ 0.4 \\ -0.1 \\ -0.7 \\ -1.2 \\ -1.8 \\ -2.3 \\ -2.9 \\ -3.4 \end{pmatrix} kip$$

Barrier Loads:

$$M_{barrier\_c} := \begin{pmatrix} 0 \\ 2.9 \\ 4.9 \\ 6 \\ 6.2 \\ 5.5 \\ 4 \\ 1.6 \\ -1.8 \\ -6 \\ -11.1 \end{pmatrix} \cdot kip \cdot ft \qquad V_{barrier\_c} := \begin{pmatrix} 0.9 \\ 0.6 \\ 0.4 \\ 0.2 \\ -0.1 \\ -0.3 \\ -0.5 \\ -0.8 \\ -1 \\ -1.2 \\ -1.5 \end{pmatrix} \cdot kip$$

Design Truck, Left Span, +M:

$$M_{truck\_pc} := \begin{pmatrix} 0 \\ 158 \\ 254 \\ 309.7 \\ 323.2 \\ 312 \\ 285.2 \\ 228.9 \\ 141.5 \\ 12.5 \\ 0 \end{pmatrix} \cdot kip \cdot ft \qquad V_{truck\_pc} := \begin{pmatrix} 50.8 \\ 42.1 \\ 33.9 \\ 26.4 \\ 20 \\ 14.4 \\ 8.8 \\ 4.1 \\ 0 \\ 0 \\ 0 \end{pmatrix} \cdot kip$$

All Truck and Tandem loads were calculated by applying a moving load and recording the respective moment and shear envelopes.

Design Truck, Left Span, -M:

$$M_{truck\_nc} := \begin{pmatrix} 0 \\ -19.6 \\ -39.2 \\ -58.8 \\ -78.4 \\ -98 \\ -117.6 \\ -137.2 \\ -156.8 \\ -176.4 \\ -211.4 \end{pmatrix} \cdot kip \cdot ft \qquad V_{truck\_nc} := \begin{pmatrix} -5.2 \\ -5.2 \\ -7.4 \\ -11.5 \\ -16.6 \\ -22.6 \\ -30.3 \\ -37.8 \\ -44.9 \\ -50.3 \\ -56.8 \end{pmatrix} \cdot kip$$

Design Tandem, Left Span, +M:

$$M_{tandem\_pc} := \begin{pmatrix} 0 \\ 150.3 \\ 252 \\ 318.8 \\ 343.2 \\ 335.2 \\ 300.7 \\ 237.8 \\ 158.5 \\ 59 \\ 0 \end{pmatrix} \cdot kip \cdot ft \qquad V_{tandem\_pc} := \begin{pmatrix} 46.7 \\ 40.1 \\ 33.6 \\ 27.4 \\ 22.9 \\ 17.3 \\ 12.1 \\ 7.5 \\ 4.5 \\ 1.2 \\ 0 \end{pmatrix} \cdot kip$$

Design Tandem, Left Span, -M:

$$M_{tandem\_nc} := \begin{pmatrix} 0 \\ -17.8 \\ -35.6 \\ -53.4 \\ -71.2 \\ -89 \\ -106.8 \\ -124.6 \\ -142.4 \\ -160.2 \\ -178 \end{pmatrix} \cdot kip \cdot ft \qquad V_{tandem\_nc} := \begin{pmatrix} -4.7 \\ -4.7 \\ -8.3 \\ -14.8 \\ -21.1 \\ -25.7 \\ -31.4 \\ -36.7 \\ -41.4 \\ -44.5 \\ -48.1 \end{pmatrix} \cdot kip$$

Design Lane, Left Span, +M:

$$M_{lane\_pc} := \begin{pmatrix} 0 \\ 34.9 \\ 60.8 \\ 77.6 \\ 85.5 \\ 84.4 \\ 74.3 \\ 55.1 \\ 27 \\ 0 \\ 0 \end{pmatrix} \cdot kip \cdot ft \qquad V_{lane\_pc} := \begin{pmatrix} 10.5 \\ 8.1 \\ 5.7 \\ 3.3 \\ 0.9 \\ -1.5 \\ -3.9 \\ -6.3 \\ -8.7 \\ -11.1 \\ -13.5 \end{pmatrix} \cdot kip$$

Calculated by applying design lane load to left span only

Design Lane, Left Span, -M:

$$M_{lane\_nc} := \begin{pmatrix} 0 \\ -5.6 \\ -11.2 \\ -16.9 \\ -22.5 \\ -28.1 \\ -33.7 \\ -39.4 \\ -45 \\ -50.6 \\ -56.2 \end{pmatrix} \cdot kip \cdot ft \qquad V_{lane\_nc} := \begin{pmatrix} -1.5 \\ -1.5 \\ -1.5 \\ -1.5 \\ -1.5 \\ -1.5 \\ -1.5 \\ -1.5 \\ -1.5 \\ -1.5 \\ -1.5 \end{pmatrix} \cdot kip$$

Calculated by applying design lane load to both spans

Loads Acting Before Composite Action is Established:

Self Weight of Beam:

$w_{sw} := \gamma_b \cdot A_b = 0.975 \frac{kip}{ft}$ *Self-weight of beam at time of release*

$M_{swr} :=$ for $n \in 1..2$

$M_{swr_n} \leftarrow \frac{w_{sw} \cdot x_{r_n}}{2} \cdot \left(L_{des} - x_{r_n}\right)$

M_{swr}

$M_{swr}^{T} = (48.262 \quad 157.95) \cdot kip \cdot ft$ *Moments due to self-weight of beam at release located at points of interest on simply supported beam*

$M_{swf} :=$ for $n \in 1..5$

$M_{swf_n} \leftarrow \frac{w_{sw} \cdot x_{f_n}}{2} \cdot \left(L_{des} - x_{f_n}\right)$

M_{swf}

$M_{swf}^{T} = (0 \quad 40.828 \quad 33.15 \quad 157.95 \quad 148.078) \cdot kip \cdot ft$ *Moments due to self-weight of beam at time final located at points of interest on simply supported beam*

$$V_{swf} := \left| \begin{array}{l} \text{for } n \in 1..5 \\ V_{swf_n} \leftarrow w_{sw} \cdot \left(\frac{L_{des}}{2} - x_{f_n} \right) \\ V_{swf} \end{array} \right.$$

$V_{swf}^{T} = (17.55 \;\; 15.112 \;\; 15.6 \;\; 0 \;\; 4.387) \cdot kip$

Shears due to self-weight of beam at time final located at points of interest on simply supported beam

Self-Weight of CIP Concrete:

$w_d := \gamma_d \cdot \left(h_d \cdot b_b + 2 \cdot h_{web} \cdot b_{fl} \right)$

$w_d = 0.9 \frac{kip}{ft}$ *Self-weight of CIP concrete at time of release*

$$M_{deck} := \left| \begin{array}{l} \text{for } n \in 1..5 \\ M_{deck_n} \leftarrow \frac{w_d \cdot x_{f_n}}{2} \cdot \left(L_{des} - x_{f_n} \right) \\ M_{deck} \end{array} \right.$$

$M_{deck}^{T} = (0 \;\; 37.687 \;\; 30.6 \;\; 145.8 \;\; 136.687) \cdot kip \cdot ft$

Moments due to self-weight of CIP concrete at time final located at points of interest on simply supported beam

$$V_{deck} := \left| \begin{array}{l} \text{for } n \in 1..5 \\ V_{deck_n} \leftarrow w_d \cdot \left(\frac{L_{des}}{2} - x_{f_n} \right) \\ V_{deck} \end{array} \right.$$

$V_{deck}^{T} = (16.2 \;\; 13.95 \;\; 14.4 \;\; 0 \;\; 4.05) \cdot kip$

Shears due to self-weight of CIP concrete at time final located at points of interest on simply supported beam

Loads Acting on Continuous Structure:

Barrier Weight:

$M_{barrier} := Map\left(Pier_{offset}, Bearing_{offset}, x_f, x_{fc}, M_{barrier\_c} \right)$

$M_{barrier}^{T} = (0.773 \;\; 2.707 \;\; 2.32 \;\; 5.4 \;\; 6.173) \cdot kip \cdot ft$

Moment caused by barrier weight acting on continuous structure

$V_{barrier} := Map\left(Pier_{offset}, Bearing_{offset}, x_f, x_{fc}, V_{barrier\_c} \right)$

$V_{barrier}^{T} = (0.82 \;\; 0.62 \;\; 0.66 \;\; -0.313 \;\; -0.06) \cdot kip$

Shear caused by barrier weight acting on continuous structure

Future Wearing Surface:

$M_{fws} := Map\left(Pier_{offset}, Bearing_{offset}, x_f, x_{fc}, M_{fws\_c} \right)$

$M_{fws}^{T} = (1.76 \;\; 6.16 \;\; 5.28 \;\; 12.467 \;\; 14.233) \cdot kip \cdot ft$

Moment caused by future wearing surface weight acting on continuous structure

$V_{fws} := Map\left(Pier_{offset}, Bearing_{offset}, x_f, x_{fc}, V_{fws\_c}\right)$

$V_{fws}^{T} = (1.867\ \ 1.533\ \ 1.6\ \ -0.733\ \ -0.033)\cdot kip$

Shear caused by future wearing surface weight acting on continuous structure

Positive Moment Envelope:

$$Max_{vehicle}(truck, tandem) := \left| \begin{array}{l} \text{for } n \in 1..last(truck) \\ \quad \left| \begin{array}{l} Vehicle_n \leftarrow truck_n \text{ if } truck_n > tandem_n \\ Vehicle_n \leftarrow tandem_n \text{ otherwise} \end{array} \right. \\ Vehicle \end{array} \right.$$

$M_{vehicle\_pc} := Max_{vehicle}\left(M_{truck\_pc}, M_{tandem\_pc}\right)$

Positive moment envelop caused by greater of truck and tandem loads for tenth points

$M_{vehicle\_pc}^{T} = (0\ \ 158\ \ 254\ \ 318.8\ \ 343.2\ \ 335.2\ \ 300.7\ \ 237.8\ \ 158.5\ \ 59\ \ 0)\cdot kip\cdot ft$

$M_{vehicle\_p} := Map\left(Pier_{offset}, Bearing_{offset}, x_f, x_{fc}, M_{vehicle\_pc}\right)$

Positive moment envelop caused by greater of truck and tandem loads for points of interest

$M_{vehicle\_p}^{T} = (42.133\ \ 147.467\ \ 126.4\ \ 332.9\ \ 339.947)\cdot kip\cdot ft$

$M_{lane\_p} := Map\left(Pier_{offset}, Bearing_{offset}, x_f, x_{fc}, M_{lane\_pc}\right)$

Positive moment envelop caused by lane load for points of interest

$M_{lane\_p}^{T} = (9.307\ \ 32.573\ \ 27.92\ \ 83.727\ \ 84.447)\cdot kip\cdot ft$

$$M_{LL\_p} := \left| \begin{array}{l} \text{for } n \in 1..5 \\ \quad M_{LL\_p_n} \leftarrow DF\cdot\left[M_{lane\_p_n} + (1 + DLA)\cdot M_{vehicle\_p_n}\right] \\ M_{LL\_p} \end{array} \right.$$

$M_{LL\_p}^{T} = (31.173\ \ 109.105\ \ 93.519\ \ 251.163\ \ 255.978)\cdot kip\cdot ft$

Positive moment at points of interest caused by the combination of design lane load and greater of truck and tandem load with consideration paid to distribution factors

$V_{vehicle\_pc} := Max_{vehicle}\left(V_{truck\_pc}, V_{tandem\_pc}\right)$

Shear caused by greater positive moment of truck and tandem loads for tenth points

$V_{vehicle\_pc}^{T} = (50.8\ \ 42.1\ \ 33.9\ \ 27.4\ \ 22.9\ \ 17.3\ \ 12.1\ \ 7.5\ \ 4.5\ \ 1.2\ \ 0)\cdot kip$

$V_{vehicle\_p} := Map\left(Pier_{offset}, Bearing_{offset}, x_f, x_{fc}, V_{vehicle\_pc}\right)$

Shear caused by greater positive moment of truck and tandem loads for points of interest

$V_{vehicle\_p}^{T} = (48.48\ \ 42.68\ \ 43.84\ \ 16.953\ \ 23.5)\cdot kip$

$V_{lane\_p} := Map\left(Pier_{offset}, Bearing_{offset}, x_f, x_{fc}, V_{lane\_pc}\right)$

Shear caused by lane load for points of interest

$V_{lane\_p}^{T} = (9.86\ \ 8.26\ \ 8.58\ \ -1.66\ \ 1.22)\cdot kip$

$V_{LL\_p} := \left| \begin{array}{l} \text{for } n \in 1..5 \\ \quad V_{LL\_p_n} \leftarrow DF\cdot\left[V_{lane\_p_n} + (1 + DLA)\cdot V_{vehicle\_p_n}\right] \\ V_{LL\_p} \end{array} \right.$

Shear from positive moment envelope at points of interest caused by the combination of design lane load and greater of truck and tandem load with consideration paid to distribution factors

$V_{LL\_p}^{T} = (35.464\ \ 31.02\ \ 31.909\ \ 9.965\ \ 15.492)\cdot kip$

Negative Moment Envelope:

$Min_{vehicle}(truck, tandem) := \left| \begin{array}{l} \text{for } n \in 1..last(truck) \\ \quad \left| \begin{array}{l} Vehicle_n \leftarrow truck_n \text{ if } truck_n < tandem_n \\ Vehicle_n \leftarrow tandem_n \text{ otherwise} \end{array} \right. \\ Vehicle \end{array} \right.$

$M_{vehicle\_nc} := Min_{vehicle}\left(M_{truck\_nc}, M_{tandem\_nc}\right)$

Negative moment envelop caused by lesser of truck and tandem loads for tenth points

$M_{vehicle\_nc}^{T} = (0\ \ -19.6\ \ -39.2\ \ -58.8\ \ -78.4\ \ -98\ \ -117.6\ \ -137.2\ \ -156.8\ \ -176.4\ \ -211.4)\cdot kip\cdot ft$

$M_{vehicle\_n} := Map\left(Pier_{offset}, Bearing_{offset}, x_f, x_{fc}, M_{vehicle\_nc}\right)$

Negative moment envelop caused by lesser of truck and tandem loads for points of interest

$M_{vehicle\_n}^{T} = (-5.227\ \ -18.293\ \ -15.68\ \ -99.307\ \ -75.787)\cdot kip\cdot ft$

$M_{lane\_n} := Map\left(Pier_{offset}, Bearing_{offset}, x_f, x_{fc}, M_{lane\_nc}\right)$

Negative moment envelop caused by lane load for points of interest

$M_{lane\_n}^{T} = (-1.493\ \ -5.227\ \ -4.48\ \ -28.473\ \ -21.753)\cdot kip\cdot ft$

$M_{LL\_n} := \left| \begin{array}{l} \text{for } n \in 1..5 \\ \quad M_{LL\_n_n} \leftarrow DF\cdot\left[M_{lane\_n_n} + (1 + DLA)\cdot M_{vehicle\_n_n}\right] \\ M_{LL\_n} \end{array} \right.$

$M_{LL\_n}^{T} = (-4.029 \ -14.1 \ -12.086 \ -76.592 \ -58.463)\cdot kip\cdot ft$

Negative moment at points of interest caused by the combination of design lane load and lesser of truck and tandem load with consideration paid to distribution factors

$V_{vehicle\_nc} := Min_{vehicle}\left(V_{truck\_nc}, V_{tandem\_nc}\right)$

Shear caused by lesser negative moment of truck and tandem loads for tenth points

$V_{vehicle\_nc}^{T} = (-5.2 \ -5.2 \ -8.3 \ -14.8 \ -21.1 \ -25.7 \ -31.4 \ -37.8 \ -44.9 \ -50.3 \ -56.8)\cdot kip$

$V_{vehicle\_n} := Map\left(Pier_{offset}, Bearing_{offset}, x_f, x_{fc}, V_{vehicle\_nc}\right)$

Shear caused by lesser negative moment of truck and tandem loads for points of interest

$V_{vehicle\_n}^{T} = (-5.2 \ -5.2 \ -5.2 \ -26.08 \ -20.26)\cdot kip$

$V_{lane\_n} := Map\left(Pier_{offset}, Bearing_{offset}, x_f, x_{fc}, V_{lane\_nc}\right)$

Shear caused by lane load for points of interest

$V_{lane\_n}^{T} = (-1.5 \ -1.5 \ -1.5 \ -1.5 \ -1.5)\cdot kip$

$V_{LL\_n} := \left| \begin{array}{l} \text{for } n \in 1..5 \\ \quad V_{LL\_n_n} \leftarrow DF\cdot\left[V_{lane\_n_n} + (1 + DLA)\cdot V_{vehicle\_n_n}\right] \\ V_{LL\_n} \end{array} \right.$

$V_{LL\_n}^{T} = (-4.015 \ -4.015 \ -4.015 \ -17.263 \ -13.57)\cdot kip$

Shear from negative moment envelope at points of interest caused by the combination of design lane load and lesser of truck and tandem load with consideration paid to distribution factors

5. Restraint Moments and Losses

Positive Restraint Moment:

Moment Due to Eccentric Prestressing:

$f_{pe} := 185ksi$ *Estimate of stress in prestressing strands a time of continuity*

$P_{ps} := f_{pe}\cdot A_{ps} = 955\cdot kip$ *Total force in prestressing strands*

$M_p := P_{ps}\cdot ecc = 328\cdot kip\cdot ft$ *Moment caused by prestressing strand eccentricity*

Dead Load Moments:

$M_{dp} := M_{swf_4}$ Max dead load moment due to self-weight of beam

$M_{dd} := M_{deck_4}$ Max dead load moment due to weight of deck

Estimate of Differential Shrinkage at End of Service Life of Bridge:

Shrinkage Strain in precast at time continuity is established:

$k_{vs1} := 1.45 - 0.13 \frac{VtoS_b}{in} = 0.789$ *(LRFD 5.4.2.3.2-1)*

$k_{vs} := \begin{cases} k_{vs} \leftarrow k_{vs1} & \text{if } k_{vs1} > 1 \\ 1 & \text{otherwise} \end{cases}$

$k_{vs} = 1$ *Factor for the effect of volume to surface ratio*

$k_{hs} := 2 - 0.014 H = 1.02$ *Factor for humidity* *(LRFD 5.4.2.3.3-2)*

$k_f := \frac{5}{1 + \frac{f_{ci\_b}}{ksi}} = 0.833$ *Factor for strength of concrete* *(LRFD 5.4.2.3.2-4)*

$t_{td} := t_{deck} - t_{trans} = 96$ *Time for development (days)*

$k_{td} := \frac{t_{td}}{61 - 4 \cdot \frac{f_{ci\_b}}{ksi} + t_{td}} = 0.701$ *Factor for time development* *(LRFD 5.4.2.3.2-5)*

$\varepsilon_{bid} := -0.00048 k_{vs} \cdot k_{hs} \cdot k_f \cdot k_{td}$ *(LRFD 5.4.2.3.3-1)*

$\varepsilon_{bid} = -0.0002859$ *Shrinkage strain in precast at time continuity is established*

Shrinkage Strain in Precast at Time Final:

$t_{ft} := t_{final} - t_{trans} = 19999$ *Time from transfer to final*

$k_{td2} := \frac{t_{ft}}{61 - 4 \cdot \frac{f_{ci\_b}}{ksi} + t_{ft}} = 0.998$ *Factor for time final* *(LRFD 5.4.2.3.2-5)*

$\varepsilon_{bif} := -0.00048 k_{vs} \cdot k_{hs} \cdot k_f \cdot k_{td2}$ *(LRFD 5.4.2.3.3-1)*

$\varepsilon_{bif} = -0.0004072$ *Shrinkage strain in precast at time final*

Total Precast Shrinkage Strain:

$\varepsilon_{shp} := \varepsilon_{bif} - \varepsilon_{bid}$

$\varepsilon_{shp} = -0.000121$

Shrinkage Strain in CIP at time Final:

$k_{vs2} := 1.45 - 0.13 \frac{VtoS_d}{in} = 0.935$ *(LRFD 5.4.2.3.2-1)*

$k_{vsd} := \begin{cases} k_{vsd} \leftarrow k_{vs2} & \text{if } k_{vs2} > 1 \\ 1 & \text{otherwise} \end{cases}$

$k_{vsd} = 1$ *Factor for the effect of volume to surface ratio*

$k_{hsd} := 2 - 0.014 H = 1.02$ *Factor for humidity* *(LRFD 5.4.2.3.3-2)*

$k_{fd} := \frac{5}{1 + \frac{0.8 f_{c\_d}}{ksi}} = 1.19$ *Factor for strength of concrete* *(LRFD 5.4.2.3.2-4)*

$t_{ftd} := t_{final} - t_{deck} = 19903$ *Factor for time final*

$k_{ftd} := \frac{t_{ftd}}{61 - 4 \cdot \frac{0.8 f_{c\_d}}{ksi} + t_{ftd}} = 0.998$ *Factor for time development* *(LRFD 5.4.2.3.2-5)*

$\varepsilon_{ddf} := -0.00048 k_{vsd} \cdot k_{hsd} \cdot k_{fd} \cdot k_{ftd}$ *(LRFD 5.4.2.3.3-1)*

$\varepsilon_{ddf} = -0.0005814$ *Shrinkage strain in CIP at time final*

Differential Shrinkage:

$\varepsilon_{sh} := \varepsilon_{ddf} - \varepsilon_{shp}$

$\varepsilon_{sh} = -0.00046$

Uniform Shrinkage Moment:

$e_e := h_b - y_g$ *Distance from top of precast beam to centroid of gross composite cross-section*

$A_{d2} := b_b \cdot h_d$

$A_{d2} = 504 \cdot in^2$ *Area of top portion of slab*

$\eta_2 := \frac{1}{1 + \frac{E_b \cdot A_b}{E_d \cdot A_{d2}}} \cdot \frac{1}{1 + \frac{E_s \cdot A_{s\_d}}{E_d \cdot A_{d2}}}$

$\eta_2 = 0.262$ *Transformation factor for top portion of slab and precast beam*

$M_s := \varepsilon_{sh} \cdot E_d \cdot A_{d2} \cdot \left(e_e + \frac{h_d}{2} \right) \cdot \eta_2$

$M_s = -188.72 \, kip \cdot ft$ *Shrinkage moment*

Creep Effects on Precast M_p and M_d:

Creep in Precast at Continuity:

$k_{vs3} := 1.45 - 0.13 \frac{VtoS_b}{in} = 0.789$ *(LRFD 5.4.2.3.2-1)*

$k_{vsc} := \begin{cases} k_{vsc} \leftarrow k_{vs3} & \text{if } k_{vs3} > 1 \\ 1 & \text{otherwise} \end{cases}$

$k_{vsc} = 1$ *Factor for the effect of volume to surface ratio*

$k_{hc} := 1.56 - 0.008 H = 1$ *Factor for humidity* *(LRFD 5.4.2.3.2-3)*

$k_{fc} := \frac{5}{1 + \frac{f_{ci\_b}}{ksi}} = 0.833$ *Factor for strength of concrete* *(LRFD 5.4.2.3.2-4)*

$t_{tfc} := t_{deck} - t_{trans} = 96$ *Time for development*

$k_{tfc} := \frac{t_{tfc}}{61 - 4 \cdot \frac{f_{ci\_b}}{ksi} + t_{tfc}} = 0.701$ *Factor for time development* *(LRFD 5.4.2.3.2-5)*

$\psi_{bdi} := 1.9 k_{vsc} \cdot k_{hc} \cdot k_{fc} \cdot k_{tfc} \cdot t_{trans}^{-0.118}$

$\psi_{bdi} = 1.109$ *Creep in precast coefficient at time of CIP placement due to loading at transfer*

Creep in Precast at Final:

$k_{vs4} := 1.45 - 0.13 \frac{VtoS_b}{in} = 0.789$ *(LRFD 5.4.2.3.2-1)*

$k_{vsf} := \begin{cases} k_{vsc} \leftarrow k_{vs4} & \text{if } k_{vs4} > 1 \\ 1 & \text{otherwise} \end{cases}$

$k_{vsf} = 1$ *Factor for the effect of volume to surface ratio*

$k_{hf} := 1.56 - 0.008H = 1$ *Factor for humidity* *(LRFD 5.4.2.3.2-3)*

$k_{ff} := \frac{5}{1 + \frac{f_{ci\_b}}{ksi}} = 0.833$ *Factor for strength of concrete* *(LRFD 5.4.2.3.2-4)*

$t_{tff} := t_{final} - t_{trans} = 19999$ *Time to final*

$k_{tff} := \frac{t_{tff}}{61 - 4 \cdot \frac{f_{ci\_b}}{ksi} + t_{tff}} = 0.998$ *Factor for time development* *(LRFD 5.4.2.3.2-5)*

$\psi_{bfi} := 1.9 k_{vsf} \cdot k_{hf} \cdot k_{ff} \cdot k_{tff} \cdot t_{trans}^{-0.118}$

$\psi_{bfi} = 1.58$ *Creep in precast coefficient at time final due to loading at transfer*

Creep Effects on CIP M_d and M_s:

$k_{vs5} := 1.45 - 0.13 \frac{VtoS_b}{in} = 0.789$ *(LRFD 5.4.2.3.2-1)*

$k_{vsm} := \begin{cases} k_{vsc} \leftarrow k_{vs5} & \text{if } k_{vs5} > 1 \\ 1 & \text{otherwise} \end{cases}$

$k_{vsm} = 1$ *Factor for the effect of volume to surface ratio*

$k_{hm} := 1.56 - 0.008H = 1$ *Factor for humidity* *(LRFD 5.4.2.3.2-3)*

$k_{fm} := \frac{5}{1 + \frac{f_{ci\_b}}{ksi}} = 0.833$ *Factor for strength of concrete* *(LRFD 5.4.2.3.2-4)*

$t_{tfm} := t_{final} - t_{deck} = 19903$ *Time to final*

$$k_{tfm} := \frac{t_{tfm}}{61 - 4\cdot\frac{f_{ci\_b}}{ksi} + t_{tfm}} = 0.998$$ *Factor for time development* *(LRFD 5.4.2.3.2-5)*

$\psi_{bfid} := 1.9 k_{vsf}\cdot k_{hf}\cdot k_{ff}\cdot k_{tff}\cdot t_{deck}^{-0.118}$

$\psi_{bfid} = 0.921$ *Creep in precast coefficient at time final due to loading at CIP placement*

CIP Deck Creep Coefficient at Time Final Due to Loading at CIP Placement:

$$k_{vs6} := 1.45 - 0.13\frac{VtoS_d}{in} = 0.935$$ *(LRFD 5.4.2.3.2-1)*

$k_{vsp} := \begin{cases} k_{vsc} \leftarrow k_{vs6} & \text{if } k_{vs6} > 1 \\ 1 & \text{otherwise} \end{cases}$

$k_{vsp} = 1$ *Factor for the effect of volume to surface ratio*

$k_{hp} := 1.56 - 0.008H = 1$ *Factor for humidity* *(LRFD 5.4.2.3.2-3)*

$$k_{fp} := \frac{5}{1 + \frac{0.8 f_{c\_d}}{ksi}} = 1.19$$ *Factor for strength of concrete* *(LRFD 5.4.2.3.2-4)*

$t_{tfp} := t_{final} - t_{deck} = 19903$ *Time to final*

$$k_{tfp} := \frac{t_{tfm}}{61 - 4\cdot\frac{f_{ci\_b}}{ksi} + t_{tfm}} = 0.998$$ *Factor for time development* *(LRFD 5.4.2.3.2-5)*

$\psi_{dfid} := 1.9 k_{vsp}\cdot k_{hp}\cdot k_{fp}\cdot k_{tfp}\cdot t_{deck}^{-0.118}$

$\psi_{dfid} = 1.316$ *Creep in CIP coefficient at time final due to loading at CIP placement*

M_r at Interior face of Pier:

Since a minimum girder age of 90 days is specified positive restraint moments caused by creep and shrinkage and deck slab shrinkage may be taken as zero. Computation of restraint moments shall not be required. Reinforcement will rather be calculated based on $1.2*M_{cr}$. *(LRFD 5.14.1.4.4)*

Positive Restraint Connection:

$f_r := 0.24\sqrt{f_{c\_d}\cdot ksi}$ *Conservatively assume entire section of continuity diaphragm is composed of deck concrete*

$f_r = 0.48\cdot ksi$ *Cracking Stress*

$I_{cont} := \frac{1}{12}\cdot b_{eff}\cdot h_c^3 = 93750 in^4$ *Moment of inertia of continuity diaphragm*

$y_{cont} := \frac{h_c}{2} = 12.5\,in$ *Centroid of continuity diaphragm*

$M_{cr} := \frac{I_{cont}}{y_{cont}} \cdot f_r$ *f_r is stress in bottom of beam*

$M_{cr} = 300\,kip\cdot ft$ *Cracking Moment*

$1.2 \cdot M_{cr} = 360\,kip\cdot ft$

$\beta_1 := \begin{cases} \beta_1 \leftarrow 0.85 \text{ if } f_{c\_d} \leq 4ksi \\ \beta_1 \leftarrow 0.65 \text{ if } f_{c\_d} \geq 8ksi \\ \beta_1 \leftarrow \frac{f_{c\_d} - 4ksi}{1ksi} \cdot 0.05 \text{ otherwise} \end{cases}$

$\beta_1 = 0.85$ *Stress block factor based on CIP concrete*

$y_{bar\_r} := 3in$

$d_r := h_b + h_d - h_{ws} - y_{bar\_r}$

$d_r = 22\,in$ *Depth to positive restraint moment steel*

$A_{sr6} := 0.44in^2$ *Number 6 bars*

$Num_{rbars} := 12$ *This can be represented as 6 hooked mild steel sections protruding from the end of each precast girder.*

$A_{sr} := A_{sr6} \cdot Num_{rbars} = 5.28\,in^2$

$c := \frac{A_{sr} \cdot f_y}{0.85 f_{c\_d} \cdot b_b}$

$c = 1.294in$ *Neutral axis depth*

$\frac{c}{d_r} = 0.059$

$\phi := 0.9$

$a := \beta_1 \cdot c = 1.1\,in$ *Depth of equivalent stress block*

$\phi M_{nr\_pos} := \phi \cdot A_{sr} \cdot f_y \cdot \left(d_r - \frac{a}{2}\right)$

$\phi M_{nr\_pos} = 509.7\,kip\cdot ft$

$Status\_PosRes := \begin{cases} \text{"OK"} \text{ if } \phi M_{nr\_pos} \geq 1.2 M_{cr} \\ \text{"No Good"} \text{ otherwise} \end{cases}$

Status_PosRes = "OK"

Negative Restraint Connection:

$M_s = -188.715\,kip\cdot ft$ *Differential shrinkage moment calculated above*

$weight_{ws} = 0.145\,\frac{kip}{ft}$ *Superimposed dead load from future wearing surface per beam*

$weight_{barrierperbeam} = 0.063\,\frac{kip}{ft}$ *Superimposed dead load from barriers per beam*

$w_{live} := DF\cdot w_{lane} = 0.305\,\frac{kip}{ft}$ *Live load that worst case beam will see from lane loading*

$M_{rs} := 101.9\,kip\cdot ft$ *Negative moment caused by differential shrinkage*
Solved using Risa 3-D using shrinkage moment calculated above (M_S)

$w_{supd} := weight_{ws} + weight_{barrierperbeam} = 0.208\,\frac{kip}{ft}$ *For use in Risa 3-D*

$M_{r\_supd} := -36.6\,kip\cdot ft$ *Solved using Risa 3-D for superimposed dead loads*

$M_{r\_live} := -53.8\,kip\cdot ft$ *Solved using Risa 3-D for superimposed live loads*

$M_{r\_neg} := 1.0\cdot\left(M_s + M_{r\_supd}\right) + 1.75 M_{r\_live}$ *Proportioned for strength limit state*

$M_{r\_neg} = -319.5\,kip\cdot ft$ *Negative restraint moment*

$A_{s\_d} = 3.52\,in^2$ *Area of steel in CIP deck*

$c := \frac{A_{s\_d}\cdot f_y}{0.85 f_{c\_d}\cdot b_b}$

$c = 0.863\,in$ *Neutral axis depth*

$d_{s\_d} := h_b + h_d - h_{ws} - 3in$

$\frac{c}{d_{s\_d}} = 0.039$

$\phi := 0.9$

$a := \beta_1\cdot c = 0.733\,in$ *Depth of equivalent stress block*

$\phi M_{nr\_neg} := \phi\cdot A_{s\_d}\cdot f_y\cdot\left(d_{s\_d} - \frac{a}{2}\right)$

$\phi M_{nr\_neg} = 342.672\,kip\cdot ft$

$Status\_NegRes := \begin{cases} \text{"OK"} & \text{if } \phi M_{nr\_neg} \geq -\left(M_{r\_neg}\right) \\ \text{"No Good"} & \text{otherwise} \end{cases}$

$Status\_NegRes = \text{"OK"}$ *Steel in CIP deck is enough to satisfy requirements for negative restraint moments*

Thermal Gradient:

Uniform temperature change causes no internal stress since superstructure is not restrained axially

$T_1 := 54$
$T_2 := 14$ *Degrees F* *Assumes AASHTO Temperature Zone 1*

$T_3 := 0$

$A_1 := h_d = 7 \cdot in$

$$A_{temp} := \begin{cases} 12in & \text{if } h_c \geq 16in \\ \left(h_c - 4in\right) & \text{otherwise} \end{cases}$$

$A_{temp} = 12 \cdot in$

$A_2 := A_{temp}$

$Area_1 := A_1 \cdot b_b = 504 \cdot in^2$

$Area_2 := A_2 \cdot b_b = 864 \cdot in^2$

$$I_1 := \frac{b_b \cdot A_1^{\,3}}{12} = 2058 in^4$$

$$I_2 := \frac{b_b \cdot A_2^{\,3}}{12} = 10368 in^4$$

$$\varepsilon_{gr} := \frac{\alpha}{A_b} \cdot \left(T_1 \cdot Area_1 + T_2 \cdot Area_2\right) = 0.000252$$ *Gradient strain*

$F_{gr} := E_b \cdot A_c \cdot \varepsilon_{gr} = 689 \cdot kip$

$$y_1 := y_{g\_top} - \frac{A_1}{2}$$

$y_1 = 9.723 in$

$$y_2 := y_{g\_top} - \left(A_1 + \frac{A_2}{2}\right)$$

$y_2 = 0.223 in$

$$\psi := \frac{\alpha}{I_g} \cdot \left[\left(\frac{T_1 - T_2}{2} \right) \cdot y_1 \cdot Area_1 + \left(\frac{T_1 - T_2}{\frac{A_1}{2}} \right) \cdot I_1 + \left(\frac{T_2}{2} \right) \cdot y_2 \cdot Area_2 + \left(\frac{T_2}{\frac{A_2}{2}} \right) \cdot I_2 \right]$$

$\psi = 0.000135 \frac{1}{ft}$

$FEM_{gr} := E_b \cdot I_g \cdot \psi$

$FEM_{gr} = 398.71 \cdot kip \cdot ft$ *Gradient induced fixed end moment*

$M_{gr} := 524.0 kip \cdot ft$ *From Risa 3-D with given fixed end moments*

$$T_{UG} := \frac{\frac{T_1 + T_2}{2} \cdot A_1 + T_2 \cdot A_1 + \frac{T_2 + T_3}{2} \cdot A_2}{A_1 + A_2}$$

$T_{UG} = 22.105$ *Temperature averaged over the cross-section (F)*

$T_G := T_1 - T_3$

$T_G = 54$ *Temperature gradient (F)*

$f_{ist} := E_b \cdot \left[\alpha \cdot T_G - \alpha \cdot T_{UG} + \psi \cdot \left(y_{g\_top} - h_d\right)\right]$

$f_{ist} = 1.419\,ksi$ *Stress in top precast beam due to temperature gradient*

$f_{isb} := E_b \cdot \left(\alpha \cdot T_G - \alpha \cdot T_{UG} - \psi \cdot y_g\right)$

$f_{isb} = 0.315\,ksi$ *Stress in bottom of precast beam due to temperature gradient*

$f_{istt} := E_b \cdot \left(\alpha \cdot T_G - \alpha \cdot T_{UG} + \psi \cdot y_{g\_top}\right)$

$f_{istt} = 1.849\,ksi$ *Stress in top of CIP due to temperature gradient*

6. Flexural Stress Check

At Release:

Compression is unlikely to exceed its allowable value in any sections of the deck due to the nature of this type of structural system. For this reason the stress computations will be limited to the top and bottom of the precast beam.

$f_{swrt} := \frac{M_{swr}}{S_t} = \begin{pmatrix} 0.205 \\ 0.669 \end{pmatrix} \cdot ksi$ *Stress in top of beam at release due to self-weight of the beam*

$f_{swrb} := \frac{-M_{swr}}{S_b} = \begin{pmatrix} -0.18 \\ -0.589 \end{pmatrix} \cdot ksi$ *Stress in bottom of beam at release due to self-weight of the beam*

At Final Conditions:

Self-Weight:

$f_{swt} := \frac{M_{swf}}{S_t} = \begin{pmatrix} 0 \\ 0.173 \\ 0.14 \\ 0.669 \\ 0.627 \end{pmatrix} \cdot ksi$ *Stress in top of beam at time final due to self-weight of the beam*

$f_{swb} := \frac{-M_{swf}}{S_b} = \begin{pmatrix} 0 \\ -0.152 \\ -0.124 \\ -0.589 \\ -0.552 \end{pmatrix} \cdot ksi$ *Stress in bottom of beam at time final due to self-weight of the beam*

Deck Weight:

$f_{deckt} := \frac{M_{deck}}{S_t} = \begin{pmatrix} 0 \\ 0.16 \\ 0.13 \\ 0.618 \\ 0.579 \end{pmatrix} \cdot ksi$ *Stress in top of beam at time final due to weight of CIP concrete*

$$f_{deckb} := \frac{-M_{deck}}{S_b} = \begin{pmatrix} 0 \\ -0.14 \\ -0.114 \\ -0.543 \\ -0.509 \end{pmatrix} \cdot ksi$$

Stress in bottom of beam at time final due to weight of CIP concrete

Barriers:

$$f_{barriert} := \frac{M_{barrier}}{S_{g\_t}} = \begin{pmatrix} 0.0007 \\ 0.0026 \\ 0.0022 \\ 0.0052 \\ 0.0059 \end{pmatrix} \cdot ksi$$

Stress in top of beam at time final due to weight of barriers

$$f_{barrierb} := \frac{-M_{barrier}}{S_{g\_b}} = \begin{pmatrix} -0.0014 \\ -0.0049 \\ -0.0042 \\ -0.0098 \\ -0.0112 \end{pmatrix} \cdot ksi$$

Stress in bottom of beam at time final due to weight of barriers

$$f_{barriertt} := \frac{M_{barrier}}{S_{g\_d}} = \begin{pmatrix} 0.0016 \\ 0.0055 \\ 0.0047 \\ 0.011 \\ 0.0126 \end{pmatrix} \cdot ksi$$

Stress in top of CIP topping at time final due to weight of barriers

Future wearing surface:

$$f_{fwst} := \frac{M_{fws}}{S_{g\_t}} = \begin{pmatrix} 0.0017 \\ 0.0059 \\ 0.0051 \\ 0.0119 \\ 0.0136 \end{pmatrix} \cdot ksi$$

Stress in top of beam at time final due to weight of future wearing surface

$$f_{fwsb} := \frac{-M_{fws}}{S_{g\_b}} = \begin{pmatrix} -0.0032 \\ -0.0112 \\ -0.0096 \\ -0.0226 \\ -0.0258 \end{pmatrix} \cdot ksi$$

Stress in bottom of beam at time final due to weight of future wearing surface

$$f_{fwstt} := \frac{M_{fws}}{S_{g\_d}} = \begin{pmatrix} 0.0036 \\ 0.0125 \\ 0.0107 \\ 0.0254 \\ 0.029 \end{pmatrix} \cdot ksi$$

Stress in top of CIP topping at time final due to weight of future wearing surface

Positive Moment Envelope:

$$f_{pLLt} := \frac{M_{LL\_p}}{S_{g\_t}} = \begin{pmatrix} 0.03 \\ 0.104 \\ 0.09 \\ 0.24 \\ 0.245 \end{pmatrix} \cdot ksi$$

Stress in top of beam at time final due to maximum positive moment

$$f_{pLLb} := \frac{-M_{LL\_p}}{S_{g\_b}} = \begin{pmatrix} -0.056 \\ -0.198 \\ -0.169 \\ -0.455 \\ -0.464 \end{pmatrix} \cdot ksi$$

Stress in bottom of beam at time final due to maximum positive moment

$$f_{pLLtt} := \frac{M_{LL\_p}}{S_{g\_d}} = \begin{pmatrix} 0.063 \\ 0.222 \\ 0.19 \\ 0.511 \\ 0.521 \end{pmatrix} \cdot ksi$$

Stress in top of CIP topping at time final due to maximum positive moment

Negative Moment Envelope:

$$f_{nLLt} := \frac{M_{LL\_n}}{S_{g\_t}} = \begin{pmatrix} -0.0039 \\ -0.0135 \\ -0.0116 \\ -0.0733 \\ -0.056 \end{pmatrix} \cdot ksi$$

Stress in top of beam at time final due to minimum negative moment

$$f_{nLLb} := \frac{-M_{LL\_n}}{S_{g\_b}} = \begin{pmatrix} 0.0073 \\ 0.0256 \\ 0.0219 \\ 0.1388 \\ 0.106 \end{pmatrix} \cdot ksi$$

Stress in bottom of beam at time final due to minimum negative moment

$$f_{nLLtt} := \frac{M_{LL\_n}}{S_{g\_d}} = \begin{pmatrix} -0.0082 \\ -0.0287 \\ -0.0246 \\ -0.1558 \\ -0.119 \end{pmatrix} \cdot ksi$$

Stress in top of CIP topping at time final due to minimum negative moment

Restraint Moment:

Positive restraint moments can be be neglected due to 90 day beam age specification

$$f_{rmt} := \frac{M_{r\_neg}}{S_{g\_t}} = -0.306 ksi$$

Stress in top of beam at time final due to negative restraint moment

$f_{rmb} := \frac{-M_{r\_neg}}{S_{g\_b}} = 0.579\,ksi$ *Stress in bottom of beam at time final due to negative restraint moment*

$f_{rmtt} := \frac{M_{r\_neg}}{S_{g\_d}} = -0.65\,ksi$ *Stress in top of CIP topping at time final due to negative restraint moment*

Thermal Gradient:

$f_{grt} := \frac{M_{gr}}{S_{g\_t}} + f_{ist} = 1.921\,ksi$ *Stress in top of beam at time final due to thermal gradient effects*

$f_{grb} := \frac{-M_{gr}}{S_{g\_b}} + f_{isb} = -0.635\,ksi$ *Stress in bottom of beam at time final due to thermal gradient effects*

$f_{grtt} := \frac{M_{gr}}{S_{g\_d}} + f_{istt} = 2.915\,ksi$ *Stress in top of CIP topping at time final due to thermal gradient effects*

7. Prestress Losses

At Release:

Elastic Shortening:

$P_j := f_{pj} \cdot A_{ps} = 1 \times 10^3 \cdot kip$ *Jacking force*

$$f_{cgp} := \frac{P_j}{A_b} + \frac{P_j \cdot ecc^2}{I_b} - \frac{M_{swr_2} \cdot ecc}{I_b}$$

$f_{cgp} = 1.483\,ksi$ *Sum of concrete stresses at the center of gravity of prestressing tendons due to the prestressing force after jacking and the self-weight of the member at the sections of maximum moment*

$\Delta f_{pES} := \frac{E_p}{E_{bi}} \cdot f_{cgp}$ *(LRFD C5.9.5.2.3a-1)*

$\Delta f_{pES} = 9.86\,ksi$ *Loss of prestress due to elastic shortening*

Prestress Loss at Release:

$\%Loss := \frac{\Delta f_{pES}}{f_{pj}} \cdot 100 = 4.869$

$f_{pi} := f_{pj} - \Delta f_{pES}$

$f_{pi} = 192.64\,ksi$ *Stress remaining after losses at release*

$P_i := f_{pi} \cdot A_{ps} = 994.02\,kip$ *Force at release after losses*

Loss From Transfer to CIP Placement:

$$K_{id} := \frac{1}{1 + \frac{E_p}{E_{bi}} \cdot \frac{A_{ps}}{A_b} \cdot \left(1 + \frac{A_b \cdot ecc^2}{I_b}\right) \cdot \left(1 + 0.7 \cdot \psi_{bfi}\right)}$$ *(LRFD Eq. 5.9.5.4.2a-2)*

$K_{id} = 0.891$ *Transformed steel coefficient that accounts for time-dependent interaction between concrete and bonded steel in the section for the time period between transfer and CIP placement*

$\Delta f_{pSR} := -\varepsilon_{bid} \cdot E_p \cdot K_{id}$

$\Delta f_{pSR} = 7.259\,ksi$ *Prestress loss due to shrinkage of the girder concrete between time of transfer and CIP placement*

$P_{init} := f_{pj} \cdot A_{ps} = 1045\,kip$

$S_{cgp} := \frac{I_b}{ecc} = 6578\,in^3$

$\Delta f_{pCR} := \frac{E_p}{E_{bi}} \cdot f_{cgp} \cdot \psi_{bdi} \cdot K_{id}$ *(LRFD 5.9.5.4.2b-1)*

$\Delta f_{pCR} = 9.746\,ksi$ *Creep of precast beam*

$\Delta f_{pLTid} := \Delta f_{pSR} + \Delta f_{pCR}$

$\Delta f_{pLTid} = 17.005\,ksi$ *Total prestress loss at time of CIP placement*

Loss From CIP Placement to Final:

$e_{pc} := y_g - y_{bar\_strands} = 7.477\,in$

$$K_{df} := \frac{1}{1 + \frac{E_p}{E_{bi}} \cdot \frac{A_{ps}}{A_g} \cdot \left(1 + \frac{A_g \cdot e_{pc}^2}{I_g}\right) \cdot \left(1 + 0.7 \cdot \psi_{bfi}\right)}$$ *(LRFD 5.9.5.4.3a-2)*

$K_{df} = 0.91$

$\varepsilon_{bdf} := \varepsilon_{bif} - \varepsilon_{bid}$

$\varepsilon_{bdf} = -0.000121$ *Concrete shrinkage strain of girder between time of CIP placement and final time*

$\Delta f_{pSD} := -\varepsilon_{bdf} \cdot E_p \cdot K_{df}$

$\Delta f_{pSD} = 3.146\,ksi$ *Shrinkage of concrete girder from time of CIP placement to time final*

Creep of Concrete Girder:

$\Delta P := -\Delta f_{pLTid} \cdot A_{ps} = -87.748\,kip$

$$\Delta f_{cd} := \Delta P \cdot \left(\frac{1}{A_b} + \frac{ecc^2}{I_b}\right) - \left(\frac{M_{fws_2} + M_{barrier_2}}{S_{cgp}}\right)$$

$\Delta f_{cd} = -0.165\,ksi$

$$\Delta f_{pCD} := \frac{E_p}{E_{bi}} \cdot f_{cgp} \cdot \left(\psi_{bfi} - \psi_{bdi}\right) \cdot K_{df} + \frac{E_p}{E_b} \cdot \Delta f_{cd} \cdot \psi_{bfd} \cdot K_{df}$$ *(LRFD 5.9.5.4.3b-1)*

$\Delta f_{pCD} = 3.498\,ksi$ *Creep of precast beam*

Relaxation of Prestressing Strands:

$K_L := 30$ *For low relaxation strands*

$$\Delta f_{pR1} := \frac{f_{pi}}{K_L} \cdot \left(\frac{f_{pi}}{f_{py}} - 0.55 \right)$$ *(LRFD 5.9.5.4.2c-1)*

$\Delta f_{pR1} = 1.559\,ksi$ *Steel relaxation loss from time of deck placement to time final*

$\Delta f_{pR2} := \Delta f_{pR1}$ *Permissible for low relaxation strands*

Shrinkage of CIP Deck:

$$\Delta f_{cdf} := \frac{\varepsilon_{ddf} \cdot A_d \cdot E_d}{\left(1 + 0.7 \cdot \psi_{ddf}\right)} \cdot \left(\frac{1}{A_g} - \frac{e_{pc} \cdot e_d}{I_g} \right)$$ *(LRFD 5.9.5.4.3d-2)*

$\Delta f_{cdf} = -0.154\,ksi$

$$\Delta f_{pSS} := \frac{E_p}{E_b} \cdot \Delta f_{cdf} \cdot K_{df} \cdot \left(1 + 0.7 \cdot \psi_{bdf}\right)$$ *(LRFD 5.9.5.4.3d-1)*

$\Delta f_{pSS} = -1.213\,ksi$ *Prestress gain due to shrinkage of deck composite section*

Total Prestress Loss from CIP Placement to Time Final:

$\Delta f_{pLTdf} := \Delta f_{pSD} + \Delta f_{pCD} + \Delta f_{pR2} + \Delta f_{pSS}$

$\Delta f_{pLTdf} = 6.99\,ksi$

Summary of Time-Dependent Losses:

Losses from transfer to CIP placement

$\Delta f_{pSR} = 7.259\,ksi$ *Girder shrinkage*

$\Delta f_{pCR} = 9.746\,ksi$ *Girder creep*

$\Delta f_{pR1} = 1.559\,ksi$ *Steel relaxation*

$\Delta f_{pLTid} = 17.005\,ksi$ *Total*

Losses from CIP placement to time final

$\Delta f_{pSD} = 3.146\,ksi$ *Girder shrinkage*

$\Delta f_{pCD} = 3.498\,ksi$ *Girder creep*

$\Delta f_{pR2} = 1.559\,ksi$ *Steel relaxation*

$\Delta f_{pSS} = -1.213\,ksi$ *Differential shrinkage*

$\Delta f_{pLTdf} = 6.99\,ksi$ *Total*

$\Delta f_{pLT} := \Delta f_{pLTid} + \Delta f_{pLTdf}$

$\Delta f_{pLT} = 23.995\,ksi$

$\Delta f_{PT} := \Delta f_{pES} + \Delta f_{pLT}$

$\Delta f_{PT} = 33.856\,ksi$

$P_e := P_i - \Delta f_{PT} \cdot A_{ps} = 819.324\,kip$ *Effective prestress after all losses*

$\%Loss_{tot} := \frac{\Delta f_{PT}}{f_{pj}} \cdot 100 = 16.719$ *Percentage of jacking force lost due to time dependent effects*

Effective Stress After Losses:

$$Check := \begin{cases} Check \leftarrow \text{"OK"} & \text{if } f_{pj} - \Delta f_{PT} < 0.8 f_{py} \\ Check \leftarrow \text{"No Good"} & \text{otherwise} \end{cases}$$

Check = "OK"

8. Stresses Due to Prestress

Points of interest include end of transfer length and midspan

At Release:

$P_r := P_i$

$$f_{psrb} := \begin{cases} \text{for } n \in 1..2 \\ \quad f_{psrb_n} \leftarrow P_r \cdot \left(\frac{1}{A_b} + \frac{ecc}{S_b} \right) \\ f_{psrb} \end{cases}$$

$f_{psrb}^T = (2.335 \;\; 2.335) \cdot ksi$ *Stress in bottom of prestressed beam due to prestressing at release*

$$f_{psrt} := \begin{cases} \text{for } n \in 1..2 \\ \quad f_{psrt_n} \leftarrow P_r \cdot \left(\frac{1}{A_b} - \frac{ecc}{S_t} \right) \\ f_{psrt} \end{cases}$$

$f_{psrt}^T = (-0.385 \;\; -0.385) \cdot ksi$ *Stress in top of prestressed beam due to prestressing at release*

At Final Conditions:

$$dist := \begin{cases} \text{for } n \in 1..5 \\ \quad dist_n \leftarrow x_{f_n} + \frac{L_b - L_{des}}{2} \\ dist \end{cases}$$

$dist^T = (0.5 \;\; 3 \;\; 2.5 \;\; 18.5 \;\; 14)\,ft$

$$dt := \begin{cases} \text{for } n \in 1..5 \\ \quad \begin{cases} dt_n \leftarrow 1 & \text{if } dist_n > L_t \\ dt_n \leftarrow \frac{dist_n}{L_t} & \text{otherwise} \end{cases} \\ dt \end{cases}$$

$dt^T = (0.167 \;\; 1 \;\; 0.833 \;\; 1 \;\; 1)$

$P_f := \left| \begin{array}{l} \text{for } n \in 1..5 \\ \quad P_{f_n} \leftarrow f_{pe} \cdot dt_n \cdot A_{ps} \\ P_f \end{array} \right.$

$P_f^T = (159.1 \;\; 954.6 \;\; 795.5 \;\; 954.6 \;\; 954.6) \cdot kip$

$f_{psb} := \left| \begin{array}{l} \text{for } n \in 1..5 \\ \quad f_{psb_n} \leftarrow P_{f_n} \cdot \left(\frac{1}{A_b} + \frac{ecc}{S_b} \right) \\ f_{psb} \end{array} \right.$

$f_{psb}^T = (0.374 \;\; 2.242 \;\; 1.869 \;\; 2.242 \;\; 2.242) \cdot ksi$ *Stress in bottom of prestressed beam due to prestressing at time final*

$f_{pst} := \left| \begin{array}{l} \text{for } n \in 1..5 \\ \quad f_{pst_n} \leftarrow P_{f_n} \cdot \left(\frac{1}{A_b} - \frac{ecc}{S_t} \right) \\ f_{pst} \end{array} \right.$

$f_{pst}^T = (-0.062 \;\; -0.37 \;\; -0.308 \;\; -0.37 \;\; -0.37) \cdot ksi$ *Stress in top of prestressed beam due to prestressing at time final*

9. Service Stress Check

At Release:

$f_{rb} := \left| \begin{array}{l} \text{for } n \in 1..2 \\ \quad f_{rb_n} \leftarrow f_{psrb_n} + f_{swrb_n} \\ f_{rb} \end{array} \right.$

$f_{rb}^T = (2.155 \;\; 1.746) \cdot ksi$ *Service stress at bottom of beam*

$f_{allow\_rc} := 0.6 \cdot f_{ci\_b} = 3 \cdot ksi$ *Allowable stress for compression* *(LRFD 5.9.4.1.1)*

$Status\_ServiceLSrc := \left| \begin{array}{l} \text{for } n \in 1..2 \\ \quad \left| \begin{array}{l} a_n \leftarrow \text{"OK"} \quad \text{if } f_{rb_n} \le f_{allow\_rc} \\ a_n \leftarrow \text{"No Good"} \quad \text{otherwise} \end{array} \right. \\ a \end{array} \right.$

$Status\_ServiceLSrc^T = (\text{"OK"} \quad \text{"OK"})$ *Check of service stress at bottom of beam*

$f_{rt} := \left| \begin{array}{l} \text{for } n \in 1..2 \\ \quad f_{rt_n} \leftarrow f_{psrt_n} + f_{swrt_n} \\ f_{rt} \end{array} \right.$

$f_{rt}^T = (-0.181 \;\; 0.284) \cdot ksi$ *Service stress at top of beam*

$f_{allow\_rt} := \begin{cases} -0.0948\sqrt{f_{ci\_b}\cdot ksi} & \text{if } -0.0948\sqrt{f_{ci\_b}\cdot ksi} \geq -0.2\,ksi \\ (-0.2\,ksi) & \text{otherwise} \end{cases}$ *(LRFD Table 5.9.4.1.2-1)*

$f_{allow\_rt} = -0.2\cdot ksi$ *Allowable stress for tension*

Status_ServiceLSrt := for $n \in 1..2$
$a_n \leftarrow$ "OK" if $f_{rt_n} \geq f_{allow\_rt}$
$a_n \leftarrow$ "No Good" otherwise
a

$Status\_ServiceLSrt^T = (\text{"OK"} \quad \text{"OK"})$ *Check of service stress at top of beam*

At Final Conditions:
Positive Moment Envelope:

$f_{pAllb} :=$ for $n \in 1..5$
$f_{pAllb_n} \leftarrow f_{psb_n} + f_{swb_n} + f_{deckb_n} + f_{barrierb_n} + f_{fwsb_n}$
$f_{pAllb_n} \leftarrow f_{pAllb_n} + (0.8\,f_{pLLb})_n + f_{rmb} + 0.5\,f_{grb}$
f_{pAllb}

$f_{pAllb}^T = (0.586 \quad 2.037 \quad 1.743 \quad 0.975 \quad 1.035)\cdot ksi$ *Service III Limit State (tensile stresses in bottom of beam)*

$f_{allow\_ft} := -0.19\sqrt{f_{c\_b}\cdot ksi}$

$f_{allow\_ft} = -0.537\cdot ksi$ *Allowable tensile stress* (LRFD Table 5.9.4.2.2-1)

Status_ServiceLSft := for $n \in 1..5$
$a_n \leftarrow$ "OK" if $f_{pAllb_n} \geq f_{allow\_ft}$
$a_n \leftarrow$ "No Good" otherwise
a

$Status\_ServiceLSft^T = (\text{"OK"} \quad \text{"OK"} \quad \text{"OK"} \quad \text{"OK"} \quad \text{"OK"})$ *Check of Service Level III stress at bottom of beam*

$f_{pPermt} :=$ for $n \in 1..5$
$f_{pPermt_n} \leftarrow f_{pst_n} + f_{swt_n} + f_{deckt_n} + f_{barriert_n} + f_{fwst_n}$
$f_{pPermt_n} \leftarrow f_{pPermt_n} + f_{rmt} + 0.5\,f_{grt}$
f_{pPermt}

$f_{pPermt}^T = (0.595 \quad 0.626 \quad 0.624 \quad 1.589 \quad 1.511)\cdot ksi$ *Compressive stress due to permanent loads*

$f_{allow\_fcd} := 0.45\cdot f_{c\_b}$ *(LRFD Table 5.9.4.2.1-1)*

$f_{allow\_fcd} = 3.6\cdot ksi$ *Allowable compressive stress*

$$\text{Status\_ServiceLSfcd} := \left| \begin{array}{l} \text{for } n \in 1..5 \\ \quad \left| \begin{array}{l} a_n \leftarrow \text{"OK"} \quad \text{if } f_{pPermt_n} \le f_{allow\_fcd} \\ a_n \leftarrow \text{"No Good"} \quad \text{otherwise} \end{array} \right. \\ a \end{array} \right.$$

$\text{Status\_ServiceLSfcd}^T = (\text{"OK"} \quad \text{"OK"} \quad \text{"OK"} \quad \text{"OK"} \quad \text{"OK"})$

Check of Service Level I stress at top of beam

$$f_{pAllt} := \left| \begin{array}{l} \text{for } n \in 1..5 \\ \quad \left| \begin{array}{l} f_{pAllt_n} \leftarrow f_{pst_n} + f_{swt_n} + f_{deckt_n} + f_{barriert_n} + f_{fwst_n} \\ f_{pAllt_n} \leftarrow f_{pAllt_n} + f_{pLLt_n} + f_{rmt} + 0.5 f_{grt} \end{array} \right. \\ f_{pAllt} \end{array} \right.$$

$f_{pAllt}^T = (0.625 \quad 0.73 \quad 0.713 \quad 1.829 \quad 1.756)\cdot ksi$

Compressive stress due to full dead load + live load

$f_{allow\_fcl} := 0.6 \cdot f_{c\_b}$

(LRFD Table 5.9.4.2.1-1)

$f_{allow\_fcl} = 4.8 \cdot ksi$ *Allowable compressive stress*

$$\text{Status\_ServiceLSfcl} := \left| \begin{array}{l} \text{for } n \in 1..5 \\ \quad \left| \begin{array}{l} a_n \leftarrow \text{"OK"} \quad \text{if } f_{pAllt_n} \le f_{allow\_fcl} \\ a_n \leftarrow \text{"No Good"} \quad \text{otherwise} \end{array} \right. \\ a \end{array} \right.$$

$\text{Status\_ServiceLSfcl}^T = (\text{"OK"} \quad \text{"OK"} \quad \text{"OK"} \quad \text{"OK"} \quad \text{"OK"})$

Check for compressive stress due to full dead load + live load

Negative Moment Envelope:

$$f_{nAllb} := \left| \begin{array}{l} \text{for } n \in 1..5 \\ \quad \left| \begin{array}{l} f_{nAllb_n} \leftarrow f_{psb_n} + f_{swb_n} + f_{deckb_n} + f_{barrierb_n} + f_{fwsb_n} \\ f_{nAllb_n} \leftarrow f_{nAllb_n} + f_{nLLb_n} + f_{rmb} + 0.5 f_{grb} \end{array} \right. \\ f_{nAllb} \end{array} \right.$$

$f_{nAllb}^T = (0.638 \quad 2.221 \quad 1.901 \quad 1.478 \quad 1.512)\cdot ksi$

$f_{allow\_fcn} := 0.6 \cdot f_{c\_b}$

$f_{allow\_fcn} = 4.8 \cdot ksi$ *Allowable compressive stress* *(LRFD 5.9.4.2.1)*

$$\text{Status\_ServiceLSfnc} := \left| \begin{array}{l} \text{for } n \in 1..5 \\ \quad \left| \begin{array}{l} a_n \leftarrow \text{"OK"} \quad \text{if } f_{nAllb_n} < f_{allow\_fcn} \\ a_n \leftarrow \text{"No Good"} \quad \text{otherwise} \end{array} \right. \\ a \end{array} \right.$$

Status_ServiceLSfnc^T = ("OK" "OK" "OK" "OK" "OK")

Check for compressive stress due to full dead load + live load

10. Flexural Strength Check

Positive Moment Envelope:

$$M_{rm} := \begin{pmatrix} 0 \\ 0 \\ 0 \\ 0 \\ 0 \end{pmatrix} kip\cdot ft$$

Due to specification of 90 day aging of precast beam

$$M_u := \left| \begin{array}{l} \text{for } n \in 1..5 \\ \quad M_{u_n} \leftarrow 1.25\left(M_{swf_n} + M_{deck_n} + M_{barrier_n}\right) + 1.5M_{fws_n} + 1.75M_{LL\_p_n} + M_{rm_n} \\ M_u \end{array} \right.$$

$M_u{}^T = (58.2 \;\; 301.7 \;\; 254.2 \;\; 844.7 \;\; 833)\cdot kip\cdot ft$ *Ultimate moment*

$$\beta_1 := \left| \begin{array}{l} \beta_1 \leftarrow 0.85 \text{ if } f_{c\_d} \le 4ksi \\ \beta_1 \leftarrow 0.65 \text{ if } f_{c\_d} \ge 8ksi \\ \beta_1 \leftarrow \frac{f_{c\_d} - 4ksi}{1ksi}\cdot 0.05 \text{ otherwise} \end{array} \right.$$

(LRFD 5.7.2.2)

$\beta_1 = 0.85$ *Stress block factor based on CIP concrete*

$$L_d := \left(270ksi - \frac{2}{3}\cdot f_{pe}\right)\cdot\frac{d_b}{ksi}$$

$L_d = 88\cdot in$ *Preliminary estimate*

$$K_{ld} := \left| \begin{array}{l} K_{ld} \leftarrow 1 \text{ if } h_b \le 24in \\ K_{ld} \leftarrow 1.6 \text{ otherwise} \end{array} \right.$$

(LRFD Eq. 5.11.4.2-1)

$K_{ld} = 1$

$$df := \left| \begin{array}{l} \text{for } n \in 1..5 \\ \quad \left| \begin{array}{l} df_n \leftarrow \frac{dist_n}{L_t}\cdot\frac{f_{pe}}{f_{pu}} \text{ if } dist_n < L_t \\ df_n \leftarrow \frac{f_{pe} + \left(\frac{dist_n - L_t}{K_{ld}\cdot L_d - L_t}\right)\cdot\left(f_{pu} - f_{pe}\right)}{f_{pu}} \text{ if } dist_n < K_{ld}\cdot L_d \\ df_n \leftarrow 1.0 \text{ otherwise} \end{array} \right. \\ df \end{array} \right.$$

$df^T = (0.504\ \ 0.685\ \ 0.649\ \ 1\ \ \ 1)$ *Preliminary estimate of fraction of strands are developed*

$A_{ps} :=$ for $n \in 1..5$
$\quad A_{ps_n} \leftarrow Num_{strands} \cdot df_n \cdot A_p$
A_{ps}

$A_{ps}^T = (2.598\ \ 3.536\ \ 3.348\ \ 5.16\ \ \ 5.16)\cdot in^2$ *Area of prestressing steel developed along length*

$b := b_{eff} = 72\cdot in$

$d_p := h_b + h_d - h_{ws} - y_{bar\_strands}$

$d_p = 20.7\cdot in$ *Depth to prestress*

$k := 2\cdot\left(1.04 - \frac{f_{py}}{f_{pu}}\right)$ *(LRFD 5.7.3.1.1-2)*

$k = 0.28$

$c :=$ for $n \in 1..5$ *(LRFD 5.7.3.1.1-4)*

$$c_n \leftarrow \frac{A_{ps_n}\cdot f_{pu}}{0.85 f_{c\_d}\cdot\beta_1\cdot b + k\cdot A_{ps_n}\cdot\frac{f_{pu}}{d_p}}$$

c

$c^T = (3.225\ \ 4.32\ \ 4.103\ \ 6.139\ \ 6.139)\cdot in$ *Preliminary calculation*

$h_f := h_d$ *Since section is composite height of flange is the same as the slab thickness*

$b_w :=$ for $n \in 1..5$
$\quad b_{w_n} \leftarrow b$ if $c_n \le h_f$
$\quad b_{w_n} \leftarrow b_v$ otherwise
b_w

$b_w^T = (72\ \ 72\ \ 72\ \ 72\ \ 72)\cdot in$ *Width of web*

$c :=$ for $n \in 1..5$

$$c_n \leftarrow \frac{A_{ps_n}\cdot f_{pu} - 0.85 f_{c\_d}\cdot\left(b - b_{w_n}\right)\cdot h_f}{0.85 f_{c\_d}\cdot\beta_1\cdot b_{w_n} + k\cdot A_{ps_n}\cdot\frac{f_{pu}}{d_p}}$$

c

$c^T = (3.225\ \ 4.32\ \ 4.103\ \ 6.139\ \ 6.139)\cdot in$ *Iterative calculation* *(LRFD 5.7.3.1.1-3)*

$$a := \left| \begin{array}{l} \text{for } n \in 1..5 \\ \quad a_n \leftarrow \beta_1 \cdot c_n \\ a \end{array} \right.$$

$a^T = (2.741 \;\; 3.672 \;\; 3.488 \;\; 5.219 \;\; 5.219)\cdot in$ *Depth of equivalent stress block*

$$f_{ps} := \left| \begin{array}{l} \text{for } n \in 1..5 \\ \quad f_{ps_n} \leftarrow f_{pu}\cdot\left(1 - k\cdot\frac{c_n}{d_p}\right) \\ f_{ps} \end{array} \right.$$ *(LRFD 5.7.3.1.1-1)*

$f_{ps}{}^T = (258.2 \;\; 254.2 \;\; 255 \;\; 247.6 \;\; 247.6)\cdot ksi$ *Average stress in prestressing steel at nominal bending resistance*

$$L_d := K_{ld}\cdot\left(f_{ps_1} - \frac{2}{3}\cdot f_{pe}\right)\cdot\frac{d_b}{ksi}$$ *(LRFD 5.11.4.2-1)*

$L_d = 80.934\,in$ *Development length*

$$df := \left| \begin{array}{l} \text{for } n \in 1..5 \\ \quad \left| \begin{array}{l} df_n \leftarrow \frac{dist_n}{L_t}\cdot\frac{f_{pe}}{f_{ps_n}} \quad \text{if } dist_n < L_t \\ df_n \leftarrow \frac{f_{pe} + \left(\frac{dist_n - L_t}{K_{ld}\cdot L_d - L_t}\right)\cdot\left(f_{ps_n} - f_{pe}\right)}{f_{ps_n}} \quad \text{if } dist_n < K_{ld}\cdot L_d \\ df_n \leftarrow 1.0 \quad \text{otherwise} \end{array} \right. \\ df \end{array} \right.$$

$df^T = (0.527 \;\; 0.728 \;\; 0.689 \;\; 1 \;\; 1)$ *Fraction strands are developed*

$$A_{ps} := \left| \begin{array}{l} \text{for } n \in 1..5 \\ \quad A_{ps_n} \leftarrow Num_{strands}\cdot df_n \cdot A_p \\ A_{ps} \end{array} \right.$$

$A_{ps}{}^T = (2.72 \;\; 3.755 \;\; 3.554 \;\; 5.16 \;\; 5.16)\cdot in^2$

$$c := \left| \begin{array}{l} \text{for } n \in 1..5 \\ \quad c_n \leftarrow \frac{A_{ps_n}\cdot f_{pu}}{0.85 f_{c\_d}\cdot\beta_1\cdot b + k\cdot A_{ps_n}\cdot\frac{f_{pu}}{d_p}} \\ c \end{array} \right.$$

$c^T = (3.368\ \ 4.571\ \ 4.341\ \ 6.139\ \ 6.139)\cdot in$ *Iterative calculation*

$$b_w := \left| \begin{array}{l} \text{for } n \in 1..5 \\ \quad \left| \begin{array}{l} b_{w_n} \leftarrow b \text{ if } c_n \le h_f \\ b_{w_n} \leftarrow b_v \text{ otherwise} \end{array} \right. \\ b_w \end{array} \right.$$

$b_w^T = (72\ \ 72\ \ 72\ \ 72\ \ 72)\cdot in$ *Width of web*

$$c := \left| \begin{array}{l} \text{for } n \in 1..5 \\ \quad c_n \leftarrow \dfrac{A_{ps_n}\cdot f_{pu} - 0.85 f_{c\_d}\cdot\left(b - b_{w_n}\right)\cdot h_f}{0.85 f_{c\_d}\cdot\beta_1\cdot b_{w_n} + k\cdot A_{ps_n}\cdot\dfrac{f_{pu}}{d_p}} \\ c \end{array} \right.$$

(LRFD 5.7.3.1.1-3)

$c^T = (3.368\ \ 4.571\ \ 4.341\ \ 6.139\ \ 6.139)\cdot in$ *Distance between the neutral axis and the compressive face*

$$M_n := \left| \begin{array}{l} \text{for } n \in 1..5 \\ \quad M_{n_n} \leftarrow df_n\cdot A_{ps_n}\cdot f_{ps_n}\cdot\left(d_p - \dfrac{a_n}{2}\right) \\ M_n \end{array} \right.$$

$M_n^T = (596.3\ \ 1092\ \ 986.2\ \ 1925.9\ \ 1925.9)\cdot kip\cdot ft$ *Nominal moment capacity*

$$\phi_f := \left| \begin{array}{l} \text{for } n \in 1..5 \\ \quad \left| \begin{array}{l} \phi_{f_n} \leftarrow \left[0.583 + 0.25\left(\dfrac{d_p}{c_n} - 1\right)\right] \text{ if } \left[0.583 + 0.25\left(\dfrac{d_p}{c_n} - 1\right)\right] < 1 \\ \phi_{f_n} \leftarrow 1 \text{ otherwise} \end{array} \right. \\ \phi_f \end{array} \right.$$

(LRFD Eq. 5.5.4.2.1-1)

$\phi_f^T = (1\ \ 1\ \ 1\ \ 1\ \ 1)$ *ϕ factor for flexure*

$$M_r := \left| \begin{array}{l} \text{for } n \in 1..5 \\ \quad M_{r_n} \leftarrow \phi_{f_n}\cdot M_{n_n} \\ M_r \end{array} \right.$$

$M_r^T = (596.3\ \ 1092\ \ 986.2\ \ 1925.9\ \ 1925.9)\cdot kip\cdot ft$ *Factored moment capacity*

$$Status\_ServiceLS := \left| \begin{array}{l} \text{for } n \in 1..5 \\ \quad \left| \begin{array}{l} a_n \leftarrow \text{"OK"} \text{ if } M_{u_n} \le M_{r_n} \\ a_n \leftarrow \text{"No Good"} \text{ otherwise} \end{array} \right. \\ a \end{array} \right.$$

$Status\_ServiceLS^{T} = (\text{"OK"} \quad \text{"OK"} \quad \text{"OK"} \quad \text{"OK"} \quad \text{"OK"})$ *Checks that factored nominal capacity exceeds ultimate moment*

Minimum Steel Check:

$f_r := 0.37 \cdot \sqrt{f_{c\_b} \cdot ksi}$

$f_r = 1.047\,ksi$ *Cracking stress*

$M_{cr} := S_{g\_b} \cdot \left(f_r + f_{psb_5}\right) - \left(M_{swf_5} + M_{deck_5}\right) \cdot \left(\frac{S_{g\_b}}{S_b} - 1\right)$ *(LRFD 5.7.3.3.2)*

$M_{cr} = 1514\,kip \cdot ft$ *Cracking moment*

$1.2 M_{cr} = 1817\,kip \cdot ft$

$1.33 M_{u_4} = 1123\,kip \cdot ft$

$M_{min} := \begin{cases} M_{min} \leftarrow S_{g\_b} \cdot f_r & \text{if } 1.2 M_{cr} < S_{g\_b} \cdot f_r \\ M_{min} \leftarrow 1.2 M_{cr} & \text{otherwise} \end{cases}$

$M_{min} = 1817\,kip \cdot ft$

$Status\_MinStl := \begin{cases} a \leftarrow \text{"OK"} & \text{if } M_{min} < M_{r_5} \\ a \leftarrow \text{"No Good"} & \text{otherwise} \\ a \end{cases}$

$Status\_MinStl = \text{"OK"}$ *Check for minimum steel*

Negative Moment Envelope:

$M_{LL\_nc} := DF \cdot \left[M_{lane\_nc_{11}} + (1 + DLA) \cdot M_{vehicle\_nc_{11}}\right]$

$M_{LL\_nc} = -160.941\,kip \cdot ft$ *Max negative LL moment occurs at middle pier support*

$M_{un} := 1.25\left(M_{barrier\_c_{11}}\right) + 1.5\left(M_{fws\_c_{11}}\right) + 1.75\left(M_{LL\_nc}\right)$

$M_{un} = -333.772\,kip \cdot ft$ *Max ultimate negative moment (occurs at middle pier support)*

$\beta_{1n} := \begin{cases} \beta_1 \leftarrow 0.85 & \text{if } f_{c\_b} \leq 4ksi \\ \beta_1 \leftarrow 0.65 & \text{if } f_{c\_b} \geq 8ksi \\ \beta_1 \leftarrow \frac{f_{c\_b} - 4ksi}{1ksi} \cdot 0.05 & \text{otherwise} \end{cases}$ *(LRFD 5.7.2.2)*

$\beta_{1n} = 0.65$ *Stress block factor based on precast beam concrete*

$c_n := \frac{A_{s\_d} \cdot f_y}{0.85 f_{c\_b} \cdot \beta_{1n} \cdot b_b}$ *(LRFD 5.7.3.1.1-4)*

$c_n = 0.664\,in$ *Iterative calculation*

$b_{wn} := \begin{cases} b_{wn} \leftarrow b_b & \text{if } c_n \leq h_f \\ b_{wn} \leftarrow b_v & \text{otherwise} \end{cases}$

$b_{wn} = 72 \cdot in$

$$c_n := \frac{A_{s\_d} \cdot f_y - 0.85 f_{c\_d} \cdot (b_b - b_{wn}) \cdot h_f}{0.85 f_{c\_b} \cdot \beta_{1n} \cdot b_b} \qquad \textit{(LRFD 5.7.3.1.1-3)}$$

$c_n = 0.664 in$ *Distance between the neutral axis and the compressive face for negative moment*

$a_n := \beta_{1n} \cdot c_n$

$a_n = 0.036 ft$ *Depth of equivalent stress block for negative bending*

$$\phi_f := \left| \begin{array}{l} \text{for } n \in 1..5 \\ \quad \left| \begin{array}{l} \phi_{f_n} \leftarrow \left[0.583 + 0.25 \left(\frac{d_p}{c_n} - 1 \right) \right] \text{ if } \left[0.583 + 0.25 \left(\frac{d_p}{c_n} - 1 \right) \right] < 1 \\ \phi_{f_n} \leftarrow 1 \text{ otherwise} \end{array} \right. \\ \phi_f \end{array} \right. \qquad \textit{(LRFD Eq. 5.5.4.2.1-1)}$$

$\phi_f^T = (1 \;\; 1 \;\; 1 \;\; 1 \;\; 1)$ *ϕ factor for flexure for negative bending*

$$d_s := h_c - cover_d - \frac{D_{bar\_d}}{2} = 23.75 in$$

$d_s = 23.75 in$ *Depth to steel*

$$M_{rn} := \phi_{f_5} \cdot A_{s\_d} \cdot f_y \cdot \left(d_s - \frac{a_n}{2} \right)$$

$M_{rn} = 414.204 kip \cdot ft$ *Factored moment for negative bending*

$$Status\_StrengthLSn := \left| \begin{array}{l} a \leftarrow \text{"OK"} \text{ if } -M_{un} \le M_{rn} \\ a \leftarrow \text{"No Good"} \text{ otherwise} \\ a \end{array} \right.$$

Status_StrengthLSn = "OK" *Check for minimum steel*

11. Vertical Shear Design

Critical Section for Shear:

$d_e := d_s$

$d_{v1} := d_s - \frac{a_n}{2} = 23.534 in$ *Effective shear depth (distance between resultants of tensile and compressive forces)*

$$d_{v\_min} := \left| \begin{array}{l} (0.9 d_e) \text{ if } 0.9 d_e \ge 0.72 h_c \\ (0.72 h_c) \text{ otherwise} \end{array} \right.$$

d_v need not be taken less than greater of $0.9 * d_e$ and $0.72 * h_c$

$d_{v\_min} = 21.375\,in$

$d_v := \begin{cases} d_{v1} & \text{if } d_{v1} \geq d_{v\_min} \\ d_{v\_min} & \text{otherwise} \end{cases}$

$d_v = 23.534\,in$ *Actual value for d_v*

Critical Section:

$\theta := 32.3\,deg$ *Assumption of theta*

$Crit\_sec1 := \begin{cases} d_v + \frac{L_{pad}}{2} & \text{if } d_v > 0.5\,d_v \cdot \cot(\theta) \\ \left(0.5\,d_v \cdot \cot(\theta)\right) + \frac{L_{pad}}{2} & \text{otherwise} \end{cases}$ *The distance from the face of support to the centerline of bearing is half the bearing pad length* *(LRFD 5.8.2.7)*

$Crit\_sec1 = 29.534\,in$ *Critical section for shear*

$V_u := 1.25\left(V_{swf_3} + V_{deck_3} + V_{barrier_3}\right) + 1.5\,V_{fws_3} + 1.75\,V_{LL\_p_3}$

$V_u = 96.566\,kip$ *Factored shear at 0.72*h from the face of the support*

$V_p := 0$ *Straight tendons* *(LRFD 5.8.3.4.3)*

$V_{r\_max} := \phi_v \cdot \left(0.25 \cdot f_{c\_b} \cdot b_v \cdot d_v + V_p\right)$ *(LRFD 5.8.3.3-2)*

$V_{r\_max} = 3050\,kip$ *Maximum permissible shear capacity at a section*

$Status\_V_{rmax} := \begin{cases} a \leftarrow \text{"OK"} & \text{if } V_u \leq V_{r\_max} \\ a \leftarrow \text{"No Good"} & \text{otherwise} \\ a \end{cases}$

$Status\_V_{rmax} = \text{"OK"}$ *Check for vertical shear*

$M_{uv} := 1.25\left(M_{swf_3} + M_{deck_3} + M_{barrier_3}\right) + 1.5\,M_{fws_3} + 1.75\,M_{LL\_n_3}$

$M_{uv} = 69.357\,kip \cdot ft$ *Shear contribution from the concrete*

$M_{uLB} := \begin{cases} \left(d_v \cdot V_u\right) & \text{if } \left|M_{uv}\right| < d_v \cdot V_u \\ \left|M_{uv}\right| & \text{otherwise} \end{cases}$

$M_{uLB} = 189.384\,kip \cdot ft$ *Lower bound for M_u*

$\varepsilon_s := \begin{cases} \frac{\frac{M_{uLB}}{d_v} + V_u}{E_s \cdot A_s + E_p \cdot A_p} & \text{if } \frac{\frac{M_{uLB}}{d_v} + V_u}{E_s \cdot A_s + E_p \cdot A_p} > 0 \\ 0 & \text{otherwise} \end{cases}$ *(LRFD 5.8.3.4.2-4)*

$\varepsilon_s = 0.031519$

$$\beta := \frac{4.8}{1 + 750 \cdot \varepsilon_s}$$ *(LRFD 5.8.3.4.2-1)*

$\beta = 0.1948$

$\theta := 29 + 3500 \varepsilon_s$ *(LRFD 5.8.3.4.2-3)*

$\theta = 139.316$ *(LRFD 5.8.3.4.2-3)*

$V_c := 0.0316 \beta \cdot \sqrt{f_{c\_b} \cdot ksi} \cdot b_v \cdot d_v$

$V_c = 29.5 \cdot kip$ *New value for V_C*

$$V_s := \frac{V_u}{\phi_v} - V_c$$

$V_s = 77.791 \cdot kip$ *Required V_S*

$$A_v := \frac{V_s}{f_y \cdot d_v \cdot \cot(\theta \cdot deg)}$$ *(LRFD C5.8.3.3-1)*

$$A_v = -0.568 \frac{in^2}{ft}$$

$$Spac := -\left(\frac{2 \cdot A_{shearbar}}{A_v} \right)$$

$Spac = 8.446 in$ *Stirrup spacing*

$$A_{v\_min} := 0.0316 \sqrt{f_{c\_b} \cdot ksi} \cdot \frac{b_v}{f_y}$$ *(LRFD 5.8.2.5-1)*

$$A_{v\_min} = 1.287 \frac{in^2}{ft}$$ *Minimum transverse reinforcement*

$V_{spc} := 0.1 \cdot f_{c\_b} \cdot b_v \cdot d_v$

$V_{spc} = 1356 kip$

$$Max\_spac := \begin{cases} 0.8 d_v & \text{if } V_u < V_{spc} \wedge 0.8 d_v < 24 in \\ 24 in & \text{if } V_u < V_{spc} \wedge 0.8 d_v \geq 24 in \\ 0.4 d_v & \text{if } V_u \geq V_{spc} \wedge 0.4 d_v < 12 in \\ 12 in & \text{if } V_u \geq V_{spc} \wedge 0.4 d_v \geq 12 in \end{cases}$$ *(LRFD 5.8.2.7-1) & (LRFD 5.8.2.7-2)*

$Max\_spac = 18.827 in$

$$Status\_spac := \begin{cases} a \leftarrow \text{"OK"} & \text{if } Spac \leq Max\_spac \\ a \leftarrow \text{"No Good"} & \text{otherwise} \\ a \end{cases}$$

Status_spac = "OK" *Check for vertical shear reinforcement spacing*

12. Longitudinal Reinforcement Check

Required Tension Tie Force:

$$A_{v\_actual} := 2 \cdot A_{shearbar} \cdot \frac{12in}{Spac}$$

$A_{v\_actual} = 0.568 in^2$ *Actual amount of transverse steel per foot*

$$V_{s\_actual\_1} := \frac{A_{v\_actual} \cdot f_y \cdot d_v \cdot \cot(\theta \cdot deg)}{12in}$$ *(LRFD 5.8.3.5)*

$V_{s\_actual\_1} = -77.8 kip$ *Actual value of V_S used based on bars and spacing specified*

$$V_{s\_actual\_max} := \frac{V_u}{\phi_v}$$

$V_{s\_actual\_max} = 107.3 kip$ *Upper limit of V_S*

$$V_{s\_actual} := \begin{cases} V_{s\_actual\_1} & \text{if } V_{s\_actual\_1} < V_{s\_actual\_max} \\ V_{s\_actual\_max} & \text{otherwise} \end{cases}$$

$V_{s\_actual} = -77.791 kip$ *Lesser of V_S calculated and V_S max*

$$F_{L\_reqd} := \left(\frac{V_u}{\phi_v} - 0.5 V_{s\_actual} - V_p \right) \cdot \cot(\theta \cdot deg)$$ *(LRFD Eq. 5.8.3.5-2)*

$F_{L\_reqd} = -170.1 kip$ *Required tension tie force*

Provided Tension Tie Force:

The stress in the strands at a given section depends on the location of the section with respect to the end of the precast section. If the section is between the end of the beam and L_t (see figure), a linear interpolation is performed using a stress variation of 0.0 at the end of the beam to f_{pe} at a distance of L_t from the end of the precast section. If the section is to the right of L_t but to the left of L_d, then the stress is interpolated between f_{pe} and f_{ps}. If the section is to the right of L_d, then the stress is assumed to be a constant value of f_{ps}.

$$x_{FB} := \frac{L_b - L_{des}}{2} + \frac{L_{pad}}{2}$$

$x_{FB} = 1 ft$ *Distance from physical end of beam to face of bearing*

$A_{str} := Num_{strands} \cdot A_p = 5.16 in^2$ *Area of prestressing steel*

$$F_{L\_prov} := \begin{cases} \left(A_{str} \cdot f_{pe} \cdot \frac{x_{FB}}{L_t} \right) & \text{if } \left(x_{FB} < L_t \right) \\ \left(A_{str} \cdot f_{pe} \right) & \text{if } \left(x_{FB} > L_d \right) \\ \left[A_{str} \cdot \left[f_{pe} + \frac{x_{FB} - K_{ld} \cdot L_d + L_t}{K_{ld} \cdot L_d - L_t} \cdot \left(f_{ps} - f_{pe} \right) \right] \right] & \text{otherwise} \end{cases}$$

Finds provided tension tie force from figure

$F_{L\_prov} = 318.2\,kip$

$$Status\_V_1 := \begin{cases} a \leftarrow \text{"OK"} & \text{if } F_{L\_prov} \geq -F_{L\_reqd} \\ a \leftarrow \text{"No Good"} & \text{otherwise} \\ a \end{cases}$$

$Status\_V_1 = \text{"OK"}$ *Check for provided tension tie force*

Refined Estimate of Provided Tension Tie Force:

Additional tensile capacity from the strands can be utilized if the force in the strands is computed at the point of intersection of the bearing crack and centroid of the strands.

$$x_c := \left(\frac{L_b - L_{des}}{2}\right) + \left(\frac{L_{pad}}{2}\right) + ecc \cdot \cot(\theta \cdot deg)$$

$x_c = 7.204\,in$ *Distance from end of beam to point of intersection of assumed crack and center of gravity of effective strands measured from end of beam*

$$F_{L\_prov\_c} := \begin{cases} \left(A_{str} \cdot f_{pe} \cdot \frac{x_c}{L_t}\right) & \text{if } (x_c < L_t) \\ \left(A_{str} \cdot f_{pe}\right) & \text{if } (x_c > L_d) \\ \left[A_{str} \cdot \left[f_{pe} + \frac{x_c - K_{ld} \cdot L_d + L_t}{K_{ld} \cdot L_d - L_t} \cdot (f_{ps} - f_{pe})\right]\right] & \text{otherwise} \end{cases}$$

Finds provided tension tie force from figure

$F_{L\_prov\_c} = 191 \cdot kip$

$$Status\_V_{1c} := \begin{cases} a \leftarrow \text{"OK"} & \text{if } F_{L\_prov\_c} \geq -F_{L\_reqd} \\ a \leftarrow \text{"No Good"} & \text{otherwise} \\ a \end{cases}$$

$Status\_V_{1c} = \text{"OK"}$ *Check for provided tension tie force*

13. Interface Shear Design

Based on recommendations from PCI Bridge Design Manual following a strength limit state approach.

$$v_{uh\_s} := \frac{V_u}{d_v \cdot b_v}$$

$$v_{nh\_reqd1} := \frac{v_{uh\_s}}{\phi_v}$$

$v_{nh\_reqd1} = 0.0633\,ksi$

$A_{cv} := b_v \cdot 1ft = 864\,in^2$ *Area of concrete considered to be engaged in interface shear transfer*

$A_{vf} := 0in^2$ *Area of interface shear reinforcement crossing the sear plane within the area A_{cv}*

$V_{nhr} := v_{nh\_reqd1} \cdot A_{cv}$

$V_{nhr} = 54.709\,kip$

Interface is CIP concrete slab on clean, roughened beam surface (no reinforcement crossing shear plane)

$c := 0.135\,ksi$ *Cohesion factor*

$\mu := 1$ *Friction factor*

$K_1 := 0.2$ *Fraction of concrete strength available to resist interface shear*

$K_2 := 0.8\,ksi$ *Limiting interface shear resistance*

Check for Maximum Allowable Shear:

$P_c := 0$ *Net compressive stress normal to shear plane*

$V_{ni\_max1} := K_1 \cdot f_{c\_d} \cdot A_{cv}$ *(LRFD 5.8.4.1-4)*

$V_{ni\_max1} = 691.2\,kip$

$V_{ni\_max2} := K_2 \cdot A_{cv}$ *(LRFD 5.8.4.1-5)*

$V_{ni\_max2} = 691.2\,kip$

$$V_{nh\_max} := \begin{cases} V_{ni\_max1} & \text{if } V_{ni\_max1} \le V_{ni\_max2} \\ V_{ni\_max2} & \text{otherwise} \end{cases}$$ *(LRFD 5.8.4.1-2)*

$V_{ni} := c \cdot A_{cv} + \mu \cdot \left(A_{vf} \cdot f_y + P_c\right)$ *Nominal shear resistance of the interface plane* (LRFD 5.8.4.1-3)

$$V_{nh\_prov} := \begin{cases} V_{ni} & \text{if } V_{ni} \le V_{nh\_max} \\ V_{nh\_max} & \text{otherwise} \end{cases}$$

$V_{nh\_prov} = 116.64\,kip$ *Lesser of calculated value and maximum allowed*

$V_{nh\_reqd} := v_{nh\_reqd1} \cdot A_{cv}$

$V_{nh\_reqd} = 54.709\,kip$

$$Status\_V_{nh\_prov} := \begin{cases} \text{"OK"} & \text{if } V_{nhr} < V_{nh\_prov} \\ \text{"No Good"} & \text{otherwise} \end{cases}$$

$Status\_V_{nh\_prov} = \text{"OK"}$

14. Spalling Forces

If the maximum spalling stress on the end face of the girder is less than the direct tensile strength of the concrete, then spalling reinforcement is not required when the member depth is less than 22".

$f_{r\_dts} := -0.23\sqrt{f_{c\_b} \cdot ksi}$

$f_{r\_dts} = -0.651 \cdot ksi$ *Direct tensile strength* *(LRFD C5.4.2.7)*

$P_{jack} := A_{ps_4} \cdot f_{pj}$

$P_{jack} = 1045\,kip$

$$\sigma_s := \frac{-P_{jack}}{A_b}\cdot\left(0.1206\frac{ecc^2}{h_b\cdot d_b} - 0.0256\right)$$

$\sigma_s = -0.183\,ksi$ *Maximum spalling stress*

$$Status\_Spalling := \begin{cases} \text{"OK"} & \text{if } \sigma_s > f_{r\_dts} \\ \text{"No Good"} & \text{otherwise} \end{cases}$$

Status_Spalling = "OK" *Check against spalling*

15. Transverse Load Distribution

$d_{cgs} := h_c - y_{bar\_strands}$

$d_{cgs} = 20.7\cdot in$ *Depth to center of prestressing strands*

$$d_{trans} := h_c - 4in - \frac{d_b}{2} - \frac{0.75in}{2}$$

$d_{trans} = 20.33\,in$

$$\alpha := \frac{d_{cgs}}{d_{trans}}$$

$\alpha = 1.018$

$A_{l\_mild} := 0in^2$ *Area of mild longitudinal reinforcement in tension at the strength limit state*

$$k_{mild} := \begin{cases} \dfrac{\frac{100\cdot\sqrt{ft}}{\sqrt{L_{des}}}}{100} & \text{if } \dfrac{\frac{100\cdot\sqrt{ft}}{\sqrt{L_{des}}}}{100} \le 50\% \\ (50\%) & \text{otherwise} \end{cases}$$

$k_{mild} = 16.667\%$

$$k_{ps} := \begin{cases} \dfrac{\frac{100\cdot\sqrt{ft}}{\sqrt{L_{des}}}\cdot\frac{f_{pe}}{f_y}}{100} & \text{if } \dfrac{\frac{100\cdot\sqrt{ft}}{\sqrt{L_{des}}}\cdot\frac{f_{pe}}{f_y}}{100} \le 50\% \\ (50\%) & \text{otherwise} \end{cases}$$

$k_{ps} = 50\cdot\%$

$A_{l\_ps} := A_{ps_2} = 3.755\,in^2$

$A_{tld} := k_{mild}\cdot A_{l\_mild} + \alpha\cdot k_{ps}\cdot A_{l\_ps}$

$A_{tld} = 1.912\,in^2$

$A_{tld\_per\_ft} := \frac{A_{tld}}{S} = 0.319\frac{in^2}{ft}$ *Longitudinal reinforcement is per beam width*

$A_{num6} := 0.44in^2$ *Number 6 bars for transverse bars*

$$S_{ld\_spac\_max} := \frac{A_{num6}}{A_{tld\_per\_ft}}$$

$S_{ld\_spac\_max} = 16.568\,in$

$S_{ld\_spac} := 12in$ *Transverse load distribution reinforcement spacing*

$$Status\_trans\_spac := \begin{cases} \text{"OK"} & \text{if } S_{ld\_spac} \le S_{ld\_spac\_max} \\ \text{"No Good"} & \text{otherwise} \end{cases}$$

$Status\_trans\_spac = \text{"OK"}$

16. Reflective Crack Control Reinforcement

$$\rho_{cr\_req} := \frac{6 \cdot \sqrt{f_{c\_d} \cdot psi}}{f_y}$$ *(LRFD 5.14.4.3.3f-1)*

$A_{scr\_req} := \rho_{cr\_req} \cdot (h_b - h_{fl}) \cdot 1ft$

$A_{scr\_req} = 1.138\,in^2$ *Required area of reinforcement of reflective crack control per unit length of span*

$$A_{ld} := \frac{2 \cdot S_{ld\_spac} \cdot A_{num6}}{1ft}$$

$A_{ld} = 0.88\,in^2$

$A_{cr\_cage\_req} := A_{scr\_req} - A_{ld}$

$A_{cr\_cage\_req} = 0.258\,in^2$ *Required area of cage reinforcement needed*

$S_{cage\_spac} := 12in$ *Provide stirrups at 12" O.C. spacing*

$A_{scage} := 0.31in^2$ *Number 5 bars*

$$A_{cr\_cage\_prov} := A_{scage} \cdot \left(\frac{1ft}{S_{cage\_spac}} \right)$$

$A_{cr\_cage\_prov} = 0.31\,in^2$

$A_{scr\_prov} := A_{ld} + A_{cr\_cage\_prov}$

$A_{scr\_prov} = 1.19\,in^2$

$$Status\_A_{scrack} := \begin{cases} \text{"OK"} & \text{if } A_{scr\_req} < A_{scr\_prov} \\ \text{"No Good"} & \text{otherwise} \end{cases}$$

$Status\_A_{scrack} = \text{"OK"}$

17. Bottom Flange Reinforcement

$w_{flng\_sw} := h_{fl} \cdot 12in \cdot \gamma_b$

$w_{flng\_sw} = 0.0375\frac{kip}{ft}$ *Self-weight of flange per 1' strip*

$w_{flng\_cip} := \left(h_c - h_{fl}\right)\cdot 12in\cdot\gamma_d$

$w_{flng\_cip} = 0.275\frac{kip}{ft}$ *Weight CIP over flange per 1' strip*

$w_{const} := 10psf$ *Assumption of construction live load*

$w_{flng\_LL} := w_{const}\cdot 12in$

$w_{flng\_LL} = 0.01\frac{kip}{ft}$ *Construction live load per 1' strip*

$b_{cant} := b_{fl} = 1ft$ *Length of cantilever*

$$M_{flng\_sw} := \frac{w_{flng\_sw}\cdot\left(b_{cant}\right)^2}{2}$$

$M_{flng\_sw} = 0.0187kip\cdot ft$ *Moment at base of flange due to self-weight of beam*

$$M_{flng\_cip} := \frac{w_{flng\_cip}\cdot\left(b_{cant}\right)^2}{2}$$

$M_{flng\_cip} = 0.137kip\cdot ft$ *Moment at base of flange due to CIP concrete*

$$M_{flng\_LL} := \frac{w_{flng\_LL}\cdot\left(b_{cant}\right)^2}{2}$$

$M_{flng\_LL} = 0.005kip\cdot ft$ *Moment at base of flange due to construction LL*

$M_{u\_flng} := 1.25\cdot\left(M_{flng\_sw} + M_{flng\_cip}\right) + 1.75\cdot M_{flng\_LL}$

$M_{u\_flng} = 0.204kip\cdot ft$ *Strength Limit State I*

$A_{s\_flng} := 0.11in^2$ *Number 3 bars*

$$c_{flng} := \frac{A_{s\_flng}\cdot f_y}{0.85 f_{c\_b}\cdot\beta_1\cdot 12in}$$

$c_{flng} = 0.095in$ *Distance between the neutral axis and the compressive face*

$$\beta_{1p} := \begin{cases} \beta_1 \leftarrow 0.85 & \text{if } f_{c\_b} \le 4ksi \\ \beta_1 \leftarrow 0.65 & \text{if } f_{c\_b} \ge 8ksi \\ \beta_1 \leftarrow \dfrac{f_{c\_b} - 4ksi}{1ksi}\cdot 0.05 & \text{otherwise} \end{cases}$$

$\beta_{1p} = 0.65$ *Stress block factor*

$a_{flng} := \beta_{1p}\cdot c_{flng}$

$a_{flng} = 0.062in$ *Depth of equivalent stress block*

$d_{sv} := h_{fl} - 1in - 0.5in - \frac{0.5in}{2}$

$d_s = 1.25 \cdot in$ *Depth to steel*

$$M_{n\_flng} := A_{s\_flng} \cdot f_y \cdot \left(d_s - \frac{a_{flng}}{2} \right)$$

$M_{n\_flng} = 0.67 \cdot kip \cdot ft$ *Nominal moment capacity at base of flange*

$$\phi_{f\_flng} := \begin{cases} 0.75 \text{ if } 0.65 + 0.15 \left(\frac{d_s}{c_{flng}} - 1 \right) \le 0.75 \\ 0.9 \text{ if } 0.65 + 0.15 \left(\frac{d_s}{c_{flng}} - 1 \right) \ge 0.9 \\ \left[0.65 + 0.15 \left(\frac{d_s}{c_{flng}} - 1 \right) \right] \text{ otherwise} \end{cases}$$

$\phi_{f\_flng} = 0.9$ *ϕ factor for flange*

$M_{r\_flng} := \phi_{f\_flng} \cdot M_{n\_flng}$

$M_{r\_flng} = 0.603 \, kip \cdot ft$ *Factored capacity of flange*

$$Status\_StrengthLS_{flng} := \begin{cases} \text{"OK"} \text{ if } M_{u\_flng} \le M_{r\_flng} \\ \text{"No Good"} \text{ otherwise} \end{cases}$$

$Status\_StrengthLS_{flng} = \text{"OK"}$ *Check of flange bending*

Use #3 bars @ 12" O.C. in bottom flange

APPENDIX D - CRACK DOCUMENTATION

The maximum crack width over the joint and in the specimen overall as well as the propagation height of the largest overall crack and the crack over the joint were documented at each load step for each specimen. This data is displayed in Tables 1-4. (NOTE: The number in brackets indicates the number of times cycled at that load. Crack widths were measured in millimeters and converted to inches.)

Table A-10: Crack Documentation for Extended Bar Specimen

Load	Behavior	Largest Crack Width	Joint Crack Width	Largest Crack Height	Joint Crack Height
(kip)		*(in.)*	*(in.)*	*(in.)*	*(in.)*
5	No Cracking	0	0	0	0
10	No Cracking	-	-	-	-
20	No Cracking	-	-	-	-
25	No Cracking	-	-	-	-
30	No Cracking	-	-	-	-
40	No Cracking	-	-	-	-
50	No Cracking	-	-	-	-
60	No Cracking	-	-	-	-
70	No Cracking	-	-	-	-
80	No Cracking	-	-	-	-
90	Crack at Interface (Only One Side)	0.004	-	17.625	-
90 *[5]*	Some Propagation	-	-	-	-
90 *[8]*	Crack in CIP Near Joint	0.008	0.004	-	-
90 *[9]*	No Propagation	-	-	-	-
90 *[10]*	No Propagation	-	-	-	-
100	No Propagation	-	-	-	-
110	Crack at Other Interface	0.012	-	-	-
120	Crack Under Load (Only One Side)	-	-	-	-
130	Crack Under Load (Other Side)	0.016	-	-	-
140	Some Propagation	0.020	-	17.875	-
150	Some Propagation	0.024	-	19.5	7.375
160	Some Propagation	0.030	0.008	21.25	-
170	Some Propagation	0.039	-	-	-
180	Some Propagation	0.049	-	21.875	-
190	Some Propagation	0.069	-	22	-
200	Additional Crack Under Load (Only One Side)	0.079	-	-	-
210	Some Propagation	0.098	-	-	9.375
220	Some Propagation	0.118	-	-	-
230	Some Propagation	0.157	-	22.375	-
240	Additional Crack Under Load (Other Side)	-	0.012	22.125	-
250	Some Propagation	-	-	-	-
260	Excessive Cracking Throughout (FAIL)	0.197	0.059	22.875	-

Table A-11: Crack Documentation for Embedded Plate Inverted-T Specimen

Load	Behavior	Largest Crack Width	Joint Crack Width	Largest Crack Height	Joint Crack Height
(kip)		*(in.)*	*(in.)*	*(in.)*	*(in.)*
5	No Cracking	0	0	0	0
10	No Cracking	-	-	-	-
20	No Cracking	-	-	-	-
25	No Cracking	-	-	-	-
30	No Cracking	-	-	-	-
40	No Cracking	-	-	-	-
50	No Cracking	-	-	-	-
60	No Cracking	-	-	-	-
70	No Cracking	-	-	-	-
80	No Cracking	-	-	-	-
90	No Cracking	-	-	-	-
100	Crack at Vertical Interface (Only One Side)	0.008	-	18.125	-
100 *[5]*	Some Propagation	-	-	-	-
100 *[8]*	No Propagation	-	-	-	-
100 *[9]*	No Propagation	-	-	-	-
100 *[10]*	No Propagation	-	-	-	-
110	Crack at Vertical Interface (Other Side) & Crack at Joint	-	-	21.125	-
120	Some Propagation	0.009	-	-	-
130	Some Propagation	-	-	-	-
140	Crack at Load (Both Sides)	0.015	-	20.5	19.5
150	Some Propagation	0.019	-	-	-
160	Some Propagation	0.030	-	-	-
170	Some Propagation	0.045	-	21.125	-
180	Some Propagation	0.059	-	21.5	20.625
190	Additional Crack at Load (One Sides)	0.079	-	22	-
200	Additional Crack at Load (Other Sides) & Crack at Joint	0.098	0.008	-	21.875
210	Major Growth at Joint	0.157	0.157	23.125	23
220	Some Propagation	0.236	0.236	-	-
225	FAIL	1.968	1.968	24.25	24.25

Table A-12: Crack Documentation for Embedded Plate Tapered Specimen

Load	Behavior	Largest Crack Width	Joint Crack Width	Largest Crack Height	Joint Crack Height
(kip)		*(in.)*	*(in.)*	*(in.)*	*(in.)*
5	No Cracking	0	0	0	0
10	No Cracking	-	-	-	-
20	No Cracking	-	-	-	-
25	No Cracking	-	-	-	-
30	No Cracking	-	-	-	-
40	No Cracking	-	-	-	-
50	No Cracking	-	-	-	-
60	No Cracking	-	-	-	-
70	No Cracking	-	-	-	-
80	No Cracking	-	-	-	-
90	No Cracking	-	-	-	-
100	No Cracking	-	-	-	-
110	Crack at Interface & Vert. Crack (Same Side)	0.002	-	18.875	-
110 *[5]*	Crack at Interface & Vert. Crack (Other Side)	-	-	20.875	-
110 *[8]*	Some Propagation	0.004	-	-	-
110 *[9]*	Some Propagation	-	-	22.75	-
110 *[10]*	No Propagation	-	-	-	-
110 *[11]*	No Propagation	-	-	-	-
120	No Propagation	-	-	-	-
130	Some Propagation	-	-	-	-
140	Crack Under Load (Only One Side)	0.008	-	-	-
150	Some Propagation	0.010	-	-	-
160	Some Propagation	0.016	-	-	-
170	Some Propagation	0.059	-	-	-
180	Some Propagation	0.079	-	-	-
190	New Crack at Joint	0.138	0.004	-	12.75
200	Some Propagation	-	-	-	13.625
210	Some Propagation	0.157	0.006	23.75	15.375
220	Some Propagation	0.197	0.010	-	16.625
230	New Crack	-	0.016	-	-
240	Some Propagation & Spalling	0.236	0.018	-	-
250	Some Propagation	0.256	0.020	-	17.875
260	Some Propagation	0.276	-	-	-
270	Some Propagation	0.315	0.024	-	-
280	Some Propagation	-	-	-	-
290	Some Propagation	0.394	0.028	-	-
300	Some Propagation	0.433	-	-	18.5

Table A-13: Crack Documentation for No Connection Specimen

Load	Behavior	Largest Crack Width	Joint Crack Width	Largest Crack Height	Joint Crack Height
(kip)		*(in.)*	*(in.)*	*(in.)*	*(in.)*
5	No Cracking	0	0	0	0
10	No Cracking	-	-	-	-
20	No Cracking	-	-	-	-
25	No Cracking	-	-	-	-
30	No Cracking	-	-	-	-
40	No Cracking	-	-	-	-
50	No Cracking	-	-	-	-
60	Crack at Joint	0.003	0.003	19	19
60 *[5]*	Some Propagation	-	-	-	-
60 *[8]*	No Propagation	-	-	-	-
60 *[9]*	No Propagation	-	-	-	-
60 *[10]*	Some Propagation	-	-	-	-
60 *[11]*	No Propagation	-	-	-	-
60 *[12]*	No Propagation	-	-	-	-
70	Some Propagation	0.012	0.012	20.5	20.5
80	Some Propagation	0.018	0.018	-	-
90	Crack Through Precast	0.079	0.020	22.5	-
90*	Major Crack Through Precast (FAIL)	0.315	-	24	-

APPENDIX E - ADDITIONAL STRAIN GAGE DATA

The following sections include the strain gage results that were not included in the Results and Discussion chapters.

Extended Bar

Figure 1 shows the strain in the extended bars on the left side of the specimen. These values reflect the same behavior seen in the extended bars from the right side that was discussed in the body of the thesis. Figure 2 shows the strain in the two concrete embedment gages that were placed 12 in. above bottom of precast. Figure 3 presents the strains in the gages that were embedded 1 in. above the precast to CIP vertical interface. This plot shows that both sides of the specimen exhibited similar behavior and that there was a good distribution of stress throughout the test.

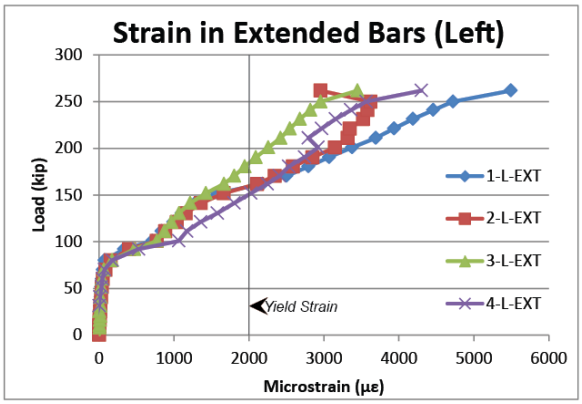

Figure A-7: Strain in Extended Bar Steel (Left Side) (6 in. Above Bottom of Precast)

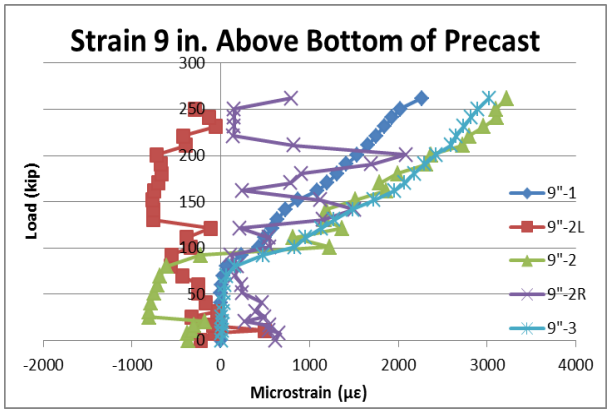

Figure A-8: Strain in Row of Gages 9 in. Above Bottom of Precast

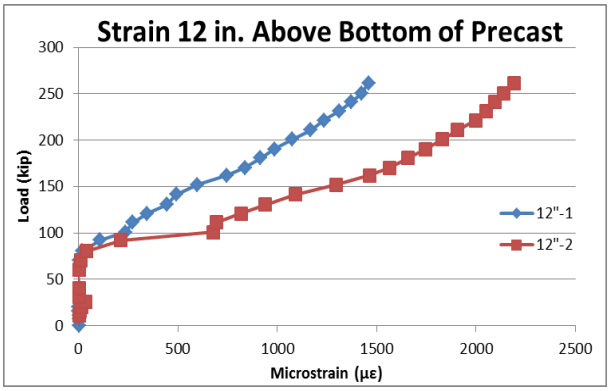

Figure A-9: Strain in Two Gages 12 in. Above Bottom of Precast

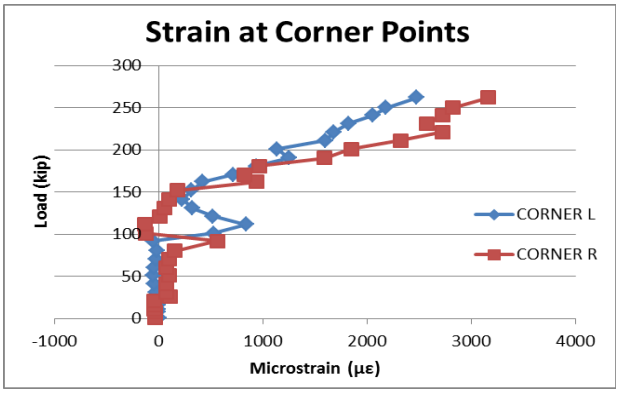

Figure A-10: Strain in Two Gages at Corner Points of Interface (19 in. Above Bottom of Precast)

Embedded Plate Inverted-T

Figure 4 shows the strain in the concrete embedment gages that were placed at the same elevation as the extended and drop bars of the other tests. Figure 5 shows that the strain above the vertical interface was the same for both sides of the test specimen, which supports that the load was evenly distributed throughout the specimen.

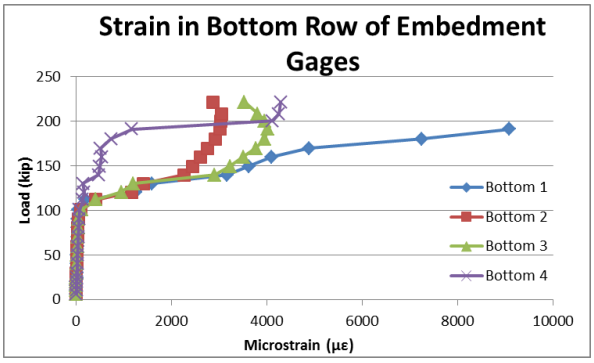

Figure A-11: Strain in Bottom Row of Embedment Gages (5 in. Above Bottom of Precast)

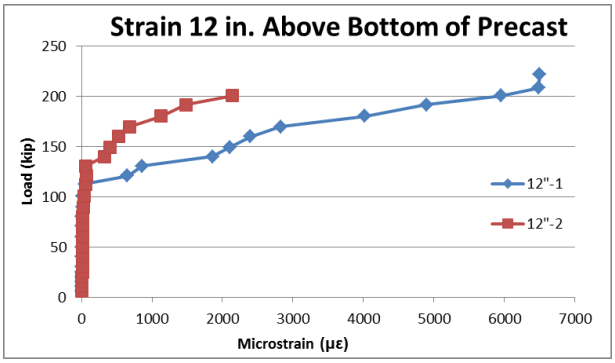

Figure A-12: Strain in Two Gages 12 in. Above Bottom of Precast

Embedded Plate Tapered

Figure 6 shows the strain in the tension steel located behind the embedded plate connection on the left side of the specimen. These gages produced results that were not consistent with the right side. Gage 2-L-EMB never worked and 1-L-EMB and 4-L-EMB exhibited behavior that indicates a loss of bond between the strain gages and the rebar at low levels of strain by comparison to what was recorded by the gages attached to the right side of the specimen. Figure 7 presents the strains in the gages that were embedded 1 in. above the precast to CIP vertical interface. This plot shows that both sides of the specimen exhibited similar behavior and that though limited, there was distribution of stress throughout the test. Figure 8 shows that the region of steel and concrete around the top mat of T&S steel remained increasingly compressive throughout the test. This indicates that the neutral axis never approached this region as it did for the other specimens during the course of loading. Figure 8 shows the uniform distribution of strains and therefore stresses in the drop bars.

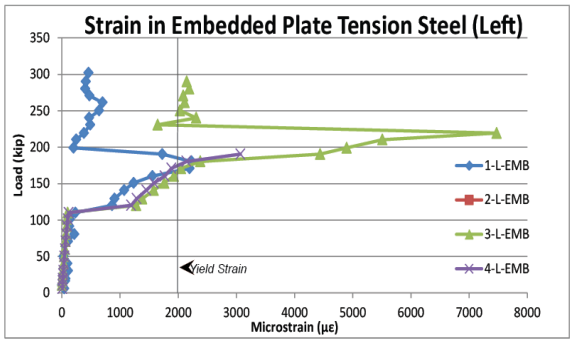

Figure A-13: Strain in Embedded Plate Tension Steel (Left Side) (1.5 in. Above Bottom of Precast)

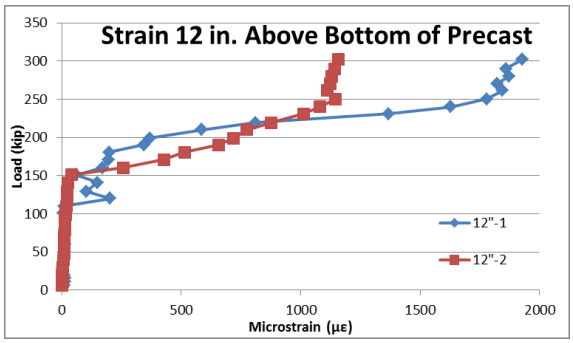

Figure A-14: Strain in Two Gages 12 in. Above Bottom of Precast

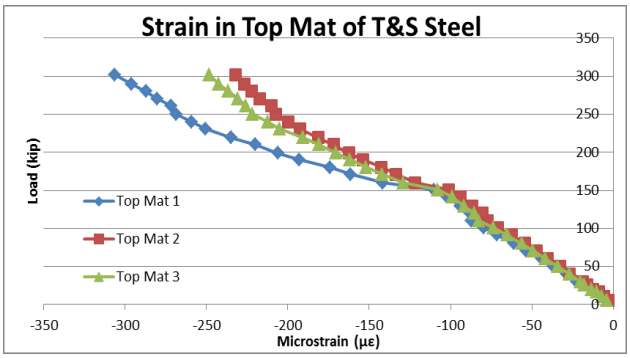

Figure A-15: Strain in Gages Attached to Top Mat of T&S Steel (22.5 in. Above Bottom of Precast)

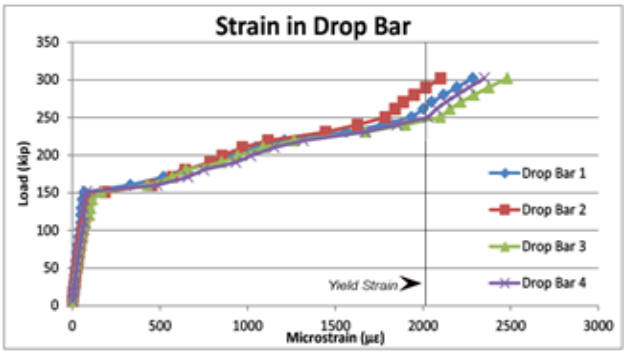

Figure A-16: Strain in Drop Bar (5 in. Above Bottom of Precast)

No Connection

Figure 10 shows the strain at the gages located above the tapered interface. The small magnitude of these results limits what can be taken from them. The behavior does, however, indicate that there was not a uniform distribution of strain throughout the test specimen. This reinforces what was observed visually. All of the cracking took place on one side of the specimen while the other remained almost entirely intact.

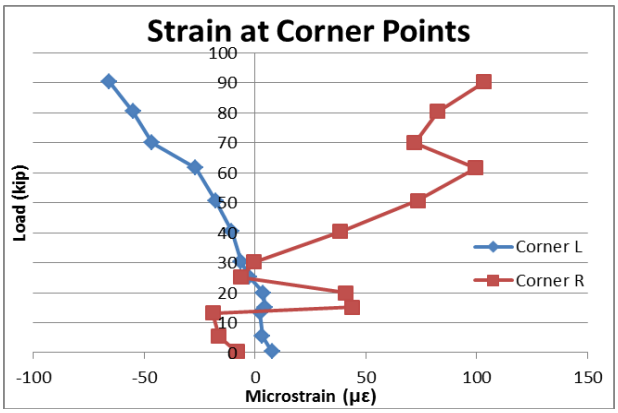

Figure A-17: Strain in Two Gages at Corner Points of Interface (19 in. Above Bottom of Precast)

APPENDIX F - STRESS IN SPECIMENS AT GIVEN APPLIED LOADS

$c := \frac{25in - 3in}{2} = 11 \cdot in$ *Distance to neutral axis*

$I := \frac{1}{12} \cdot 4ft \cdot (25in - 3in)^3 = 42592 \cdot in^4$ *Moment of inertia*

$x := \frac{11.5ft}{2} - 3ft = 2.75 \cdot ft$ *Length between support and applied load*

$M = x \cdot P$ *Moment at joint*

$\sigma = \frac{M \cdot c}{I}$ *Stress at joint*

$DLA := 1.33$ *Impact Factor*

$\sigma_{serv} := DLA \cdot 0.13ksi = 0.173 \cdot ksi$ *Service level stress (0.13 ksi is from finite element model)*

$w_{self} := 25in \cdot 4ft \cdot 0.15 \frac{kip}{ft^3} = 1.25 \cdot \frac{kip}{ft}$ *Distributed Self Weight of Specimen*

$P_{beam} := \frac{9.5ft \cdot 70 \frac{lbf}{ft}}{2} = 0.332 \cdot kip$ *Point loads applied because spreader bar weight*

$M_{exist} := P_{beam} \cdot x + \frac{1}{8} \cdot w_{self} \cdot (11.5ft)^2 = 21.578 \cdot kip \cdot ft$ *Existing moment in specimen*

$\sigma_{exist} := \frac{M_{exist} \cdot c}{I} = 0.067 \cdot ksi$ *Existing stress in specimen*

$P_{serv} := 2 \cdot \frac{(\sigma_{serv} - \sigma_{exist}) \cdot I}{c \cdot x} = 24.88 \cdot kip$ *Applied load required to induce service tensile stress at joint*

$\sigma(\Omega) := \left(\sigma_{exist} + \frac{\frac{\Omega}{2} \cdot x \cdot c}{I} \right)$ *Stress at joint with given applied loads*

$$loads := \begin{pmatrix} 5 \\ 10 \\ 15 \\ 20 \\ 25 \\ 30 \\ 40 \\ 50 \\ 60 \\ 70 \\ 80 \\ 90 \\ 100 \\ 110 \\ 120 \end{pmatrix} \cdot kip \qquad \sigma(loads) = \begin{pmatrix} 0.09 \\ 0.11 \\ 0.13 \\ 0.15 \\ 0.17 \\ 0.19 \\ 0.24 \\ 0.28 \\ 0.32 \\ 0.37 \\ 0.41 \\ 0.45 \\ 0.49 \\ 0.54 \\ 0.58 \end{pmatrix} \cdot ksi \qquad \frac{\sigma(loads)}{\sigma_{serv}} = \begin{pmatrix} 0.51 \\ 0.63 \\ 0.76 \\ 0.88 \\ 1 \\ 1.13 \\ 1.37 \\ 1.62 \\ 1.87 \\ 2.11 \\ 2.36 \\ 2.6 \\ 2.85 \\ 3.1 \\ 3.34 \end{pmatrix}$$

Applied Loads

Stress at joint due to applied loads

Ratio of applied load stress to service load stress

APPENDIX G – DESIGN NOMINAL AND CRACKING LOADS

Nominal Strength

Extended Bar

Over the Longitudinal Joint

$d_{s\_ext} := 19in$ *Depth to extended bar steel*

$A_{s\_ext} := 8 \cdot \left(0.44in^2\right) = 3.52in^2$ *Area of extended bar steel*

$d_{s\_top} := 4in$ *Depth to top steel*

$A_{s\_top} := 8 \cdot \left(0.2in^2\right) = 1.6in^2$ *Area of top steel*

$A_s := A_{s\_ext} + A_{s\_top}$ *Area of steel*

$\left(f_y := 60ksi\right)$ *Strength of steel*

$f'_c := 4000psi$ *Compressive strength of concrete*

$b := 48in$ *Width of section*

$\left(a := \frac{A_s \cdot f_y}{0.85 f'_c \cdot b}\right)$

$(a) = 1.882in$ *Depth of Whitney Stress block*

$\left(\beta_1 := 1.05 - 0.05 \frac{f'_c}{ksi}\right)$

$\left(\beta_1\right) = 0.85$ *Beta factor*

$\left(c := \frac{a}{\beta_1}\right)$

$(c) = 2.215in$ *Depth to neutral axis*

$M_{n1} := A_{s\_ext} \cdot f_y \cdot \left(d_{s\_ext} - \frac{a}{2}\right) + A_{s\_top} \cdot f_y \cdot \left(d_{s\_top} - \frac{a}{2}\right)$

$\left(M_{n1}\right) = 4107.7kip \cdot in$ *Nominal moment capacity*

$w_{self} := 0.15 \frac{kip}{ft^3} \cdot 25in \cdot 48in = 1.25 \frac{kip}{ft}$ *Self-weight of specimen*

$M_{self} := \frac{w_{self} \cdot (138in)^2}{8} = 247.969kip \cdot in$ *Moment due to self-weight*

$M := M_{n1} - M_{self} = 3.86 \times 10^3 \cdot kip \cdot in$ *Moment that needs to be applied*

$P := \frac{M}{2.75ft} = 116.961kip$ *Point load to cause moment*

$Nominal_{load} := 2 \cdot P = 233.921kip$ *Total applied load to cause moment*

$\varepsilon_s := \frac{0.003}{c} \cdot \left(d_{s\_ext} - c\right) = 0.023$ *Strain in extreme tension steel*

At Vertical Precast to CIP Interface & At Minimum Depth of Concrete

$d_{s\_ext} := 19in$ *Depth to extended bar steel*

$A_{s\_ext} := 4 \cdot \left(0.44in^2\right) = 1.76in^2$ *Area of extended bar steel*

$d_{s\_top} := 4in$ *Depth to top steel*

$A_{s\_top} := 8 \cdot \left(0.2in^2\right) = 1.6in^2$ *Area of top steel*

$A_s := A_{s\_ext} + A_{s\_top}$ *Area of steel*

$\left(f_y := 60ksi\right)$ *Strength of steel*

$f'_c := 4000psi$ *Compressive strength of concrete*

$b := 48in$ *Width of section*

$\left(a := \frac{A_s \cdot f_y}{0.85 f'_c \cdot b}\right)$

$(a) = 1.235in$ *Depth of Whitney Stress block*

$\left(\beta_1 := 1.05 - 0.05 \frac{f'_c}{ksi}\right)$

$\left(\beta_1\right) = 0.85$ *Beta factor*

$\left(c := \frac{a}{\beta_1}\right)$

$(c) = 1.453in$ *Depth to neutral axis*

$M_{n1} := A_{s\_ext} \cdot f_y \cdot \left(d_{s\_ext} - \frac{a}{2}\right) + A_{s\_top} \cdot f_y \cdot \left(d_{s\_top} - \frac{a}{2}\right)$

$\left(M_{n1}\right) = 2265.9kip \cdot in$ *Nominal moment capacity*

$w_{self} := 0.15\frac{kip}{ft^3} \cdot 25in \cdot 48in = 1.25\frac{kip}{ft}$ *Self-weight of specimen*

$M_{self} := \frac{w_{self} \cdot (138in)^2}{8} = 247.969kip \cdot in$ *Moment due to self-weight*

$M := M_{n1} - M_{self} = 2.018 \times 10^3 \cdot kip \cdot in$ *Moment that needs to be applied*

$P := \frac{M}{2.75ft} = 61.149kip$ *Point load to cause moment*

$Nominal_{load} := 2 \cdot P = 122.298kip$ *Total applied load to cause moment* **<<<CONTROLS**

$\varepsilon_s := \frac{0.003}{c} \cdot \left(d_{s\_ext} - c\right) = 0.036$ *Strain in extreme tension steel*

Embedded Plate Inverted-T

Over the Longitudinal Joint - At Vertical/Tapered Precast to CIP Interface - At Minimum Depth of Concrete

$d_{s\_emb} := 23.5in$ *Depth to transverse connection steel*

$A_{s\_emb} := 4 \cdot \left(0.44in^2\right) = 1.76in^2$ *Area of transverse connection steel*

$d_{s\_top} := 4in$ *Depth to top steel*

$A_{s\_top} := 8 \cdot \left(0.2in^2\right) = 1.6in^2$ *Area of top steel*

$A_s := A_{s\_emb} + A_{s\_top}$ *Area of steel*

$\left(f_y := 60ksi\right)$ *Strength of steel*

$f'_c := 4000psi$ *Compressive strength of concrete*

$b := 48in$ *Width of section*

$\left(a := \frac{A_s \cdot f_y}{0.85 f'_c \cdot b}\right)$

$(a) = 1.235in$ *Depth of Whitney Stress block*

$\left(\beta_1 := 1.05 - 0.05 \frac{f'_c}{ksi}\right)$

$\left(\beta_1\right) = 0.85$ *Beta factor*

$\left(c := \frac{a}{\beta_1}\right)$

$(c) = 1.453in$ *Depth to neutral axis*

$M_{n1} := A_{s\_emb} \cdot f_y \cdot \left(d_{s\_emb} - \frac{a}{2}\right) + A_{s\_top} \cdot f_y \cdot \left(d_{s\_top} - \frac{a}{2}\right)$

$\left(M_{n1}\right) = 2741.1kip \cdot in$ *Nominal moment capacity*

$w_{self} := 0.15 \frac{kip}{ft^3} \cdot 25in \cdot 48in = 1.25 \frac{kip}{ft}$ *Self-weight of specimen*

$M_{self} := \frac{w_{self} \cdot (138in)^2}{8} = 247.969kip \cdot in$ *Moment due to self-weight*

$M := M_{n1} - M_{self} = 2.493 \times 10^3 \cdot kip \cdot in$ *Moment that needs to be applied*

$P := \frac{M}{2.75ft} = 75.549kip$ *Point load to cause moment*

$Nominal_{load} := 2 \cdot P = 151.098kip$ *Total applied load to cause moment* **<<<<CONTROLS**

$\varepsilon_s := \frac{0.003}{c} \cdot \left(d_{s\_emb} - c\right) = 0.046$ *Strain in extreme tension steel*

Embedded Plate Tapered

Over the Longitudinal Joint - At Vertical/Tapered Precast to CIP Interface

$d_{s\_emb} := 23.5in$ *Depth to transverse connection steel*

$A_{s\_emb} := 4 \cdot (0.44in^2) = 1.76in^2$ *Area of transverse connection steel*

$d_{s\_top} := 4in$ *Depth to top steel*

$A_{s\_top} := 4 \cdot (0.2in^2) = 0.8in^2$ *Area of top steel*

$d_{s\_drop} := 20in$ *Depth to drop steel*

$A_{s\_drop} := 4 \cdot (0.2in^2) = 0.8in^2$ *Area of drop steel*

$A_s := A_{s\_emb} + A_{s\_top} + A_{s\_drop}$ *Area of steel*

$(f_y := 60ksi)$ *Strength of steel*

$f'_c := 4000psi$ *Compressive strength of concrete*

$b := 48in$ *Width of section*

$\left(a := \frac{A_s \cdot f_y}{0.85 f'_c \cdot b}\right)$

$(a) = 1.235in$ *Depth of Whitney Stress block*

$\left(\beta_1 := 1.05 - 0.05 \frac{f'_c}{ksi}\right)$

$(\beta_1) = 0.85$ *Beta factor*

$\left(c := \frac{a}{\beta_1}\right)$

$(c) = 1.453in$ *Depth to neutral axis*

$M_{n1} := A_{s\_emb} \cdot f_y \cdot \left(d_{s\_emb} - \frac{a}{2}\right) + A_{s\_top} \cdot f_y \cdot \left(d_{s\_top} - \frac{a}{2}\right) + A_{s\_drop} \cdot f_y \cdot \left(d_{s\_drop} - \frac{a}{2}\right)$

$(M_{n1}) = 3509.1kip \cdot in$ *Nominal moment capacity*

$w_{self} := 0.15 \frac{kip}{ft^3} \cdot 25in \cdot 48in = 1.25 \frac{kip}{ft}$ *Self-weight of specimen*

$M_{self} := \frac{w_{self} \cdot (138in)^2}{8} = 247.969kip \cdot in$ *Moment due to self-weight*

$M := M_{n1} - M_{self} = 3.261 \times 10^3 \cdot kip \cdot in$ *Moment that needs to be applied*

$P := \frac{M}{2.75ft} = 98.822kip$ *Point load to cause moment*

$Nominal_{load} := 2 \cdot P = 197.643\,kip$ *Total applied load to cause moment*

$\varepsilon_s := \frac{0.003}{c} \cdot \left(d_{s\_emb} - c\right) = 0.046$ *Strain in extreme tension steel*

At Minimum Depth of Concrete

$d_{s\_emb} := 23.5in$ *Depth to transverse connection steel*

$A_{s\_emb} := 4 \cdot \left(0.44in^2\right) = 1.76\,in^2$ *Area of transverse connection steel*

$d_{s\_top} := 4in$ *Depth to top steel*

$A_{s\_top} := 8 \cdot \left(0.2in^2\right) = 1.6in^2$ *Area of top steel*

$A_s := A_{s\_emb} + A_{s\_top}$ *Area of steel*

$\left(f_y := 60ksi\right)$ *Strength of steel*

$f'_c := 4000psi$ *Compressive strength of concrete*

$b := 48in$ *Width of section*

$\left(a := \frac{A_s \cdot f_y}{0.85 f'_c \cdot b}\right)$

$(a) = 1.235in$ *Depth of Whitney Stress block*

$\left(\beta_1 := 1.05 - 0.05 \frac{f'_c}{ksi}\right)$

$\left(\beta_1\right) = 0.85$ *Beta factor*

$\left(c := \frac{a}{\beta_1}\right)$

$(c) = 1.453in$ *Depth to neutral axis*

$M_{n1} := A_{s\_emb} \cdot f_y \cdot \left(d_{s\_emb} - \frac{a}{2}\right) + A_{s\_top} \cdot f_y \cdot \left(d_{s\_top} - \frac{a}{2}\right)$

$\left(M_{n1}\right) = 2741.1\,kip \cdot in$ *Nominal moment capacity*

$w_{self} := 0.15 \frac{kip}{ft^3} \cdot 25in \cdot 48in = 1.25 \frac{kip}{ft}$ *Self-weight of specimen*

$M_{self} := \frac{w_{self} \cdot (138in)^2}{8} = 247.969\,kip \cdot in$ *Moment due to self-weight*

$M := M_{n1} - M_{self} = 2.493 \times 10^3 \cdot kip \cdot in$ *Moment that needs to be applied*

$P := \frac{M}{2.75ft} = 75.549\,kip$ *Point load to cause moment*

$Nominal_{load} := 2 \cdot P = 151.098\,kip$ *Total applied load to cause moment* **<<<<CONTROLS**

$\varepsilon_s := \frac{0.003}{c} \cdot \left(d_{s\_emb} - c\right) = 0.046$ *Strain in extreme tension steel*

No Connection

At Over the Longitudinal Joint

$d_{s\_drop} := 20in$ *Depth to steel*

$A_{s\_drop} := 4 \cdot (0.44in^2) = 1.76in^2$ *Area of steel*

$d_{s\_top} := 5.5in$ *Depth to steel in top layer*

$A_{s\_top} := 4 \cdot (0.2in^2) = 0.8in^2$ *Area of steel in top layer*

$A_s := A_{s\_drop} + A_{s\_top}$ *Total area of steel*

$(f_y := 60ksi)$ *Strength of steel*

$f'_c := 4000psi$ *Compressive strength of concrete*

$b := 48in$ *Width of section*

$\left(a := \frac{A_s \cdot f_y}{0.85 f'_c \cdot b}\right)$

$(a) = 0.941in$ *Depth of Whitney Stress block*

$\left(\beta_1 := 1.05 - 0.05 \frac{f'_c}{ksi}\right)$

$(\beta_1) = 0.85$ *Beta factor*

$\left(c := \frac{a}{\beta_1}\right)$

$(c) = 1.107in$ *Depth to neutral axis*

$M_{n1} := A_{s\_drop} \cdot f_y \cdot \left(d_{s\_drop} - \frac{a}{2}\right) + A_{s\_top} \cdot f_y \cdot \left(d_{s\_top} - \frac{a}{2}\right)$

$(M_{n1}) = 2303.7kip \cdot in$ *Nominal moment capacity*

$w_{self} := 0.15 \frac{kip}{ft^3} \cdot 25in \cdot 48in = 1.25 \frac{kip}{ft}$ *Self-weight of specimen*

$M_{self} := \frac{w_{self} \cdot (138in)^2}{8} = 247.969kip \cdot in$ *Moment due to self-weight*

$M := M_{n1} - M_{self} = 2.056 \times 10^3 \cdot kip \cdot in$ *Moment that needs to be applied*

$P := \frac{M}{2.75ft} = 62.295kip$ *Point load to cause moment*

$Nominal_{load} := 2 \cdot P = 124.591kip$ *Total applied load to cause moment*

$\varepsilon_s := \frac{0.003}{c} \cdot (d_{s\_drop} - c) = 0.051$ *Strain in extreme tension steel*

At Vertical/Tapered Precast to CIP Interface

$d_{s\_drop} := 20in$ *Depth to drop bar steel*

$A_{s\_drop} := 4 \cdot \left(0.44in^2\right) = 1.76in^2$ *Area of drop bar steel*

$d_{s\_3} := 23in$ *Depth to bottom row of reinforcement*

$A_{s\_3} := 3 \cdot \left(0.11in^2\right) = 0.33in^2$ *Area of steel in bottom row of reinforcement*

$d_{s\_top} := 2.5in$ *Depth to steel in top layer*

$A_{s\_top} := 4 \cdot \left(0.2in^2\right) = 0.8in^2$ *Area of steel in top layer*

$A_s := A_{s\_drop} + A_{s\_3} + A_{s\_top}$ *Total area of steel*

$\left(f_y := 60ksi\right)$ *Strength of steel*

$f'_c := 4000psi$ *Compressive strength of concrete*

$b := 48in$ *Width of section*

$$\left(a := \frac{A_s \cdot f_y}{0.85 f'_c \cdot b}\right)$$

$(a) = 1.063in$ *Depth of Whitney Stress block*

$$\left(\beta_1 := 1.05 - 0.05 \frac{f'_c}{ksi}\right)$$

$\left(\beta_1\right) = 0.85$ *Beta factor*

$$\left(c := \frac{a}{\beta_1}\right)$$

$(c) = 1.25in$ *Depth to neutral axis*

$$M_{n1} := A_{s\_drop} \cdot f_y \cdot \left(d_{s\_drop} - \frac{a}{2}\right) + A_{s\_3} \cdot f_y \cdot \left(d_{s\_3} - \frac{a}{2}\right) + A_{s\_top} \cdot f_y \cdot \left(d_{s\_top} - \frac{a}{2}\right)$$

$\left(M_{n1}\right) = 2595.3kip \cdot in$ *Nominal moment capacity*

$w_{self} := 0.15 \frac{kip}{ft^3} \cdot 25in \cdot 48in = 1.25 \frac{kip}{ft}$ *Self-weight of specimen*

$M_{self} := \frac{w_{self} \cdot (138in)^2}{8} = 247.969kip \cdot in$ *Moment due to self-weight*

$M := M_{n1} - M_{self} = 2.347 \times 10^3 \cdot kip \cdot in$ *Moment that needs to be applied*

$P := \frac{M}{2.75ft} = 71.131kip$ *Point load to cause moment*

$Nominal_{load} := 2 \cdot P = 142.261kip$ *Total applied load to cause moment*

$\varepsilon_s := \frac{0.003}{c} \cdot \left(d_{s\_3} - c\right) = 0.052$ *Strain in extreme tension steel*

At Minimum Depth of CIP Concrete

$d_{s\_3} := 23in$ *Depth to steel*

$A_{s\_3} := 3 \cdot \left(0.11in^2\right) = 0.33in^2$ *Area of steel*

$d_{s\_top} := 5.5in$ *Depth to drop bar steel*

$A_{s\_top} := 4 \cdot \left(0.44in^2\right) = 1.76in^2$ *Area of drop bar steel*

$d_{s\_top2} := 2.5in$ *Depth to steel in top layer*

$A_{s\_top2} := 4 \cdot \left(0.2in^2\right) = 0.8in^2$ *Area of steel in top layer*

$A_s := A_{s\_3} + A_{s\_top} + A_{s\_top2}$ *Total area of steel*

$\left(f_y := 60ksi\right)$ *Strength of steel*

$f'_c := 4000psi$ *Compressive strength of concrete*

$b := 48in$ *Width of section*

$\left(a := \frac{A_s \cdot f_y}{0.85 f'_c \cdot b}\right)$

$(a) = 1.063in$ *Depth of Whitney Stress block*

$\left(\beta_1 := 1.05 - 0.05 \frac{f'_c}{ksi}\right)$

$\left(\beta_1\right) = 0.85$ *Beta factor*

$\left(c := \frac{a}{\beta_1}\right)$

$(c) = 1.25in$ *Depth to neutral axis*

$M_{n1} := A_{s\_3} \cdot f_y \cdot \left(d_{s\_3} - \frac{a}{2}\right) + A_{s\_top} \cdot f_y \cdot \left(d_{s\_top} - \frac{a}{2}\right) + A_{s\_top2} \cdot f_y \cdot \left(d_{s\_top2} - \frac{a}{2}\right)$

$\left(M_{n1}\right) = 1064.1kip \cdot in$ *Nominal moment capacity*

$w_{self} := 0.15 \frac{kip}{ft^3} \cdot 25in \cdot 48in = 1.25 \frac{kip}{ft}$ *Self-weight of specimen*

$M_{self} := \frac{w_{self} \cdot (138in)^2}{8} = 247.969kip \cdot in$ *Moment due to self-weight*

$M := M_{n1} - M_{self} = 816.113kip \cdot in$ *Moment that needs to be applied*

$P := \frac{M}{2.75ft} = 24.731kip$ *Point load to cause moment*

$Nominal_{load} := 2 \cdot P = 49.461kip$ *Total applied load to cause moment* **<<<<CONTROLS**

$\varepsilon_s := \frac{0.003}{c} \cdot \left(d_{s\_3} - c\right) = 0.052$ *Strain in extreme tension steel*

Cracking Moments/Loads

Extended Bar

$M_{selfweight} := M_{self}$

$CIP_{deepdepth} := 22in$ *Depth of CIP portion at section*

$width := 48in$ *Width of section*

$A_{CIPdeep} := CIP_{deepdepth} \cdot width$ *Area of CIP region at section*

$A_{deckbottom} := 4 \cdot \left(0.44in^2\right) = 1.76in^2$ *Area of steel in bottom of section*

$A_{decktop} := 8 \cdot \left(0.2in^2\right) = 1.6in^2$ *Area of steel in top of section*

$\eta := 8.04$ *Modular ratio*

$A_{trasnsformed} := A_{CIPdeep} + \left(A_{decktop} + A_{deckbottom}\right) \cdot (\eta - 1) = 1.08 \times 10^3 \cdot in^2$ *Transformed area*

$d_{s\_top} := 4in$ *Depth to top steel*

$d_{s\_bottom} := 18.825in$ *Depth to bottom steel*

$f_{cCIP} := 4000psi$ *Design strength of CIP concrete*

$$y_{bottomtrasnformed.1} := \frac{A_{CIPdeep} \cdot \frac{CIP_{deepdepth}}{2} + A_{deckbottom} \cdot (\eta - 1) \cdot d_{s\_bottom}}{A_{trasnsformed}}$$

$$y_{bottomtrasnformed.2} := \frac{A_{decktop} \cdot (\eta - 1) \cdot d_{s\_top}}{A_{trasnsformed}}$$

$y_{bottomtrasnformed} := y_{bottomtrasnformed.1} + y_{bottomtrasnformed.2} = 11.017in$ *Centroid*

$\left(I_{cipgross} := \frac{1}{12} \cdot width \cdot CIP_{deepdepth}^{3} = 0.018m^4\right)$ *Gross moment of inertia*

$I_{transformed.1} := I_{cipgross} + A_{deckbottom} \cdot (\eta - 1) \cdot \left(y_{bottomtrasnformed} - d_{s\_bottom}\right)^2$

$I_{transformed.2} := A_{decktop} \cdot (\eta - 1) \cdot \left(d_{s\_top} - y_{bottomtrasnformed}\right)^2$

$I_{transformed} := I_{transformed.1} + I_{transformed.2} = 4.39 \times 10^4 in^4$ *Transformed moment of inertia*

$f_{raci} := 7.5\sqrt{f_{cCIP} \cdot psi} = 474.342psi$ *Rupture stress on CIP concrete*

$c_{cip} := \frac{CIP_{deepdepth}}{2} = 11 \cdot in$ *Centroid of CIP section*

$M_{crackingacitransformed} := \frac{f_{raci} \cdot I_{transformed}}{y_{bottomtrasnformed}} = 1.89 \times 10^{3} \cdot kip \cdot in$ *Transformed cracking moment*

$P_{acitransformed} := \frac{\left(M_{crackingacitransformed} - M_{selfweight}\right)}{2.75ft \cdot 12\frac{in}{ft}} = 49.767kip$ *Point load required to cause cracking*

$P_{totalacitransformed} := P_{acitransformed} \cdot 2 = 99.535kip$ *Total applied load required to cause cracking*

Embedded Plate

$CIP_{deepdepth} := 22in$ *Depth of CIP portion at section*

$width := 48in$ *Width of section*

$A_{CIPdeep} := CIP_{deepdepth} \cdot width$ *Area of CIP region at section*

$A_{deckbottom} := 4 \cdot \left(0.44in^2\right) = 1.76in^2$ *Area of steel in bottom of section*

$A_{decktop} := 8 \cdot \left(0.2in^2\right) = 1.6in^2$ *Area of steel in top of section*

$\eta := 8.04$ *Modular ratio*

$A_{trasnsformed} := A_{CIPdeep} + \left(A_{decktop} + A_{deckbottom}\right) \cdot (\eta - 1) = 1.08 \times 10^{3} \cdot in^2$ *Transformed area*

$d_{s\_top} := 4in$ *Depth to top steel*

$d_{s\_bottom} := 23.5in$ *Depth to bottom steel*

$f_{cCIP} := 4000psi$ *Design strength of CIP concrete*

$y_{bottomtrasnformed.1} := \frac{A_{CIPdeep} \cdot \frac{CIP_{deepdepth}}{2} + A_{deckbottom} \cdot (\eta - 1) \cdot d_{s\_bottom}}{A_{trasnsformed}}$

$y_{bottomtrasnformed.2} := \frac{A_{decktop} \cdot (\eta - 1) \cdot d_{s\_top}}{A_{trasnsformed}}$

$y_{bottomtrasnformed} := y_{bottomtrasnformed.1} + y_{bottomtrasnformed.2} = 11.07in$ *Centroid*

$\left(I_{cipgross} := \frac{1}{12} \cdot width \cdot CIP_{deepdepth}^{3} = 0.018m^4\right)$ *Gross moment of inertia*

$I_{transformed.1} := I_{cipgross} + A_{deckbottom} \cdot (\eta - 1) \cdot \left(y_{bottomtrasnformed} - d_{s\_bottom}\right)^2$

$I_{transformed.2} := A_{decktop} \cdot (\eta - 1) \cdot \left(d_{s\_top} - y_{bottomtrasnformed}\right)^2$

$I_{transformed} := I_{transformed.1} + I_{transformed.2} = 4.507 \times 10^{4} in^4$ *Transformed moment of inertia*

$f_{raci} := 7.5\sqrt{f_{cCIP} \cdot psi} = 474.342psi$ *Rupture stress on CIP concrete*

$c_{cip} := \frac{CIP_{deepdepth}}{2} = 11 \cdot in$ *Centroid of CIP section*

$M_{crackingacitransformed} := \frac{f_{raci} \cdot I_{transformed}}{y_{bottomtrasnformed}} = 1.931 \times 10^{3} \cdot kip \cdot in$ *Transformed cracking moment*

$P_{acitransformed} := \frac{\left(M_{crackingacitransformed} - M_{selfweight}\right)}{2.75ft \cdot 12\frac{in}{ft}} = 51.006kip$ *Point load required to cause cracking*

$P_{totalacitransformed} := P_{acitransformed} \cdot 2 = 102.012kip$ *Total applied load required to cause cracking*

No Connection

$CIP_{deepdepth} := 22in$ *Depth of CIP portion at section*

$width := 48in$ *Width of section*

$A_{CIPdeep} := CIP_{deepdepth} \cdot width$ *Area of CIP region at section*

$A_{deckbottom} := 4 \cdot \left(0.44in^2\right) = 1.76in^2$ *Area of steel in bottom of section*

$A_{decktop} := 4 \cdot \left(0.2in^2\right) = 0.8in^2$ *Area of steel in top of section*

$\eta := 8.04$ *Modular ratio*

$A_{trasnsformed} := A_{CIPdeep} + \left(A_{decktop} + A_{deckbottom}\right) \cdot (\eta - 1) = 1.074 \times 10^{3} \cdot in^2$ *Transformed area*

$d_{s\_top} := 2.5in$ *Depth to top steel*

$d_{s\_bottom} := 20in$ *Depth to bottom steel*

$f_{cCIP} := 4000psi$ *Design strength of CIP concrete*

$$y_{bottomtrasnformed.1} := \frac{A_{CIPdeep} \cdot \frac{CIP_{deepdepth}}{2} + A_{deckbottom} \cdot (\eta - 1) \cdot d_{s\_bottom}}{A_{trasnsformed}}$$

$$y_{bottomtrasnformed.2} := \frac{A_{decktop} \cdot (\eta - 1) \cdot d_{s\_top}}{A_{trasnsformed}}$$

$y_{bottomtrasnformed} := y_{bottomtrasnformed.1} + y_{bottomtrasnformed.2} = 11.059in$ *Centroid*

$\left(I_{cipgross} := \frac{1}{12} \cdot width \cdot CIP_{deepdepth}^{3} = 0.018m^4\right)$ *Gross moment of inertia*

$I_{transformed.1} := I_{cipgross} + A_{deckbottom} \cdot (\eta - 1) \cdot \left(y_{bottomtrasnformed} - d_{s\_bottom}\right)^2$

$I_{transformed.2} := A_{decktop} \cdot (\eta - 1) \cdot \left(d_{s\_top} - y_{bottomtrasnformed}\right)^2$

$I_{transformed} := I_{transformed.1} + I_{transformed.2} = 4.4 \times 10^{4}\,in^{4}$ *Transformed moment of inertia*

$f_{raci} := 7.5\sqrt{f_{cCIP} \cdot psi} = 474.342\,psi$ *Rupture stress on CIP concrete*

$c_{cip} := \frac{CIP_{deepdepth}}{2} = 11 \cdot in$ *Centroid of CIP section*

$M_{crackingacitransformed} := \frac{f_{raci} \cdot I_{transformed}}{y_{bottomtrasnformed}} = 1.887 \times 10^{3} \cdot kip \cdot in$ *Transformed cracking moment*

$P_{acitransformed} := \frac{\left(M_{crackingacitransformed} - M_{selfweight}\right)}{2.75ft \cdot 12\frac{in}{ft}} = 49.668kip$ *Point load required to cause cracking*

$P_{totalacitransformed} := P_{acitransformed} \cdot 2 = 99.336kip$ *Total applied load required to cause cracking*